

APPLICATION OF NYSTRÖM METHOD FOR THE SOLUTION OF TIME  
DOMAIN ELECTRIC FIELD INTEGRAL EQUATION

A THESIS SUBMITTED TO  
THE DEPARTMENT OF ELECTRICAL AND ELECTRONICS ENGINEERING  
OF  
MIDDLE EAST TECHNICAL UNIVERSITY

BY

GÖKHUN SELÇUK

IN PARTIAL FULFILLMENT OF THE REQUIREMENTS  
FOR  
THE DEGREE OF DOCTOR OF PHILOSOPHY  
IN  
ELECTRICAL AND ELECTRONICS ENGINEERING

SEPTEMBER 2014



Approval of the thesis:

**APPLICATION OF NYSTRÖM METHOD FOR THE SOLUTION OF TIME  
DOMAIN ELECTRIC FIELD INTEGRAL EQUATION**

submitted by **GÖKHUN SELÇUK** in partial fulfillment of the requirements for the  
degree of **Doctor of Philosophy in Electrical and Electronics Engineering**  
**Department, Middle East Technical University** by,

Prof. Dr. Canan Özgen  
Dean, Graduate School of **Natural and Applied Sciences**

\_\_\_\_\_

Prof. Dr. Gönül Turhan Sayan  
Head of Department, **Electrical and Electronics Engineering**

\_\_\_\_\_

Prof. Dr. S. Sencer Koç  
Supervisor, **Electrical and Electronics Engineering Dept., METU**

\_\_\_\_\_

**Examining Committee Members**

Prof. Dr. Mustafa Kuzuoğlu  
Electrical and Electronics Engineering Dept., METU

\_\_\_\_\_

Prof. Dr. S. Sencer Koç  
Electrical and Electronics Engineering Dept., METU

\_\_\_\_\_

Prof. Dr. Ayhan Altıntaş  
Electrical and Electronics Engineering Dept., Bilkent University

\_\_\_\_\_

Prof. Dr. Gülbin Dural  
Electrical and Electronics Engineering Dept., METU

\_\_\_\_\_

Assoc. Prof. Dr. Lale Alatan  
Electrical and Electronics Engineering Dept., METU

\_\_\_\_\_

**Date:** September 19, 2014

**I hereby declare that all information in this document has been obtained and presented in accordance with academic rules and ethical conduct. I also declare that, as required by these rules and conduct, I have fully cited and referenced all material and results that are not original to this work.**

Name, Last Name : Gökhan Selçuk

Signature:

## ABSTRACT

### APPLICATION OF NYSTRÖM METHOD FOR THE SOLUTION OF TIME DOMAIN ELECTRIC FIELD INTEGRAL EQUATION

Selçuk, Gökhun

Ph. D., Department of Electrical and Electronics Engineering

Supervisor : Prof. Dr. S. Sencer Koç

September 2014, 109 Pages

Solution of surface scattering problems with electric field integral equation (EFIE) requires careful treatment of singularities introduced by the 3D dyadic Green's function when source and observation points are close to each other or coincide. One may either utilize the divergence conforming basis and testing functions to reduce the order of singularity or directly deal with singularities via analytical singularity extraction methods. The latter method is not a commonly used one although it enables use of less complicated pulse-like basis functions and no attempt is done to apply it in time domain. In this study a new time domain formulation for EFIE is obtained. Self-cell contribution is evaluated by an efficient treatment of hypersingular integrals. By using Hadamard finite part interpretation new formulas are introduced for hypersingular integrals on planar surfaces. Also same interpretation is used to obtain explicit expressions for hypersingular integrals on nonplanar surfaces and these expressions improve the accuracy significantly. Close cell contribution is evaluated by increasing the number of quadrature points and applying interpolation. Explicit marching on in time (MOT) scheme along with new formulation is applied to solve transient scattering from perfectly electric conductor (PEC) surfaces. Agreement with analytical results is obtained.

Keywords: Electric Field Integral Equation, Singularity Extraction, Hadamard Finite Part, Transient Scattering

## ÖZ

### ZAMAN UZAMINDA ELEKTRİK ALAN TÜMLEVSEL DENKLEMİNİN ÇÖZÜMÜ İÇİN NYSTRÖM YÖNTEMİNİN UYGULANMASI

Selçuk, Gökhan  
Doktora, Elektrik ve Elektronik Mühendisliği Bölümü  
Tez Yöneticisi : Prof. Dr. S. Sencer Koç

Eylül 2014, 109 Sayfa

Yüzey saçılım problemlerinin elektrik alan tümlevsel denklem (EATD) yöntemiyle çözümü, kaynak noktası ile gözlem noktasının yakın olduğu ya da çakıştığı durumlarda, 3B ikici Green işlevinin tekilliklerinin dikkatli şekilde ele alınmasını gerektirmektedir. Tekilliğin seviyesinin düşürülmesi için ıraksaklık uyumlu temel ve test fonksiyonlarına başvurulabileceği gibi, bu tekillikler direkt olarak analitik tekilik özütleme yöntemleri ile de ele alınabilir. İkinci yöntem daha basit darbe benzeri temel fonksiyonlarını kullanmayı olanaklı kılmasına rağmen yaygın olarak kullanılmamaktadır ve yöntemin zaman bölgesinde kullanımı için hiçbir teşebbüs yapılmamıştır. Bu çalışmada EATD için zaman uzamında yeni bir formülasyon elde edilmiştir. Öz-hücre etkisi, hipertekil tümlevin etkin şekilde ele alınması ile hesaplanmıştır. Hadamard sonlu parça yaklaşımı kullanılarak düzlemsel yüzeylerde hipertekil tümlevler için yeni formüller elde edilmiştir. Aynı yaklaşım düzlemsel olmayan yüzeylerde de hipertekil tümlevler için açık ifadelerin bulunmasında kullanılmış ve bu ifadeler hassasiyeti önemli ölçüde artırmıştır. Yakın hücre etkisi tümlev noktalarının artırılması ve aradeğerleme uygulanması ile hesaplanmıştır. Yeni formülasyon kullanılarak zamanda açık ilerleme (ZAI) şeması ile mükemmel elektriksel iletken (MEİ) yüzeylerden geçici saçılım problemi çözülmüştür. Analitik sonuçlarla uyum elde edilmiştir.

Anahtar Kelimeler : Elektrik Alan Tümlevsel Denklemi, Tekillik Özütleme, Hadamard Sonlu Parça, Geçici Saçınım

to Mahir, Hakan, Cemile

## **ACKNOWLEDGEMENTS**

I would like to thank to my supervisor Prof. Dr. S. Sencer Koç for his valuable guidance and recommendations throughout the thesis. Without his ideas this study would hardly be finished.

I am also grateful to the members of Thesis Supervising Committee, Prof. Dr. Mustafa Kuzuoğlu and Prof. Dr. Ayhan Altıntaş for their comments, criticism and time.

I would also like to thank to Abidin Taşkiran for his support, understanding and encouragement in workplace.

Finally I would like to thank my family members; my wife Cemile, my two-year old son Hakan, our new baby Mahir and my parents Mehmet and Sakine for their continuous support throughout my life.



## TABLE OF CONTENTS

ABSTRACT.....	v
ÖZ.....	vi
ACKNOWLEDGEMENTS.....	viii
TABLE OF CONTENTS.....	ix
LIST OF TABLES.....	xii
LIST OF FIGURES.....	xiii
CHAPTERS	
1. INTRODUCTION.....	1
2. INTEGRAL EQUATION METHODS FOR COMPUTATIONAL ELECTROMAGNETICS.....	5
2.1 Overview of Computational Electromagnetics.....	5
2.1.1 Differential Equation Methods.....	6
2.1.2 Integral Equation Methods.....	7
2.1.3 Other Methods.....	8
2.2 Maxwell's Equations.....	9
2.3 Boundary Conditions.....	10
2.4 Vector Potential Formulation.....	11
2.4.1 Magnetic Vector Potential.....	11
2.4.2 Electric Vector Potential.....	14
2.5 Equivalence Theorems.....	14
2.5.1 Volume Equivalence Principle.....	15

2.5.2 Surface Equivalence Principle.....	17
2.6 Surface Integral Equations.....	20
2.6.1 Electric Field Integral Equation.....	20
2.6.2 Magnetic Field Integral Equation.....	21
3. NYSTRÖM METHOD FOR THE SOLUTION OF INTEGRAL EQUATIONS.....	23
3.1 The Method of Moments.....	23
3.1.1 Selection of Basis Functions.....	23
3.1.2 MoM Solution to EFIE with RWG Basis Functions.....	27
3.2 The Locally Corrected Nyström Method.....	28
3.2.1 Formulation of LCN Method.....	30
3.2.2 Advantages of LCN Method.....	32
4. SINGULAR INTEGRALS AND THEIR EVALUATION.....	35
4.1 Weakly Singular Integrals and Their Evaluation.....	37
4.2 Strongly Singular Integrals and Their Evaluation.....	44
4.2.1 Contour Integration Method.....	44
4.2.2 Limiting Procedure.....	46
4.3 Hypersingular Integrals and Their Evaluation.....	50
4.3.1 Contour Integration for Flat Surfaces.....	52
4.3.2 Hadamard Finite Part Interpretation.....	56
4.4 Hypersingular Integrals on Nonplanar Surfaces.....	59
4.4.1 Taylor Series Expansion of Surface Function.....	61
4.4.2 Bicubic Spline Representation of Surface Function.....	64

4.5 Numerical Results.....	67
4.5.1 Scattering from Dielectric Cube.....	67
4.5.2 Scattering from PEC Cylinder ( $TM_z$ Polarization).....	68
4.5.3 Scattering from PEC Cylinder ( $TE_z$ Polarization).....	70
5. A TIME DOMAIN NYSTROM METHOD FOR THE SOLUTION OF EFIE.....	73
5.1 Formulation.....	74
5.1.1 Conventional Formulation for TDEFIE.....	75
5.1.2 Nyström Method for the Solution of TDEFIE.....	77
5.2 Numerical Results .....	81
5.2.1 Electrically Large Plate.....	82
5.2.2 PEC Cylinder.....	83
5.2.3 PEC Strip.....	85
6. CONCLUSION.....	87
REFERENCES.....	89
APPENDICES	
A. NUMERICAL INTEGRATION AND QUADRATURE RULES.....	95
B. EQUIVALENCE OF FINITE PART INTEGRALS TO PHYSICAL FIELDS.....	100
C. REQUIREMENT ON THE DENSITY FUNCTION FOR THE EXISTENCE OF FINITE PART OF A HYPER SINGULAR INTEGRAL.....	107
CURRICULUM VITAE.....	109

## LIST OF TABLES

### TABLES

Table 4.1 Results obtained for weakly singular integrals on square patch.....	43
Table 4.2 Results obtained for nearly weakly singular integrals on square patch.....	43
Table 4.3 Results obtained for nearly strongly singular integrals on square patch.....	49
Table 4.4 Results obtained for strongly singular integrals on square patch.....	49
Table 4.5 The components of hypersingular dyadic on a triangle with random shape.....	58
Table 4.6 Comparison of (4.52) with analytical solution for $a=2$ .....	63
Table 4.7 Comparison of (4.52) with analytical solution for $a=5$ .....	63
Table 4.8 Comparison of (4.58) with exact results.....	66
Table A.1 Relative performance of quadrature rules.....	98

## LIST OF FIGURES

### FIGURES

Figure 2.1 Field geometry for actual problem and equivalent problem (a) actual problem (b) equivalent problem.....	16
Figure 2.2 Physical equivalent for scattering from a PEC object (a) actual problem (b) equivalent problem.....	18
Figure 3.1 RWG Basis Function.....	27
Figure 4.1 Exclusion zone in the domain of integration.....	37
Figure 4.2 Triangular patch on which the singular integral is defined.....	40
Figure 4.3 The square patch over which weakly singular integral is defined.....	42
Figure 4.4 The surface $S$ over which strongly singular integral is defined and the extracted surface $S_\epsilon$ .....	47
Figure 4.5 Nonplanar surface $\Omega$ and its projection $D$ on $u_1u_2$ plane.....	60
Figure 4.6 Accuracy of $I_{22}$ with different approximations of surface function.....	66
Figure 4.7. Geometry for dielectric cube scattering problem.....	67
Figure 4.8. Bistatic radar cross section of dielectric cube with $a=0.15\lambda$ for both vertical and horizontal polarizations.....	68
Figure 4.9. Bistatic radar cross section of dielectric cube with $a=0.05\lambda$ for both vertical and horizontal polarizations.....	69
Figure 4.10 Geometry of the PEC cylinder problem (TM <sup>z</sup> polarization).....	69
Figure 4.11 Current induced on PEC cylinder versus angle for TM <sup>z</sup> polarization.....	70

Figure 4.12 Current induced on PEC cylinder versus angle for $TE^z$ polarization.....	70
Figure 4.13 Accuracy obtained for $TE^z$ scattering problem when number of nodes is increased.....	71
Figure. 5.1 Geometry for PEC plane problem.....	82
Figure. 5.2 Amplitude of induced current on PEC plate.....	83
Figure. 5.3 Geometry for PEC cylinder problem.....	84
Figure. 5.4 Amplitude of induced current on cylinder.....	84
Figure. 5.5 Amplitude of induced current on PEC strip.....	85
Figure B.1 The geometry over which (4.43) is defined.....	98

## CHAPTER 1

### INTRODUCTION

Time domain integral equation (TDIE) methods are used extensively to analyze transient scattering and radiation problems. The major advantages of TDIE methods over finite difference time domain (FDTD) and time domain finite element (TD-FEM) methods are that, TDIEs require lesser unknowns and they do not use artificial absorbing boundary conditions (ABC) to truncate the computational domain. Despite its advantages TDIEs are plagued by late time stability and computational complexity. In this study these two shortcomings of TDIE methods are addressed. This is achieved by using the well-known Nyström method for the solution of time domain electric field integral equation (TDEFIE).

Nyström method is basically a frequency domain method purposed in [1-3] for the solution of integral equation methods in electromagnetics. The main idea of the procedure is to replace the surface integrals of the basis and testing functions in the conventional method of moments (MoM) procedure with quadrature rules. Since evaluation of kernel of EFIE at selected quadrature nodes is computationally more efficient and simpler than evaluating surface integrals, Nyström method offers faster precomputation phase than MoM procedure and reduces computational complexity by eliminating basis and testing functions.

One drawback of the Nyström method is that quadrature rules are accurate only for smooth kernels but electromagnetic problems involve singular kernels. Because of this, quadrature rules can only be used for far cell interactions and special care should be exercised to compute near cell and self-cell interactions. Moreover, Nyström method does not use divergence conforming basis and testing functions to which the differential operators of the free space Green's function can be transferred. Therefore the method introduces weakly singular, strongly singular

and hypersingular integrals with  $1/R$ ,  $1/R^2$  or  $1/R^3$  terms in the kernel, respectively. The remedy with singular kernels is to modify the kernel so that the modified kernel produces correct field at quadrature nodes. This is referred to local corrections. Although local corrections increase computational complexity, they are only required for a small number of interactions and do not affect total computational cost drastically.

One contribution of this study is in evaluation of hypersingular integrals which arise in the solution of EFIE via Nyström method. Although the literature dealing with evaluation of weakly singular and strongly singular integrals is extensive, few studies address evaluation of hypersingular integrals for the solution of electromagnetic problems. A Cauchy principal value like approach in the limiting sense is used in [4] and a similar approach along with Stoke's theorem is used in [5] to obtain simpler formulas. Hypersingular surface integrals are converted to regular line integrals on curvilinear patches in [6] but explicit formulas are not introduced. Here we evaluate hypersingular integrals based on Hadamard finite part (HFP) interpretation. Hadamard finite part interpretation neglects the divergent part of the integral and keeps the finite part which in fact gives the correct value for the physical field. The advantage of using HFP interpretation is twofold. First the resulting explicit expressions for flat surfaces are simpler compared to other expressions previously introduced in the literature. Secondly HFP interpretation can easily be adapted for evaluation of hypersingular integrals on nonplanar surfaces. Numerical tests have shown that the new expressions for hypersingular integrals on flat surfaces are as accurate as previously introduced ones. Moreover, on curvilinear elements we have obtained improved accuracy and have shown that when scattering from nonplanar surfaces is considered, the new formulas introduce higher rate of convergence for the solution compared to flat face discretization. Having obtained ready to use explicit expressions for hypersingular integrals, the computational complexity for the method is reduced without sacrificing accuracy.



Despite its advantages in frequency domain, Nyström method was not considered for time domain scattering problems. The main contribution of this study is utilization of Nyström method for analysis of transient electromagnetic phenomena, specifically for the solution of TDEFIE. Unlike MoM procedure, which introduces a set of temporal and spatial basis and testing functions for the unknown current density, we used samples of current at selected quadrature nodes and specific time instants to formulate EFIE. The spatial integrals are again approximated by quadrature rules. The time derivative and the integral of the current density are approximated by backward difference scheme and numerical integration respectively. One problem in time domain Nyström scheme is that; due to the retarded interactions, the values of current density at arbitrary time instant are required for marching on in time. Since the method only uses samples of current at specific instants, the delayed interactions are evaluated by using interpolation in time. By numerical studies we have shown that quite accurate results can be obtained by the purposed procedure. Moreover late time stability is improved by interpolation process and no stabilization technique is necessary for the procedure.

The thesis is organized as follows. Chapter 2 introduces an overview of computational electromagnetics and presents some fundamental theorems for derivation of integral equations. In Chapter 3 frequency domain MoM procedure and Nyström method are introduced. Chapter 4 is devoted to evaluation of singular integrals and their accuracies. Here we introduce the novel formulas obtained for hypersingular integrals for both flat and curvilinear surfaces. In chapter 5 we introduce the new formulation for TDEFIE using Nyström method and present some numerical results. Chapter 6 concludes the thesis and future studies are discussed.



## **CHAPTER 2**

# **INTEGRAL EQUATION METHODS FOR COMPUTATIONAL ELECTROMAGNETICS**

### **2.1 Overview of Computational Electromagnetics**

Electromagnetic systems play an important role in today's technology since they form the fundamental part of many applications such as telecommunications, radar, medical diagnosis and electronic warfare. Understanding the behavior of electromagnetic wave in different media along with radiation and scattering mechanisms is essential for the synthesis of such systems. The construction of these systems as well as analysis and testing ultimately require solution of Maxwell's equations for the system of interest. Although expressions for the behavior of electromagnetic waves can be obtained analytically for a limited number of cases, numerical analysis offers extensive application area and has gained wide attention with the advent of fast computers. Computational electromagnetics basically involves the development and application of numerical algorithms for the solution of Maxwell's equations [7].

With diverse application areas and the wide attention on the topic, there is a variety of methods to solve Maxwell's equations. Here we try to give a brief overview of computational electromagnetics in order to introduce integral equation methods as a part of a bigger framework. The methods in computational electromagnetic can be categorized according to the form of Maxwell's equation they use. Differential equation methods use Maxwell's equations in differential form and integral equation methods use these equations in integral form to construct their algorithms. Methods in computational electromagnetic can also be classified according to whether they use Maxwell's equations in time domain or in frequency domain and categorized as time domain or frequency domain

techniques, respectively. Here we use the first criteria and categorize the methods as differential equation methods and integral equation methods. The distinction between time domain and frequency domain techniques will be emphasized later in chapter 5.

### **2.1.1 Differential Equation Methods**

Maxwell's equations in differential form are point relations and relate the field values at these points. Therefore in application of differential equation techniques, every point in space should be discretized and the unknowns are the field values at these points.

A very popular and the oldest technique using differential equations is the finite difference time domain method (FDTD) introduced by Yee in the mid-1960s [8]. This method samples the electromagnetic field in a finite volume at distinct points in a space lattice and equally spaced instants in time. Electromagnetic phenomenon is modeled automatically by imposing time domain curl equations via finite differences and marching in time. The data on each sample point at a given instant is effected only by neighboring points at the previous instant so that there is no need to store the history of field values and this reduces required memory size. Therefore the memory storage and running time requirements are proportional to the number of unknowns. However the field values should be defined at each space lattice and this increases the number of unknowns. Also numerical wave radiation conditions such as absorbing boundary conditions (ABCs) should be employed to eliminate spurious, nonphysical reflections from the borders of the problem space.

The transmission line matrix method (TLM) [9] uses a similar principle but does not use Maxwell's curl equations directly. The computational domain is considered as a mesh of transmission lines connecting the nodes. The electromagnetic field is modeled as wave pulses propagating in these lines and scattered at the nodes. Similar to FDTD method the computational domain is

whole space where fields exist. Also no back-storage in time is required other than the field values in the adjacent nodes at the previous time.

Another commonly used frequency-domain technique is the finite element method (FEM) [10] where each cell is referred to as an element. The method is employed for the solution of frequency-domain boundary value electromagnetic problems by using a variational form. The method is often used for computing field distribution in complex, closed regions such as cavities and waveguides [11]. Similar to FDTD method the solution domain must be truncated making FEM unsuitable for scattering and radiation problems unless combined with a boundary integral equation approach [12].

The main advantage of differential equation methods is that, they can easily handle inhomogeneous dielectric media such as biological tissues, geophysical strata and shielding metal structures having complex interior loading [7]. Also nonlinear media is easily incorporated with these methods since the characteristics of the media are involved in the equations for each element. Moreover for time domain problems no back-storage in time is required as the new field values are only determined by the present values and for frequency domain methods the system matrix is sparse due to local interactions. On the other hand a major drawback of differential equation methods is the requirement to discretize whole problem space which increases the number of unknowns drastically especially for problems with open regions. Open region problems can be treated by absorbing boundary conditions but these conditions can also introduce errors. Another disadvantage is stability and dispersion problems which require additional efforts for compensation [13].

### **2.1.2 Integral Equation Methods**

Integral equation methods set up an equation which relates the electromagnetic field to the unknown sources by using the boundary conditions on the surface or within the volume. These equations are not general and should be derived based on the type of scattering geometry and on the characteristics of material content. These can be either volume integral equations or surface integral equations.

Whereas volume integral equations set up an integro-differential equation relating polarization currents within the volume to total field, surface integral equations try to find unknown surface currents whether electric, magnetic or both.

The main advantage of integral equation methods over differential equation methods is that integral equation methods only discretize the space where sources exists. This discretization reduces the number of unknowns especially for open problems and is suitable for antenna radiation and scattering problems. Nevertheless the disadvantage is that, since there is interaction between all elements in the solution domain, the system matrix is dense for frequency domain problems and the required computer memory is proportional to  $N^2$  where  $N$  is the number of unknowns. For time domain problems on the other hand storage of all previous current values is required so that the required memory is proportional to  $N^2T$  where  $T$  is the number of time steps. Recently a multilevel fast multipole method (MLFMM) [47], is introduced to reduce the memory requirement for integral equation methods. Instead of allowing interaction between each element directly the scheme groups far cell elements and interactions are evaluated on a group by group level so that the required memory is proportional to  $N\log(N)$ . Another important disadvantage of the integral equation methods, which is one of the research topics of this study, is the complex source-field relation due to different orders of singularities introduced by the Green's function itself and its derivatives.

### **2.1.3 Other Methods**

As mentioned, computational electromagnetic is an extensive research area and the techniques for numerical solution of electromagnetic problems cannot be categorized only as differential equation methods or integral equation methods. Below we name some of the methods that cannot be classified within the two aforementioned methods.

Geometrical theory of diffraction (GTD) [15] uses ray optics to analyze electromagnetic wave propagation. The amplitude and the phase of the field value on a ray are determined by Fermat's principle. At diffraction points new waves are

launched whose amplitudes are determined for a number of canonical shapes. The method offers fast solution especially for electrically large objects but is not as accurate as the previously mentioned methods since it is a high frequency approximation. Also the method estimates infinite field between the border of illuminated and shadow regions. In order to overcome this defect a uniform theory of diffraction (UTD) [16] is developed which introduces new coefficients for the amplitude of diffracted rays and eliminates infinite field. Time domain techniques based on GTD and UTD [17] is also introduced for the solution of transient scattering problems.

Physical optics (PO) is also a high frequency method for the solution of Maxwell's equations and uses source-field relations similar to integral equation methods. Whereas integral equation methods evaluate for the current density directly, PO uses high frequency approximation for the current density. PO is widely used in reflector antenna problems and radar cross section (RCS) problems but its application area is limited since it does not account for the diffracted fields unless used with physical theory of diffraction (PTD) [18,19]. PTD is used to supplement PO solution by adding the effects of nonuniform currents at the diffracting edges.

Apart from the above mentioned methods, there are also hybrid methods which combine powerful aspects of two different methods into a single method. An example is a combination of finite element method with boundary integral method (FE-BI) [10]. A commercial EM simulation software [20] uses GTD along with integral equation methods to provide both accurate and fast solutions.

## **2.2 Maxwell's Equations**

Integral equation methods use source-field relations to set up the system of equations for a given problem. Since these relations are obtained utilizing Maxwell's equations, they will be introduced here for the sake of completeness.

For a homogenous medium with constitutive parameters  $\epsilon$  and  $\mu$ , frequency domain Maxwell's equations can be written as,

$$\vec{\nabla} \times \vec{E}(\vec{r}) = -j\omega\mu\vec{H}(\vec{r}) - \vec{M}(\vec{r}) \quad (2.1)$$

$$\vec{\nabla} \times \vec{H}(\vec{r}) = \vec{J}(\vec{r}) + j\omega\epsilon\vec{E}(\vec{r}) \quad (2.2)$$

$$\vec{\nabla} \cdot \vec{D}(\vec{r}) = \rho_e(\vec{r}) \quad (2.3)$$

$$\vec{\nabla} \cdot \vec{B}(\vec{r}) = \rho_m(\vec{r}) \quad (2.4)$$

where  $\vec{E}(\vec{r})$  is the electric field intensity in V/m,  $\vec{H}(\vec{r})$  is the magnetic field intensity in A/m,  $\vec{D}(\vec{r})$  is the electric flux density in C/m<sup>2</sup> and  $\vec{B}(\vec{r})$  is the magnetic flux density in Wb/m<sup>2</sup>. Also  $\vec{J}(\vec{r})$  is the volume electric current density in A/m<sup>2</sup>,  $\vec{M}(\vec{r})$  is the volume magnetic current density in V/m<sup>2</sup>,  $\rho_e(\vec{r})$  is the volume electric charge density in C/m<sup>3</sup> and  $\rho_m(\vec{r})$  is the volume magnetic charge density in Wb/m<sup>3</sup>. Finally  $\omega$  is the angular frequency in rad/s,  $\epsilon$  is the permittivity of medium in F/m and  $\mu$  is the permeability of medium in H/m. In writing (2.1)-(2.4)  $e^{j\omega t}$  convention is used, and this will be suppressed throughout the thesis.

The electric field intensity is related to the electric flux density with,

$$\vec{D}(\vec{r}) = \epsilon\vec{E}(\vec{r}) \quad (2.5)$$

and magnetic field intensity is related to magnetic flux density with,

$$\vec{B}(\vec{r}) = \mu\vec{H}(\vec{r}) \quad (2.6)$$

which are called as constitutive relations.

### 2.3 Boundary Conditions

At a boundary between two media with constitutive parameters  $\epsilon_1, \mu_1$  and  $\epsilon_2, \mu_2$  the boundary conditions can be written as,

$$\hat{n} \times \vec{E}_2(\vec{r}) = \hat{n} \times \vec{E}_1(\vec{r}) - \vec{M}_s(\vec{r}) \quad (2.7)$$

$$\hat{n} \times \vec{H}_2(\vec{r}) = \hat{n} \times \vec{H}_1(\vec{r}) + \vec{J}_s(\vec{r}) \quad (2.8)$$

$$\hat{n} \cdot \vec{D}_2(\vec{r}) = \hat{n} \cdot \vec{D}_1(\vec{r}) + \rho_e(\vec{r}) \quad (2.9)$$

$$\hat{n} \cdot \vec{B}_2(\vec{r}) = \hat{n} \cdot \vec{B}_1(\vec{r}) + \rho_m(\vec{r}) \quad (2.10)$$

where  $\hat{n}$  is the unit vector normal to the boundary and pointing from region 2 to region 1. For the special case when region 1 is a perfect electrically conducting



(PEC) object, the fields inside object are zero and the boundary conditions can be written as,

$$\hat{n} \times \vec{E}_2(\vec{r}) = 0 \quad (2.11)$$

$$\hat{n} \times \vec{H}_2(\vec{r}) = \vec{J}_s(\vec{r}) \quad (2.12)$$

$$\hat{n} \cdot \vec{D}_2(\vec{r}) = \rho_e(\vec{r}) \quad (2.13)$$

$$\hat{n} \cdot \vec{B}_2(\vec{r}) = 0 \quad (2.14)$$

## 2.4 Vector Potential Formulation

Although Maxwell's equations can be used to directly obtain field values from the source function in many cases it may be difficult or impossible to directly solve these equations for the fields [11]. It is therefore a common practice to introduce auxiliary vector potentials as intermediate steps to solve for the field values  $\vec{E}(\vec{r})$  and  $\vec{H}(\vec{r})$  from the known source functions. The most common vector potentials are the magnetic vector potential  $\vec{A}(\vec{r})$  and the electric field potential  $\vec{F}(\vec{r})$ . It should be noted that although the field quantities are physically measurable quantities, for most engineers the vector potentials are only mathematical tools which ease the derivation of field from the sources [21].

### 2.4.1 Magnetic Vector Potential

The magnetic vector potential  $\vec{A}(\vec{r})$  is derived first. This potential is useful in solving the electromagnetic field generated by a given electric current  $\vec{J}(\vec{r})$ . Much of the discussion here is borrowed from [22].

Since the magnetic field  $\vec{H}(\vec{r})$  is solenoidal, it can be written as a curl of another vector  $\vec{A}(\vec{r})$ , so that one writes;

$$\vec{H}(\vec{r}) = \frac{1}{\mu} \vec{\nabla} \times \vec{A}(\vec{r}) \quad (2.15)$$

Using (2.1), (2.15) can be written as,

$$\vec{\nabla} \times \vec{E}(\vec{r}) = -j\omega \vec{\nabla} \times \vec{A}(\vec{r}) \quad (2.16)$$

Rewriting (2.16) gives

$$\vec{\nabla} \times (\vec{E}(\vec{r}) + j\omega\vec{A}(\vec{r})) = 0 \quad (2.17)$$

Since the curl of the term within the parentheses is zero, it can be written as the gradient of a scalar so that

$$\vec{E}(\vec{r}) = -j\omega\vec{A}(\vec{r}) - \vec{\nabla}\Phi_e(\vec{r}) \quad (2.18)$$

where  $\Phi_e(\vec{r})$  is an arbitrary electric scalar potential. Using the identity

$$\vec{\nabla} \times \vec{\nabla} \times \vec{A} = \vec{\nabla}(\vec{\nabla} \cdot \vec{A}) - \nabla^2 \vec{A} \quad (2.19)$$

and take curl of both sides of (2.15), we can write,

$$\mu\vec{\nabla} \times \vec{H} = \vec{\nabla}(\vec{\nabla} \cdot \vec{A}) - \nabla^2 \vec{A} \quad (2.20)$$

and using also (2.2) leads to,

$$\mu\vec{J} + j\omega\mu\epsilon\vec{E} = \vec{\nabla}(\vec{\nabla} \cdot \vec{A}) - \nabla^2 \vec{A} \quad (2.21)$$

The electric field intensity in (2.21) is substituted using (2.18) so we can write

$$\mu\vec{J} + j\omega\mu\epsilon(-j\omega\vec{A} - \vec{\nabla}\Phi_e) = \vec{\nabla}(\vec{\nabla} \cdot \vec{A}) - \nabla^2 \vec{A} \quad (2.22)$$

Reorganization of (2.22) leads to

$$\nabla^2 \vec{A} + k^2 \vec{A} = -\mu\vec{J} + \vec{\nabla}(\vec{\nabla} \cdot \vec{A} + j\omega\mu\epsilon\Phi_e) \quad (2.23)$$

where  $k = \omega^2\mu\epsilon$  is the wavenumber.

The curl of the magnetic vector potential was selected in (2.15), but we are still free to choose the divergence of the potential. We select the divergence of  $\vec{A}$  such that the second term on the RHS of (2.23) is eliminated. So by using,

$$\vec{\nabla} \cdot \vec{A} = -j\omega\mu\epsilon\Phi_e \quad (2.24)$$

we can simplify (2.23) to,

$$\nabla^2 \vec{A} + k^2 \vec{A} = -\mu\vec{J} \quad (2.25)$$

This is the Helmholtz equation for the magnetic potential so that  $\vec{A}$  can be obtained from  $\vec{J}$  by using,

$$\vec{A}(\vec{r}) = \mu \iiint_V G(\vec{r}, \vec{r}') \vec{J}(\vec{r}') dV' \quad (2.26)$$

where  $G(\vec{r}, \vec{r}')$  is the solution of scalar Helmholtz equation,

$$\nabla^2 G(\vec{r}, \vec{r}') + k^2 G(\vec{r}, \vec{r}') = -\delta(\vec{r}, \vec{r}') \quad (2.27)$$

and is given by,

$$G(\vec{r}, \vec{r}') = \frac{e^{-jk|\vec{r}-\vec{r}'|}}{4\pi|\vec{r}-\vec{r}'|} \quad (2.28)$$

This derivation leads to a formula relating the electric field to magnetic vector potential  $\vec{A}$  and scalar potential  $\Phi_e$ ,

$$\vec{E} = -j\omega\vec{A} - \vec{\nabla}\Phi_e = -j\omega\vec{A} - \frac{j}{\omega\mu\epsilon} \vec{\nabla}(\vec{\nabla} \cdot \vec{A}) \quad (2.29)$$

Substituting (2.26) into (2.29) leads to the final formula relating the electric field to the current,

$$\vec{E}(\vec{r}) = -j\omega\mu \iiint_V \frac{e^{-jk|\vec{r}-\vec{r}'|}}{4\pi|\vec{r}-\vec{r}'|} \vec{J}(\vec{r}') dV' - \frac{j\omega\mu}{k^2} \vec{\nabla} \left( \vec{\nabla} \cdot \iiint_V \frac{e^{-jk|\vec{r}-\vec{r}'|}}{4\pi|\vec{r}-\vec{r}'|} \vec{J}(\vec{r}') dV' \right) \quad (2.30)$$

Also by using (2.15)

$$\vec{H}(\vec{r}) = \vec{\nabla} \times \iiint_V \frac{e^{-jk|\vec{r}-\vec{r}'|}}{4\pi|\vec{r}-\vec{r}'|} \vec{J}(\vec{r}') dV' \quad (2.31)$$

### 2.4.2 Electric Vector Potential

By symmetry of the Maxwell's equations we can also define an electric vector potential  $\vec{F}$ . The procedure for the magnetic potential is summarized below for the electric potential without giving details,

$$\vec{E} = \frac{1}{\varepsilon} \vec{\nabla} \times \vec{F} \quad (2.32)$$

$$\Phi_m = -\frac{1}{j\omega\mu\varepsilon} \vec{\nabla} \cdot \vec{F} \quad (2.33)$$

$$\nabla^2 \vec{F} + k^2 \vec{F} = -\varepsilon \vec{M} \quad (2.34)$$

$$\vec{H} = -j\omega\vec{F} - \vec{\nabla}\Phi_m = -j\omega\vec{F} - \frac{j}{\omega\mu\varepsilon} \vec{\nabla}(\vec{\nabla} \cdot \vec{F}) \quad (2.35)$$

$$\vec{F}(\vec{r}) = \varepsilon \iiint_V G(\vec{r}, \vec{r}') \vec{M}(\vec{r}') dV' \quad (2.36)$$

The formulas (2.32)-(2.36) lead to a final equation relating the magnetic field  $\vec{H}$  to the magnetic currents  $\vec{M}$  as,

$$\vec{H}(\vec{r}) = -j\omega\varepsilon \iiint_V \frac{e^{-jk|\vec{r}-\vec{r}'|}}{4\pi|\vec{r}-\vec{r}'|} \vec{M}(\vec{r}') dV' - \frac{j\omega\varepsilon}{k^2} \vec{\nabla} \left( \vec{\nabla} \cdot \iiint_V \frac{e^{-jk|\vec{r}-\vec{r}'|}}{4\pi|\vec{r}-\vec{r}'|} \vec{M}(\vec{r}') dV' \right) \quad (2.37)$$

Also by using (2.32)

$$\vec{E}(\vec{r}) = \vec{\nabla} \times \iiint_V \frac{e^{-jk|\vec{r}-\vec{r}'|}}{4\pi|\vec{r}-\vec{r}'|} \vec{M}(\vec{r}') dV' \quad (2.38)$$

### 2.5 Equivalence Theorems

For the solution of electromagnetic radiation and scattering problems it is often more convenient to formulate the problem in terms of an equivalent one. In obtaining the equivalent problem, actual sources are replaced by equivalent fictitious sources which radiate the correct field in the region of interest. The

advantage of using equivalence theorems is that they eliminate the presence of obstacles in the original problem and sources radiate in a homogenous medium. Nevertheless in most cases obtaining solutions for the equivalent problem is as difficult as the original problem. On the other hand equivalent problems are useful for obtaining formulations for electric field integral equation (EFIE) and magnetic field integral equation (MFIE) and are also useful in visualizing the nature of scattered field [23]. Equivalence theorems may either introduce equivalent volume currents which are obtained by using volume equivalence principle or they introduce equivalent surface currents which are obtained by using surface equivalence principle. Volume equivalence principle is mostly used for the solution of scattering problems from inhomogeneous dielectric objects and surface equivalence principle is generally used for scattering problems from PEC objects and homogenous dielectrics.

### 2.5.1 Volume Equivalence Principle

In using volume equivalence theorem the obstacle in the problem is replaced by equivalent electric and magnetic currents,  $\vec{J}_v$  and  $\vec{M}_v$ , which radiate the scattered fields  $\vec{E}^s$  and  $\vec{H}^s$ .

In order to obtain the formulation for volume equivalence principle, it is first assumed that real sources  $\vec{J}_i$  and  $\vec{M}_i$  radiate in unbounded free space with no obstacle present and radiate fields,  $\vec{E}^{inc}$  and  $\vec{H}^{inc}$ . Since they satisfy Maxwell's equations, we can write

$$\vec{\nabla} \times \vec{E}^{inc} = -j\omega\mu_0\vec{H}^{inc} - \vec{M}_i \quad (2.39)$$

$$\vec{\nabla} \times \vec{H}^{inc} = j\omega\epsilon_0\vec{E}^{inc} + \vec{J}_i \quad (2.40)$$

When same sources radiate in the medium represented by  $(\epsilon_1, \mu_1)$  they generate fields  $\vec{E}$  and  $\vec{H}$  which satisfy,

$$\vec{\nabla} \times \vec{E} = -j\omega\mu_1\vec{H} - \vec{M}_i \quad (2.41)$$

$$\vec{\nabla} \times \vec{H} = j\omega\epsilon_1 \vec{E} + \vec{J}_i \quad (2.42)$$

Subtraction of (2.39) from (2.41) and (2.40) from (2.42) yields

$$\vec{\nabla} \times (\vec{E} - \vec{E}^0) = -j\omega(\mu_1 \vec{H} - \mu_0 \vec{H}^0) \quad (2.43)$$

$$\vec{\nabla} \times (\vec{H} - \vec{H}^0) = j\omega(\epsilon_1 \vec{E} - \epsilon_0 \vec{E}^0) \quad (2.44)$$

Next define the difference  $(\vec{E} - \vec{E}^{inc})$  and  $(\vec{H} - \vec{H}^{inc})$  as the scattered fields  $\vec{E}^s$  and  $\vec{H}^s$  such that (2.42) and (2.43) can be rewritten as,

$$\vec{\nabla} \times \vec{E}^s = -j\omega(\mu_1 - \mu_0)\vec{H} - j\omega\mu_0\vec{H}^s \quad (2.45)$$

$$\vec{\nabla} \times \vec{H}^s = j\omega(\epsilon_1 - \epsilon_0)\vec{E} + j\omega\epsilon_0\vec{E}^s \quad (2.46)$$

We define volume equivalent electric and magnetic sources  $\vec{J}_v$  and  $\vec{M}_v$  as,

$$\vec{J}_v = j\omega(\epsilon_1 - \epsilon_0)\vec{E} \quad (2.47)$$

$$\vec{M}_v = j\omega(\mu_1 - \mu_0)\vec{H} \quad (2.48)$$

which only exist within the obstacle. Using (2.47) and (2.48), (2.45) and (2.46) can be written as,

$$\vec{\nabla} \times \vec{E}^s = -\vec{M}_v - j\omega\mu_0\vec{H}^s \quad (2.49)$$

$$\vec{\nabla} \times \vec{H}^s = \vec{J}_v + j\omega\epsilon_0\vec{E}^s \quad (2.50)$$

Using (2.49) and (2.50) the fields  $\vec{E}^s$  and  $\vec{H}^s$ , radiated by equivalent sources  $\vec{J}_v$  and  $\vec{M}_v$  which exist only within the obstacle, can be found outside the material if the equivalent sources radiate in free space. It should be noted that the solution of the equivalent problem is not easier than the original problem since the equivalent sources are written in terms of unknown total fields  $\vec{E}$  and  $\vec{H}$ .

However equivalent problem provides a physical interpretation for scattering phenomena and is useful for obtaining potential integral formulation [21].

### 2.5.2 Surface Equivalence Principle

Surface equivalence is a principle in which actual sources are replaced with equivalent sources which radiate the same field in the region of interest. Surface equivalence principle help in obtaining potential integral formulations for scattering and diffraction problems and also are more suggestive of approximations. Being first introduced in [24], surface equivalence principle is a more rigorous formulation of Huygen's principle [25], which state that "each point on a primary wavefront can be considered to be a new source of a secondary spherical wave and that the secondary wavefront can be constructed as the envelope of these secondary spherical waves" [26].

For the development of the surface equivalence principle consider Figure 2.1a where actual sources  $\vec{J}_1$  and  $\vec{M}_1$  radiate fields  $\vec{E}_1$  and  $\vec{H}_1$  in free space with permittivity and permeability  $(\epsilon_0, \mu_0)$  respectively.

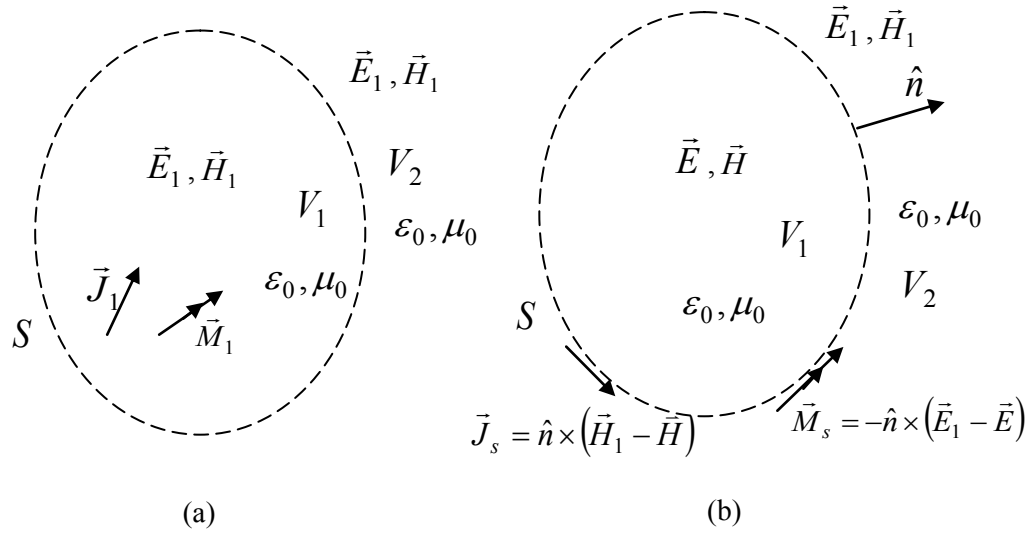


Fig 2.1 Field geometry for actual problem and equivalent problem

(a) Actual problem (b) Equivalent problem

The sources in actual problem are enclosed within an imaginary surface  $S$ . We want to develop an equivalent problem in which arbitrary fields  $\vec{E}$ ,  $\vec{H}$  are present within  $V_1$  but suitable tangential currents are introduced on  $S$  which give rise to actual fields  $\vec{E}_1$ ,  $\vec{H}_1$  within the region of interest  $V_2$ . In order to satisfy boundary conditions the surface currents are given by,

$$\hat{n} \times (\vec{E}_1(\vec{r}) - \vec{E}(\vec{r})) = -\vec{M}_s(\vec{r}) \quad (2.51)$$

$$\hat{n} \times (\vec{H}_1(\vec{r}) - \vec{H}(\vec{r})) = \vec{J}_s(\vec{r}) \quad (2.52)$$

where  $\hat{n}$  is the unit normal on  $S$  pointing from  $V_1$  to  $V_2$ . The sources in (2.51) and (2.52) radiate in unbounded free space and (2.30-31) and (2.37-38) can be used to determine fields outside the closed surface. As the equivalent problem defines tangential fields on the surface of  $S$ , from uniqueness theorem we know that they are the correct fields. When the arbitrary fields within  $S$  are assumed to be zero we get Love's equivalence principle [27] which introduces currents,

$$\hat{n} \times \vec{E}_1(\vec{r}) = -\vec{M}_s(\vec{r}) \quad (2.53)$$

$$\hat{n} \times \vec{H}_1(\vec{r}) = \vec{J}_s(\vec{r}) \quad (2.54)$$

on  $S$ .

Let us next consider scattering problem from a PEC object which is of much practical concern. Although there are alternate methods for the solution of this problem we will consider only physical equivalent which is used for scattering problems rather than radiation problems and is utilized to obtain formulations for EFIE and MFIE.

We first assume that real sources  $\vec{J}_1$  and  $\vec{M}_1$  radiate fields  $\vec{E}_1$  and  $\vec{H}_1$ , which are also assumed to be known in the absence of the scattering object. In the presence of the PEC scattering object the total fields outside the object are  $\vec{E}$ ,  $\vec{H}$  which are expressed as,



$$\vec{E}(\vec{r}) = \vec{E}_1(\vec{r}) + \vec{E}^s(\vec{r}) \quad (2.55)$$

$$\vec{H}(\vec{r}) = \vec{H}_1(\vec{r}) + \vec{H}^s(\vec{r}) \quad (2.56)$$

where  $\vec{E}^s$ ,  $\vec{H}^s$  denote scattered fields from the object as shown in Figure 2.2a.

Since the total tangential electric field on  $S$  is zero, the magnetic current is equal to zero and we can write,

$$-\hat{n} \times \vec{E}_1(\vec{r}) = \hat{n} \times \vec{E}^s(\vec{r}) \quad (2.57)$$

Also the induced electric current is equal to the total tangential magnetic field so that we can write,

$$\vec{J}_p = \hat{n} \times \vec{H}(\vec{r}) = \hat{n} \times \vec{H}_1(\vec{r}) + \hat{n} \times \vec{H}^s(\vec{r}) \quad (2.58)$$

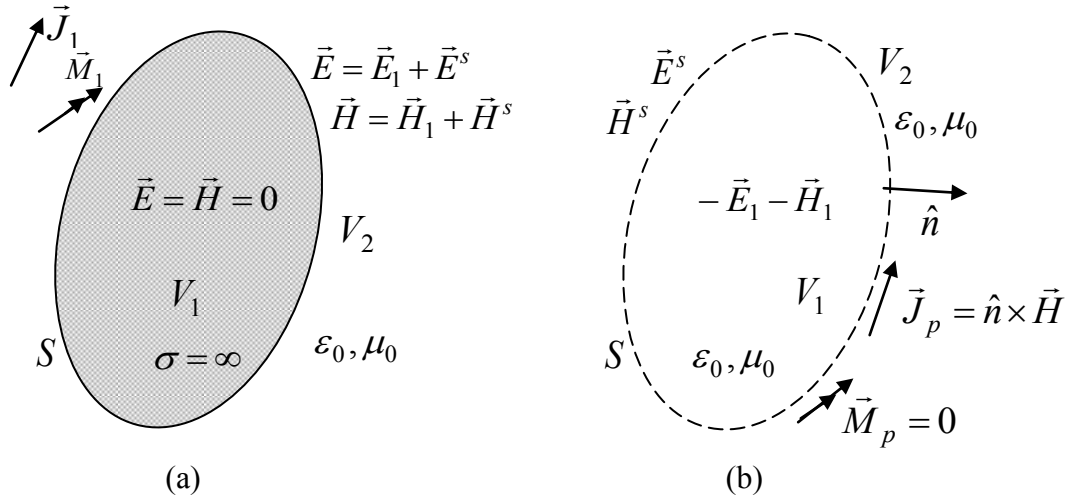


Figure 2.2 Physical equivalent for scattering from a PEC object (a) Actual problem (b) Equivalent problem.

Therefore the equivalent problem for the solution of Fig. 2.2a is that given in Fig. 2.2b. It should be remembered that the equivalent sources in (2.57) and (2.58)

radiate in unbounded free space with no object present. Since  $\vec{M}_p$  is zero and  $\vec{J}_p$  radiate in free space (2.30) and (2.31) can be used to evaluate fields outside the object. It should also be noted that the total tangential field  $\vec{H}$  is unknown so that the equivalent problem does not help in simplifying the solution. Instead the equivalent problem will be utilized to obtain potential integral formulation for the problem which is the topic of next section.

## 2.6 Surface Integral Equations

Scattering problem can be considered as radiation problems where the locally radiating currents are generated by other currents or fields. Similarly antenna analysis can be considered as a scattering problem in which the currents on the antenna are generated by an external source and RCS calculations involve incident electromagnetic field which induces currents on the scatterer that re-radiate the scattered field [11].

In radiation problems the unknown fields are found by integration of known currents  $\vec{J}$  and  $\vec{M}$ . But in scattering problems these sources are unknown and first an integral equation for the unknown currents should be obtained. After finding these sources, they can be used to evaluate the scattered fields  $\vec{E}^s$  and  $\vec{H}^s$ .

In this section we consider derivation of EFIE and MFIE for PEC objects using the physical equivalent problem which is introduced in 2.5.2.

### 2.6.1 Electric Field Integral Equation

From the physical equivalent problem in Fig 2.2b we see that there are no magnetic currents induced on the surface of the object and only electric current exists which radiate in the absence of the scattering object. The radiated field due to a known electric current source can be evaluated by using (2.30) which is rewritten here as,

$$\vec{E}(\vec{r}) = -j\omega\mu \iint_S \frac{e^{-jk|\vec{r}-\vec{r}'|}}{4\pi|\vec{r}-\vec{r}'|} \vec{J}(\vec{r}') dS' - \frac{j\omega\mu}{k^2} \vec{\nabla} \left( \vec{\nabla} \cdot \iint_S \frac{e^{-jk|\vec{r}-\vec{r}'|}}{4\pi|\vec{r}-\vec{r}'|} \vec{J}(\vec{r}') dS' \right) \quad (2.59)$$

In order to establish the integral equation we use vanishing tangential electric field on the surface of the object. That is on the surface we have,

$$-\hat{n} \times \vec{E}^i(\vec{r}) = \hat{n} \times \vec{E}^s(\vec{r}) \quad (2.60)$$

Using (2.59) and (2.60) we obtain the EFIE, which is written as,

$$\hat{n} \times \vec{E}^i(\vec{r}) = \hat{n} \times \left[ j\omega\mu \iint_S \frac{e^{-jk|\vec{r}-\vec{r}'|}}{4\pi|\vec{r}-\vec{r}'|} \vec{J}(\vec{r}') dS' + \frac{j\omega\mu}{k^2} \vec{\nabla} \left( \vec{\nabla} \cdot \iint_S \frac{e^{-jk|\vec{r}-\vec{r}'|}}{4\pi|\vec{r}-\vec{r}'|} \vec{J}(\vec{r}') dS' \right) \right] \quad (2.61)$$

on the surface of the scattering object  $S$ .

It should be noted that the del operators on the second integral on RHS of (2.61) operate on observation coordinates. When these operators are taken under the integral sign the second derivative of the free space Green's function introduce terms with  $1/R$ ,  $1/R^2$  and  $1/R^3$  singularities which are difficult to integrate. For this reason using integration by parts, electric field integral equation (EFIE) is generally written in an alternate form as,

$$\hat{n} \times \vec{E}^i(\vec{r}) = \hat{n} \times \left[ j\omega\mu \iint_S \frac{e^{-jk|\vec{r}-\vec{r}'|}}{4\pi|\vec{r}-\vec{r}'|} \vec{J}(\vec{r}') dS' + \frac{j\omega\mu}{k^2} \left( \iint_S \frac{e^{-jk|\vec{r}-\vec{r}'|}}{4\pi|\vec{r}-\vec{r}'|} \vec{\nabla}' \vec{\nabla}' \cdot \vec{J}(\vec{r}') dS' \right) \right] \quad (2.62)$$

where the del operators now act on source coordinates on current function. Depending on the type of the problem it may be advantageous to use one form over the other.

### 2.6.2 Magnetic Field Integral Equation

The physical equivalent problem in Fig. 2.2b can also be utilized to obtain magnetic field integral equation (MFIE). This time the induced current on the scattering object is related to the magnetic field intensity  $\vec{H}$ . From Fig. 2.2b the induced current on the surface is given by,

$$\hat{n} \times \{ \vec{H}^i(\vec{r}) + \vec{H}^s(\vec{r}) \} = \vec{J}(\vec{r}) \quad (2.63)$$

Also the scattered magnetic field is related to the current with,

$$\vec{H}^s(\vec{r}) = \vec{\nabla} \times \iint_S \frac{e^{-jk|\vec{r}-\vec{r}'|}}{|\vec{r}-\vec{r}'|} \vec{J}(\vec{r}') dS' \quad (2.64)$$

Since observation point is within the source region we take the limit as  $\vec{r}$  approaches the surface from the outside ( $\vec{r} \rightarrow S^+$ ). Using (2.64) in (2.63) we write,

$$\hat{n} \times \vec{H}^i(\vec{r}) + \lim_{\vec{r} \rightarrow S^+} \left[ \hat{n} \times \vec{\nabla} \times \iint_S \frac{e^{-jk|\vec{r}-\vec{r}'|}}{|\vec{r}-\vec{r}'|} \vec{J}(\vec{r}') dS' \right] = \vec{J}(\vec{r}) \quad (2.65)$$

Moving the curl operator inside the integral sign we get,

$$\hat{n} \times \vec{H}^i(\vec{r}) + \lim_{\vec{r} \rightarrow S^+} \left[ \hat{n} \times \iint_S \vec{J}(\vec{r}') \times \vec{\nabla} \frac{e^{-jk|\vec{r}-\vec{r}'|}}{|\vec{r}-\vec{r}'|} dS' \right] = \vec{J}(\vec{r}) \quad (2.66)$$

Equation (2.66) relates the incident field to the induced current on the scattering object which should be solved numerically. However the gradient of free space Green's function introduces terms with  $1/R$  and  $1/R^2$  singularities which require special care for evaluation.

In the next chapter we introduce two methods, the conventional method of moments (MoM) procedure and the locally corrected Nyström method for the solution of EFIE and MFIE. We will emphasize how the two methods overcome the difficulties introduced by singular integrals and comment on the advantages and disadvantages of both methods.

## CHAPTER 3

### NYSTRÖM METHOD FOR THE SOLUTION OF INTEGRAL EQUATIONS

Solution of EFIE and MFIE on arbitrary surfaces by analytical methods is difficult and in most cases impossible. Therefore these equations are discretized and solved numerically to yield an approximation to exact solution. The most popular method for discretization of integral equations is method of moments (MoM) procedure, whose popularity is due to the work of Harrington [28]. Nyström method which is introduced in [1-3] is told to be an alternative MoM procedure although it is in fact a form of MoM with special basis and testing functions. In this chapter we introduce MoM and Nyström procedures and mention the advantages and disadvantages of two procedures over each other.

#### 3.1 The Method of Moments

The MoM is a discretization procedure for integro-differential equations in the form,

$$\mathcal{L}f = g \quad (3.1)$$

where  $\mathcal{L}$  is the integro-differential operator,  $f$  is the unknown function and  $g$  is a known function.

The first step in MoM is the discretization of problem domain. The geometry is discretized into smaller simple geometrical pieces, usually triangles or quadrilaterals for surfaces and tetrahedra or hexahedra for volumes. If higher order accuracy is desired, the number of elements can be increased. However increasing the number of elements increases computation time since the number of unknowns is also increased. An alternative to obtain high accuracy without increasing the

number of meshes is to use curvilinear meshes to accurately represent the surface or volume under consideration. Discretization of problem domain is commonly called as meshing.

The second step is to expand the unknown function as a linear combination of expansion functions whose coefficients are unknown. So that we write,

$$f \cong f^N = \sum_{n=1}^N a_n \phi_n \quad (3.2)$$

where  $\phi_n$  are the basis functions and  $a_n$  are the unknown coefficients to be determined. It can be seen from (3.2) that the unknown function  $f$  is projected onto the space of basis functions. Therefore it is important to select proper basis functions and select  $N$  adequately large to have good approximation for  $f$  and have a small residue. The residue is defined as,

$$r^N = g - \sum_{n=1}^N a_n \mathcal{L} \phi_n \quad (3.3)$$

In writing (3.3) the linearity of operator  $\mathcal{L}$  is used. In order to find the coefficients of the basis functions, we force the residue to be orthogonal to a set of testing functions. That is,

$$\langle t_m, r^N \rangle = 0 \quad \text{for } m = 1, 2, 3, \dots, N \quad (3.4)$$

where the inner product  $\langle \cdot, \cdot \rangle$  is defined as,

$$\langle t_m, b_n \rangle = \int_S t_m b_n dS \quad (3.5)$$

Using (3.4) in (3.3) result in  $N$  equations which can be written as,

$$\langle t_m, g \rangle = \sum_{n=1}^N a_n \langle t_m, \mathcal{L} \phi_n \rangle \quad \text{for } m = 1, 2, 3, \dots, N \quad (3.6)$$

Equation (3.6) is a matrix equation in the form,

$$\bar{V} = \bar{\bar{Z}}\bar{I} \quad (3.7)$$

where  $\bar{V}$  is the excitation vector whose elements are given by  $V_m = \langle t_m, g \rangle$ ,  $\bar{\bar{Z}}$  is the impedance matrix with elements  $Z_{mn} = \langle t_m, \mathcal{L}\phi_n \rangle$  and  $\bar{I}$  represents the coefficients of basis functions and its elements are  $I_n = a_n$ .

Selection of testing functions is also important to obtain satisfactory accuracy since the coefficients in (3.7) only guarantee orthogonality to the space spanned by testing functions. If testing functions are not selected properly, the residue may have large values outside the domain spanned by testing functions. However if testing functions are selected to be within the range of  $\mathcal{L}$ , this unwanted situation is avoided [29].

The last step in MoM procedure is to solve (3.7) for unknown coefficients by using

$$\bar{I} = \bar{\bar{Z}}^{-1}\bar{V} \quad (3.8)$$

The inverse of impedance matrix can be found by LU decomposition or by Gaussian elimination which require a computation time of order  $O(N^3)$  where  $N$  is the number of unknowns. When the number of unknowns is large one may consult to iterative algorithms which require a computation time of order  $O(MN^2)$  where  $N$  is the number of unknowns and  $M$  is the number of iterations [30].

### 3.1.1 Selection of Basis Functions

Accurate representation of the current density as well as charge density within the problem domain is possible only if the appropriate basis functions are selected to expand the unknown current function. These basis functions can be either entire domain or subdomain functions depending on the domain of definition, curved or planar functions depending on the shape of the surface on which current flows and low order or high order polynomials depending on the degree of accuracy desired [31].

Although the comparison of basis function are studied extensively in the literature [32-35], the most successful and the most popular basis function used in the past 30 years is the Rao-Wilton-Glisson (RWG) basis functions defined on triangular patches [11]. These vector basis functions span over adjacent triangles and are defined as,

$$\vec{\phi}_n(\vec{r}) = \frac{L_n}{2A_n^+} \vec{\rho}_n^+(\vec{r}) \quad \text{for} \quad \vec{r} \text{ in } T_n^+ \quad (3.9)$$

$$\vec{\phi}_n(\vec{r}) = \frac{L_n}{2A_n^-} \vec{\rho}_n^-(\vec{r}) \quad \text{for} \quad \vec{r} \text{ in } T_n^- \quad (3.10)$$

where  $T_n^+$  and  $T_n^-$  are the triangles that share a common edge  $n$ ,  $L_n$  is the length of the common edge,  $\vec{r}$  is the position vector and  $A_n^+$  and  $A_n^-$  are the areas of the corresponding triangles. On  $T_n^+$ ,  $\vec{\rho}_n^+(\vec{r})$  points toward the vertex opposite to the edge and is given by,

$$\vec{\rho}_n^+(\vec{r}) = \vec{v}^+ - \vec{r} \quad \text{for} \quad \vec{r} \text{ in } T_n^+ \quad (3.11)$$

and . On  $T_n^-$ ,  $\vec{\rho}_n^-(\vec{r})$  points away from the vertex opposite to the edge and is,

$$\vec{\rho}_n^-(\vec{r}) = \vec{r} - \vec{v}^- \quad \text{for} \quad \vec{r} \text{ in } T_n^- \quad (3.12)$$

where  $v^+$  and  $v^-$  are the positions of the vertex points opposite to the common edge.

RWG basis functions are plotted in Figure 3.1. Since basis functions are defined only for adjacent triangles no basis functions assigned to boundary edges. These basis functions have no component normal to the edges other than they have assigned to. Evaluation of surface divergence of  $\phi_n(\vec{r})$  yields,

$$\vec{\nabla} \cdot \vec{\phi}_n(\vec{r}) = -\frac{L_n}{A_n^+} \quad \text{for} \quad \vec{r} \text{ in } T_n^+ \quad (3.13)$$



$$\vec{\nabla} \cdot \vec{\phi}_n(\vec{r}) = \frac{L_n}{A_n^-} \quad \text{for} \quad \vec{r} \text{ in } T_n^- \quad (3.14)$$

$$\vec{\nabla} \cdot \vec{\phi}_n(\vec{r}) = 0 \quad , \text{ otherwise} \quad (3.15)$$

Since divergence of current is proportional to the accumulated charge density, no charge is accumulated along the edge between two triangles. Since there is no charge accumulation, RWG basis functions are told to be divergence conforming.

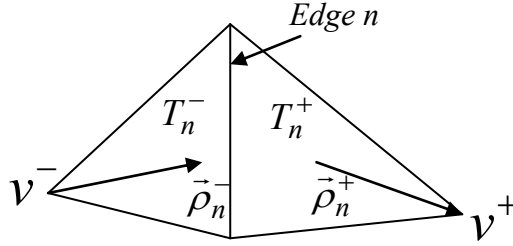


Figure 3.1 RWG Basis Function

Other basis function used in electromagnetic problems such as curl conforming as well as higher order basis functions can be found in [36].

### 3.1.2 MoM Solution to EFIE with RWG Basis Functions

In this section we write explicitly the elements of the impedance matrix  $\bar{\bar{Z}}$  and excitation vector  $\bar{V}$  for EFIE on the surface of a conducting object when RWG basis and testing function are used for the solution. We rewrite EFIE again as,

$$\hat{n}(\vec{r}) \times \vec{E}^i(\vec{r}) = j\omega\mu\hat{n}(\vec{r}) \times \iint_S \left( 1 + \frac{1}{k^2} \vec{\nabla} \vec{\nabla} \cdot \right) \sum_{n=1}^N a_n \vec{\phi}_n(\vec{r}') \frac{e^{-jkR}}{R} dS' \quad (3.16)$$

which is one equation in  $N$  unknowns. Applying  $N$  testing functions to (3.16) and distributing the vector differential operators to basis and testing functions the elements of impedance matrix  $\bar{\bar{Z}}$  can be obtained as,

$$Z_{mn} = \iint_{S_m} \iint_{S_n} \left\{ \vec{\phi}_m(\vec{r}) \cdot \vec{\phi}_n(\vec{r}') - \frac{1}{k^2} (\vec{\nabla} \cdot \vec{\phi}_m(\vec{r})) (\vec{\nabla}' \cdot \vec{\phi}_n(\vec{r}')) \right\} \frac{e^{-jkR}}{R} dS' dS \quad (3.17)$$

inserting RWG basis and testing functions in (3.17) we arrive at,

$$Z_{mn} = \frac{L_m L_n}{A_m A_n} \iint_{S_m} \iint_{S_n} \left\{ \frac{1}{4} \vec{\rho}_m^\pm(\vec{r}) \cdot \vec{\rho}_n^\pm(\vec{r}') - \frac{1}{k^2} \right\} \frac{e^{-jkR}}{R} dS' dS \quad (3.18)$$

Also the elements of excitation vector are given by,

$$b_m = -\frac{j}{\omega\mu} \iint_{S_m} \frac{L_m}{2A} \vec{\rho}_m^\pm(\vec{r}) \cdot \vec{E}^i(\vec{r}) \frac{e^{-jkR}}{R} dS \quad (3.19)$$

The source and testing integrals are performed over two RWG functions which span two triangles each. Although the evaluation of double surface integrals seems to be computationally inefficient, the major advantage of using RWG basis functions is the reduction in the order of singularity since vector differential operators are transformed to basis and testing functions. Thus the singularity in the integrand in (3.18) is only due to the Green's function itself. This is an  $1/R$  singularity so that we call the integral in (3.18) as a weakly singular integral.

### 3.2 The Locally Corrected Nyström Method

Nyström method is a relatively old procedure which was introduced by Nyström in 1930 [37] for solution of integral equations. In application of Nyström method the integration domain is divided into  $N$  pieces or patches and the integral on each patch is replaced by  $q$  point quadrature rules leading to a total of  $Nq$  unknowns to be determined. The integral equation is enforced at the nodes of the quadrature rule and a system of equations is obtained for the samples of unknown quantity, usually surface current.

The primary difference between Nyström method and MoM is that, in MoM procedure the surface current density is represented as linear combination of basis functions and the coefficients of these basis functions are to be determined by the procedure. In Nyström procedure on the other hand the unknown quantity is the samples of the surface current density at selected quadrature points. Indeed this difference can be considered as a change of basis functions and Nyström method

can be considered as MoM procedure with impulse basis and testing functions[38-39].

Both methods are high-order methods for which the accuracy can be improved by selecting smaller cells to represent the surface which result in increased unknowns to be determined. This is known as h-refinement. Another alternative to improve accuracy is the p-refinement. In MoM procedure p-refinement is achieved by using higher order polynomials to represent the current density. In Nyström procedure on the other hand p-refinement is achieved by increasing the number of quadrature points within the cell.

In Nyström method the system matrix is constructed by using quadrature rules and the entries of this matrix are the samples of kernel with appropriate weights. However in conventional MoM procedure the elements of system matrix are found by evaluating double surface integrals of the basis functions as given in (3.18). As evaluation of the kernel at selected quadrature points is computationally cheaper than evaluation of double surface integrals, Nyström method is advantageous in terms of computational cost when compared with conventional MoM procedure [40].

The drawback of classical Nyström method is that it cannot handle integral equations with singular kernels. Therefore this method in conventional form is not suitable for 3D electromagnetic scattering problems where the kernels are singular due the singularity of Green's function and its derivatives. However this drawback is alleviated in some studies either by a construction of special quadrature rule [41-42] or by using singularity extraction methods [43-44] to avoid the infinite sample.

Nyström method for the solution of electromagnetic problems gained popularity with the introduction of locally-corrected Nyström (LCN) method described in [1-3]. The LCN method alleviates the difficulty with singular kernels by replacing the samples of singular kernel with some corrected kernels which are finite and produce correct fields at quadrature nodes. The corrected kernels are found by convolution of the singular kernel with a set of basis functions and this in

turn increases computation time. However since local corrections are required only when the kernel is singular or nearly singular, it is required only for a small number of source-observation patch interactions. As for the majority of interactions classical quadrature rules are applied, LCN still offers substantially smaller matrix fill cost than conventional MoM procedure.

### 3.2.1 Formulation of LCN Method

The first step in application of Nyström method is to determine the extent of domain where local corrections should be applied and the domain where classical quadrature rules will be used. The domain of local corrections should always include the patch containing the observation point where the kernel is singular. Outside the observation patch the kernel is not singular but exhibits a rapid change in magnitude so that classical quadrature rules still fail in accuracy. The domain of local corrections should be extended until the underlying quadrature rule has desired accuracy. As the order of accuracy is dependent on the order of singularity of the kernel as well as the underlying quadrature rule, this step may require some recursive calculations until the desired accuracy is obtained.

Outside the domain of local corrections the integral is evaluated numerically by using,

$$\iint_{S_n} f(\vec{r}') G(\vec{r}_{mj} - \vec{r}') d\vec{r}' = \sum_{i=1}^q w_{ni} f(\vec{r}'_{ni}) G(\vec{r}_{mj} - \vec{r}'_{ni}) \quad (3.20)$$

for  $j = 1 \dots q$ .

In (3.20)  $w_{ni}$ 's are the weights associated to the quadrature point “ $i$ ” within source patch “ $n$ ”,  $f(\vec{r}'_{ni})$  is the value of the density function at source point “ $\vec{r}'_{ni}$ ” and  $G(\vec{r}_{mj} - \vec{r}'_{ni})$  is the kernel which is a function of distance between source point and observation point “ $\vec{r}_{mj}$ ”. The weights and nodes in (3.20) will be determined by the quadrature rule. An introduction to quadrature rules is given in appendix A.

The error for the numerical representation in (3.20) is same as the underlying quadrature rule [45]. That is for a smooth domain of integration and with regular kernel (3.20) is a high order representation of the exact integral if high order quadrature rules are used.

Unfortunately within the domain of local corrections (3.20) fail in accuracy so that the classical quadrature rules should be modified for accurate evaluation near or self patch contribution. That is instead of using (3.20), we use,

$$\iint_{S_n} f(\vec{r}') G(\vec{r}_{mj} - \vec{r}') d\vec{r}' = \sum_{i=1}^q w_{ni} f(\vec{r}'_{ni}) \tilde{G}(\vec{r}_{mj} - \vec{r}'_{ni}) \quad (3.21)$$

where  $\tilde{G}(\vec{r} - \vec{r}'_n)$  is the new corrected kernel which must be synthesized at the necessary samples. One way to achieve this is to introduce some hypothetical current functions and find a new corrected kernel such that the near fields produced by this currents are exact at quadrature nodes. The hypothetical currents are a set of basis functions  $\{B_k(\vec{r}')\}$  and we form the matrix equation,

$$\sum_{i=1}^q B_k(\vec{r}'_{ni}) \{w_{ni} \tilde{G}(\vec{r}_{mj} - \vec{r}'_{ni})\} = \iint_{S_n} B_k(\vec{r}') G(\vec{r}_{mj} - \vec{r}') d\vec{r}' \quad (3.22)$$

for  $k = 1, 2, 3, \dots, q$ . This system needs to be solved for  $w_{ni} \tilde{G}(\vec{r}_{mj} - \vec{r}'_{ni})$ . The corrected kernel obtained in (3.22) will be used in (3.21) and will accurately evaluate correct fields at sample nodes if the density function can adequately be described by the basis functions. The system of (3.22) is of order  $q$  and should be repeated for each  $\tilde{G}(\vec{r}_{mj} - \vec{r}'_{ni})$  when source and observation points are within the domain of local corrections. Since this procedure is required only for a small number of source-observation patch pairs the required set of computations is relatively inexpensive. The most expensive part in calculations in (3.22) is the singular integrals on the RHS of (3.22) [40], which is one of the topics that we deal with in this thesis.

An alternative formulation to local corrections is proposed by Tong and Chew [38], where density function is again represented as a linear combination of some basis functions,

$$f_n(\vec{r}') = \sum_{k=1}^q f_{nk} B_k(\vec{r}') \quad (3.23)$$

and the field at observation point “ $\vec{r}_{mj}$ ”, due to the current at cell  $n$  is approximated by,

$$\iint_{S_n} f(\vec{r}') G(\vec{r}_{mj} - \vec{r}') d\vec{r}' = \sum_{k=1}^q f_{nk} \iint_{S_n} B_k(\vec{r}') G(\vec{r}_{mj} - \vec{r}') d\vec{r}' \quad (3.24)$$

The alternative formulation has the same accuracy and the same computational cost as is shown in [40]. However the alternative formulation is more straightforward, as it uses an explicit set for density function and it uses correct sources in contrast to the hypothetical sources which are used in the original local corrections procedure.

### 3.2.2 Advantages of LCN Method

Some of the advantages introduced by LCN are faster precomputation, elimination of multipatch basis functions and iterative solver memory reduction as explained below.

Nyström method uses quadrature rules to evaluate impedance matrix elements in contrast to conventional MoM Galerkin procedure which evaluates double surface integrals. As evaluating the kernel at sample points is faster when compared to evaluating double surface integrals, LCN is faster in evaluating the impedance matrix elements. For a system matrix of size  $N$ , MoM Galerkin procedure needs to evaluate  $N^2$  double surface integrals, whereas LCN needs to evaluate less than  $N^2$  kernel evaluation plus  $O(N)$  calculations for local corrections. As local corrections slow down LCN, this advantage is less

pronounced for electrically small objects but more pronounced for electrically large objects.

Conventional MoM require divergence conforming basis and testing functions, such as RWG, to which vector differential operators are transferred. In order to facilitate differentiation these basis functions have certain level of continuity across the edge between adjacent patches. As shown previously in this section, an important property of the RWG basis functions is that, their normal components are continuous across the patch boundaries and no charge is accumulated along the boundary. But it has been shown in [46] that the requirement for such basis functions vanish for high-order codes because the continuity of the source distribution is achieved as a consequence of accurate evaluation of integrals.

When used with iterative solvers the memory demand of LCN can be reduced from  $O(N^2)$  to  $O(N)$ . The maximum memory is required when all elements of system matrix are stored and the minimum demand is for elements belonging local corrections. Storing only elements belonging to local corrections is practical because evaluation of other elements is fast. It is shown that the memory requirement for multilevel fast multipole method (MLFMM) for conventional MoM procedure is  $O(N \log N)$ [47].

Despite the above mentioned advantages of LCN, one important disadvantage of Nyström method is the requirement to accurately evaluate singular integrals of different orders. Since there are no divergence conforming basis and testing functions to which the vector differential of Green's function can be transferred, the kernel of the integrals are the derivatives of Green's function which are difficult to evaluate. Chapter 4 deals with evaluation of singular integrals and obtains explicit formulas for singular integrals. Therefore the difficulty of evaluation of singular integrals is alleviated with ready to use expressions.





## CHAPTER 4

### SINGULAR INTEGRALS AND THEIR EVALUATION

It was shown in the previous section that integral equation methods for the evaluation of EM problems finally lead to matrix equations of type,

$$\bar{V} = \bar{\bar{Z}}\bar{I} \quad (4.1)$$

Where  $\bar{V}$  is a vector related to the excitation fields,  $\bar{I}$  represents unknown source function within or on the scattering body and  $\bar{\bar{Z}}$  is the impedance matrix constructed such that the entry  $Z_{mn}$  evaluates the field on patch  $m$  due to the current on patch  $n$ . Specifically, evaluation of  $Z_{mn}$  requires evaluation of integrals whose kernels are free space Green's function, its first derivative and in some cases, like Nyström method, its second derivative. When source and observation points are sufficiently separated, elements of the impedance matrix can be effectively and accurately evaluated using quadrature rules. However, quadrature rules fail in accuracy whenever source and observation points are close to each other and even may become infinite when they coincide. Free space Green's function exhibits singularity of order  $1/R$  whereas the first derivative involves terms with  $1/R$  and  $1/R^2$  singularities. Finally the second derivative of the Green's function involves terms with  $1/R$ ,  $1/R^2$  and  $1/R^3$  singularities with  $R$  being the distance between observation point and the source point.

An integral is said to be singular if the integrand becomes infinite at some point within the integration domain. Nevertheless, such integrals may still exist since the value of integral does not depend on the value of the integrand at some finite number of isolated points. Rather it depends on the behavior of the integrand in the neighborhood of the singular point. Before evaluation of the integral one requires to know whether the integral exists in an ordinary sense or in a special

sense. For that purpose an infinitesimal zone  $\Omega_\epsilon$  around singular point is excluded from the integration domain  $\Omega$  and then  $\Omega_\epsilon$  is made to shrink to singular point. Generally,  $\Omega_\epsilon$  is the intersection of  $\Omega$  with a ball of radius  $\epsilon$  centered at the singular point as plotted in Figure 4.1. Thus one is interested in the integral,

$$\lim_{\epsilon \rightarrow 0} \int_{\Omega - \Omega_\epsilon} f(x) dx \quad (4.2)$$

If the integral exists independently of the shape of the exclusion zone  $\Omega_\epsilon$ , singularity is integrable in the ordinary sense and it is called a *weak singularity*. However, the integral is still considered to be an improper one.

An example for weakly singular integral is the surface integral of the free space Green's function. As the exclusion zone consider a disk with radius  $\epsilon$  around the singular point as shown in Fig. 4.1. The integrand increases at the rate  $1/\epsilon$  as  $\epsilon \rightarrow 0$ . However, the area of the disk decreases with  $\epsilon^2$  so the contribution from an infinitesimal surface element around singularity diminishes as the area of the surface approaches zero. Thus one has,

$$\lim_{\epsilon \rightarrow 0} \int_{\Omega - \Omega_\epsilon} \frac{e^{-jkR}}{R} dS = \int_{\Omega} \frac{e^{-jkR}}{R} dS \quad (4.3)$$

which is the formal definition for weak singularity.

The first derivative of the Green's function on the other hand, includes a term with  $1/R^2$  singularity and this requires special treatment. For this case the integrand increases at the rate  $1/\epsilon^2$  as  $\epsilon \rightarrow 0$  and the area of the surface element decreases at the same rate  $\epsilon^2$ . Thus contribution from an infinitesimal element is a finite value although it does not diverge. This finite value depends on the shape of the extracted zone. It is said that the integral exists in the *Cauchy principal value* (CPV) sense if the limit in (4.2) is finite assuming  $\Omega_\epsilon$  to be symmetric. The singularity for which CPV integral exists is called a *strong singularity*.

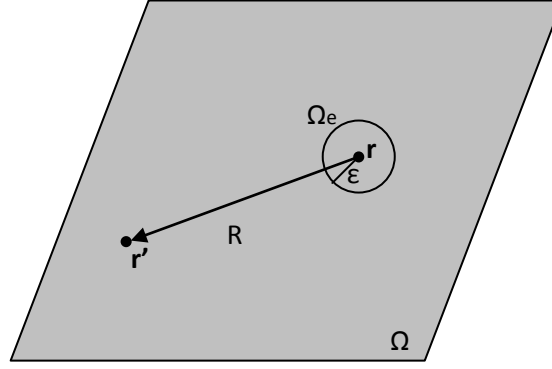


Figure 4.1 Exclusion zone in the domain of integration

Finally, if the singularity of the integrand is stronger than CPV integrals, which occurs when the second derivative of the Green's function is evaluated, then the integral is said to be a *hypersingular integral*. In electromagnetic problems hypersingular surface integrals involving  $1/R^3$  terms are encountered. For this case the increase rate of the integrand is  $1/\varepsilon^3$  and the contribution from an infinitesimal surface element diverges as its area shrinks to zero. Nevertheless, one can still specify the coefficients of the particular divergent terms as well as the finite part of such an integral. Based on the ideas of Hadamard, it can be shown that finite part of such integrals still has a meaning in evaluation of real physical fields [48]. This approach in evaluation of hypersingular integrals is called Hadamard finite part interpretation. In following sections it will be shown that hypersingular integrals arising in EFIE formulation can be interpreted in the Hadamard finite part sense and accurate results can be obtained.

It is also important to mention that the literature dealing with singular integrals is extensive. So is the nomenclature adopted for the definitions of singular integrals. In this study we adopted the definition utilized in boundary element method (BEM) where surface integrals containing  $1/R$  singularity is said to be a weakly singular, the integrals containing  $1/R^2$  terms are said to be strongly singular and the integrals with  $1/R^3$  terms are said to be hypersingular [49-51]. EM community on the other hand uses a different convention where  $1/R$  singularity is termed as strong singularity,  $1/R^2$  singularity is called

hypersingularity and the integrals involving  $1/R^3$  terms are said to be super-hypersingular [5, 52]. The reason why we adopted the convention of BEM is that, the contribution of this study is mainly due to the evaluation of surface integrals with  $1/R^3$  terms. The methods for evaluation of such integrals were well known and applied since 1990's for the solution of crack problems [53], acoustic and elastic wave scattering problems [50] and fluid flow problems by BEM. The attention of EM community for the evaluation of such integrals is only recent and few papers are published in this area [4]. In this study we applied some of the methods borrowed from BEM to find explicit formulas for hypersingular integrals and observed that the resulting formulas are far simpler than those previously published in literature and still have the same accuracy. Also we introduced new explicit formulas for the evaluation of hypersingular integrals on curved surfaces and showed that these new formulas increase accuracy by numerical tests.

In this chapter first the evaluation of weakly singular integrals is introduced, following with some numerical test for accuracy analysis. Secondly, strongly singular integrals are handled and then we introduce the novel interpretation to hypersingular integrals and new explicit formulas for flat triangular patch surfaces. Lastly the modified hypersingular kernel on curved surfaces is introduced and accuracy analysis is conducted.

#### 4.1 Weakly Singular Integrals and Their Evaluation

Consider the integral,

$$I = \iint_{\Omega} \bar{J}(\bar{r}') \frac{e^{-jkR}}{R} d\Omega \quad (4.4)$$

which appears on the RHS of (2.62) for the solution of EFIE. According to the definitions given above the integral is a weakly singular integral as long as the current function  $\bar{J}(\bar{r}')$  has a smooth behavior and is bounded in integration domain. Here we will assume that  $\bar{J}(\bar{r}')$  is constant, however, the derivation for

any other smooth function is straightforward. Using Taylor series expansion of exponential term,

$$e^{-jkR} = 1 + \frac{(-jkR)}{1!} + \frac{(-jkR)^2}{2!} + \frac{(-jkR)^3}{3!} + \dots \quad (4.5)$$

it is obvious that evaluation of the singular integral,

$$I = \iint_{\Omega} \frac{1}{R} d\Omega \quad (4.6)$$

to a high accuracy is enough for accurate evaluation of (4.4) since the remaining terms of the Taylor series expansion are not singular and can be handled by quadrature rules.

Evaluation of weakly singular integrals can either be done by using quadrature rules or by using analytical approaches. The advantage of using quadrature rules is that they do not require any regularization of the integrand and can directly handle (4.4). In addition to this no extra coordinate transformation is required and quadrature rules can easily be applied in the global coordinate system. Accuracy of the method depends on the number of quadrature points selected, and their positions as well as the weighting factor applied to each quadrature point [1]. Nevertheless, quadrature rules fail in accuracy whenever the number of integration points is not large enough. To save computation time and meanwhile preserve accuracy one needs to consult to analytical methods. Most commonly used procedure for the analytical solution of weakly singular integrals is Duffy transform [54]. The method basically converts the integral to a polar coordinate system and the Jacobian of the transformation removes the singularity.

Let us evaluate the singular integral in (4.4) on a flat triangular patch as plotted in Figure 4.2

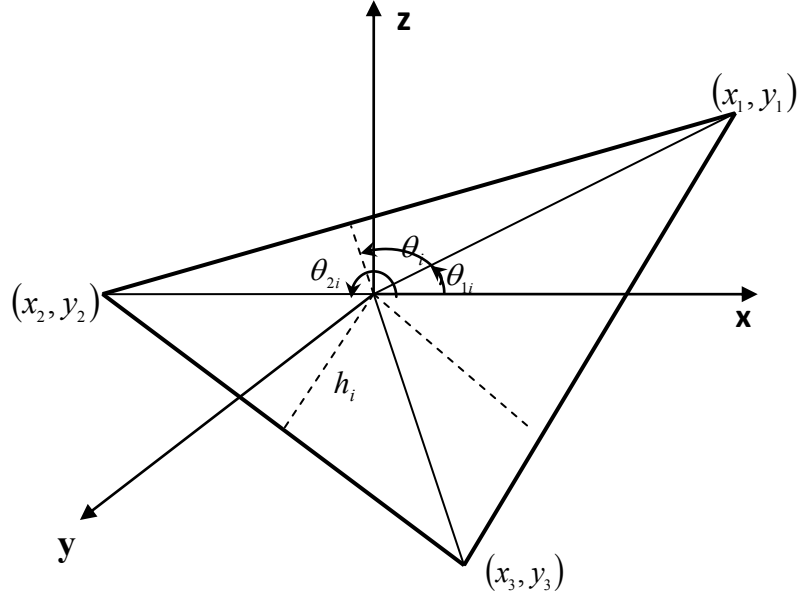


Figure 4.2 Triangular patch on which the singular integral is defined

The triangular patch is assumed to lie on the  $xy$ -plane and the observation point is located at the origin of the coordinate system. The patch is divided into three subtriangles each having their common vertex at the observation point. The height of each triangle is defined by  $h_i$ . One of the edges of each subtriangle is at an angle  $\theta_{1i}$  from the  $x$ -axis and the second edge is at an angle  $\theta_{2i}$ . Also  $\theta_i$  is defined as the angle between  $x$ -axis and drawn height line of each subtriangle. The vertices of the triangular patch are located at points  $(x_i, y_i)$  with  $i=1,2,3$ . In polar coordinate system the integral in (4.6) can be written in the form,

$$I = \sum_{i=1}^3 I_i \quad \text{with} \quad I_i = \int_{\theta_{1i}}^{\theta_{2i}} \int_0^{R_i(\theta)} \frac{1}{R} R dR d\theta \quad (4.7)$$

In inner integral in (4.7), radial integration is evaluated from  $R = 0$  to  $R = R_i(\theta)$  where  $R_i(\theta)$  is given by,

$$R_i(\theta) = \frac{h_i}{\cos(\theta - \theta_i)} \quad (4.8)$$

The weak singularity is removed by the Jacobian of transformation and one is left with an integral in angular coordinates. Using (4.8), (4.7) can be rewritten as,

$$I_i = \int_{\theta_{1i}}^{\theta_{2i}} \frac{h_i}{\cos(\theta - \theta_i)} d\theta \quad (4.9)$$

Using the integral table [75], one obtains the final result as,

$$I_i = h_i \left\{ \ln |\sec(\theta_{2i} - \theta_i) + \tan(\theta_{2i} - \theta_i)| - \ln |\sec(\theta_{1i} - \theta_i) + \tan(\theta_{1i} - \theta_i)| \right\} \quad (4.10)$$

A final point to be mentioned in evaluation of weakly singular integrals is that the derived formulas are not only valid for triangular patches but also for any other surface that can be divided into subtriangles with a common vertex point which coincides with the observation point. For a square patch for example one can divide the square patch into four subtriangles and write,

$$I = \sum_{i=1}^4 I_i \quad (4.11)$$

where the definition of  $I_i$  is the same as given above.

*Numerical tests:*

The validity of the formulas above is demonstrated by two numerical examples.

In the first case we consider a square patch whose corners lie at points  $(1,1)$ ,  $(-1,1)$ ,  $(1,-1)$  and  $(-1,-1)$ . The singular point is centered at the origin  $(0,0)$  as shown in Figure 4.3. We evaluate the surface integral,

$$I = \int_{-1}^1 \int_{-1}^1 \frac{1}{\sqrt{x^2 + y^2}} dx dy \quad (4.12)$$

and compare the results obtained by analytical method using (4.10) with the results obtained by using quadrature rules.

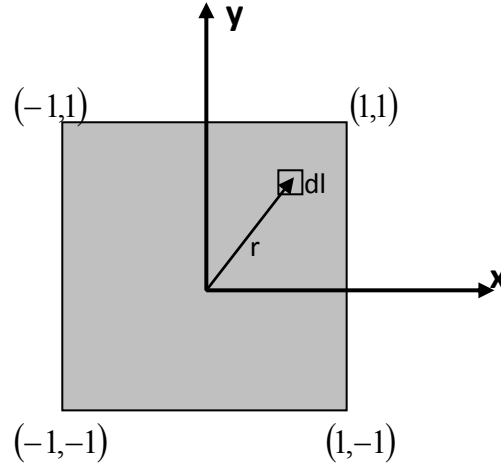


Figure 4.3 The square patch over which weakly singular integral is defined

Quadrature rule approximate the integral in (4.12) by,

$$I = \int_{-1}^1 \int_{-1}^1 \frac{1}{\sqrt{x^2 + y^2}} dx dy = \sum_{i=1}^N \sum_{j=1}^N f(i, j) w_{ij} \quad (4.13)$$

in which  $f(i, j)$  is the value of the integrand at the  $ij^{th}$  point and  $w_{ij}$  is the weight function associated with that point. In this problem square patch is divided into  $N^2$  elements each having equal area with side length  $dl = 2/N$  and have their center points at  $(x_i, y_j)$ . Thus we have

$$f(i, j) = \frac{1}{\sqrt{x_i^2 + y_j^2}} \quad \text{and} \quad w_{ij} = dS = \frac{4}{N^2} \quad (4.14)$$

Table 4.1 shows analytical results as well as the results calculated using quadrature rules with different  $N$ . The percentage accuracy is also included for reference.

As expected accuracy of quadrature rules increase as the number of points is increased. However accuracy analysis shows that to obtain a tenfold improvement in accuracy, number of quadrature points must be increased by a factor of 100. This behavior of quadrature rules requires excess computation time and their use is not favorable when high accuracy is a concern.



Table 4.1 Results obtained for weakly singular integral on a square patch

Analytical Result	Quadrature Rule	$N$	Accuracy (%)
7.0509886	6.3496212	$10^1$	$1.0 \times 10^1$
7.0509886	6.9738148	$10^2$	$1.1 \times 10^0$
7.0509886	7.0431969	$10^3$	$1.1 \times 10^{-1}$
7.0509886	7.0502087	$10^4$	$1.1 \times 10^{-2}$
7.0509886	7.0509107	$10^5$	$1.2 \times 10^{-3}$

As a second problem we consider the same integral as in (4.12) but this time observation point does not lie within the patch. Rather, the observation point is selected outside the source patch but close to it. Since the integrand still has a near singular behavior, quadrature rules are not very accurate at those regions and the integral is nearly weakly singular. In this problem the observation point is again at the origin whereas the square patch has its corners at  $(-3, -1)$ ,  $(-3, 1)$ ,  $(-1, -1)$  and  $(-1, 1)$ . Table 4.2 presents the results obtained by analytical formula (4.10) as well as quadrature rules.

Table 4.2 Results obtained for nearly weakly singular integral on a square patch

Analytical Result	Quadrature Rule	$N$	Accuracy (%)
2.07609947180	2.05858319517	$10^1$	$0.9 \times 10^0$
2.07609947180	2.07589164576	$10^2$	$1.0 \times 10^{-2}$
2.07609947180	2.07609735600	$10^3$	$1.0 \times 10^{-4}$
2.07609947180	2.07609945061	$10^4$	$1.0 \times 10^{-6}$
2.07609947180	2.07609947158	$10^5$	$1.1 \times 10^{-8}$

Table 4.2 shows that unlike the singular case, nearly singular integrals obtain greater accuracy with fewer number of quadrature points. Accuracy with  $10^8$  quadrature points in singular case can be achieved with only  $10^4$  points in nearly singular case. Also it should be noted that for a tenfold increase in accuracy, it suffices to increase the number of quadrature points by a factor of 10. This was 100 for singular case.

## 4.2 Strongly Singular Integrals and Their Evaluation

Strongly singular integrals are those for which contribution from an infinitesimal element around the singular point does not vanish as its size diminishes around singular point but rather remains finite. Because of this finite contribution, conventional quadrature rules fail to yield correct results even if very high number of quadrature points is employed and singular point is excluded from integration domain. For nearly strongly singular integrals however, quadrature rules may produce accurate results with large number of quadrature points, but this is not an effective solution if computation time and memory are taken into account. So an analytical treatment before numerical calculation is necessary in most cases.

Treatment of strongly singular integrals in numerical evaluation of electromagnetic problems is relatively old [55, 56] and primarily deals with integrands whose singularities are due to  $1/R^3$  terms defined in a specified volume. Later [57] introduced a numerical procedure to evaluate strongly singular integrals with  $1/R^2$  terms defined on surfaces.

Two common approaches exist for analytical treatment of strongly singular integrals which are also valid for evaluation of nearly strongly integrals. First method uses vector identity and evaluates the integral on the contour of the integration domain. The resulting integral is not singular when observation point does not lie on the contour of the integration domain. Second method uses a limiting procedure by first assuming the observation point to lie just above the source patch at  $(0,0,h)$ . After evaluating the nearly singular integral the limit  $h \rightarrow 0$  is evaluated yielding the final result. In this study both methods will be presented.

### 4.2.1 Contour Integration Method

Vector identities can be helpful for evaluation of integrals whose integrands contain gradients of functions. The major advantage is the reduction of the

dimension of the integration domain. That is volume integrals are reduced to surface integrals around the boundary and surface integrals are reduced to line integrals around the surface. Another advantage is the reduction in the complexity of the integrand. Since it removes one of the derivatives the order of singularity is also reduced. A form of the theorem can be stated as [21],

$$\iint_S \nabla A(\vec{r}) dS = \int_{\partial S} \hat{n} A(\vec{r}) dl \quad (4.15)$$

where  $A(\vec{r})$  is a scalar function defined on the surface  $S$ ,  $\partial S$  is the boundary contour of the surface and  $\hat{n}$  is the outward normal to  $\partial S$ . Similar to the case for weakly singular integrals the integration domain is considered to be a flat triangular patch on  $xy$ -plane and singular point is located at the center of the coordinate system as shown in Fig. 4.2. Moreover, for a triangular patch  $\hat{n} = n_x \hat{a}_x + n_y \hat{a}_y$  is constant and (4.15) can be decomposed into two integrals with,

$$\begin{aligned} I_x &= \iint_S \frac{\partial A(\vec{r})}{\partial x} dS = \int_{\partial S} n_x A(\vec{r}) dl \\ I_y &= \iint_S \frac{\partial A(\vec{r})}{\partial y} dS = \int_{\partial S} n_y A(\vec{r}) dl \end{aligned} \quad (4.16)$$

The surface integral is represented as a sum of three integrals each corresponding to an edge of the triangle, thus

$$I_x = \sum_{i=1}^3 I_{xi} \text{ with } I_{xi} = \int_{\Gamma_i} n_{xi} A(\vec{r}) d\Gamma_i \quad (4.17)$$

and

$$I_y = \sum_{i=1}^3 I_{yi} \text{ with } I_{yi} = \int_{\Gamma_i} n_{yi} A(\vec{r}) d\Gamma_i \quad (4.18)$$

As an example consider the strongly singular integral,

$$\iint_S \frac{\partial}{\partial x} \left( \frac{1}{\sqrt{x^2 + y^2}} \right) dS \quad (4.19)$$

which appears in MFIE formulation in surface scattering problems. Using (4.16) one can write the equality,

$$\iint_S \frac{\partial}{\partial x} \left( \frac{1}{\sqrt{x^2 + y^2}} \right) dS = \sum_{i=1}^3 \int_{\Gamma_i} n_{xi} \left( \frac{1}{\sqrt{x^2 + y^2}} \right) d\Gamma_i \quad (4.20)$$

Also from (4.8) and from Fig 4.2 one can write,

$$\left( \frac{1}{\sqrt{x^2 + y^2}} \right) = \frac{\cos(\theta - \theta_i)}{h_i} \quad (4.21)$$

and finally one obtains an explicit formula for (4.19) as

$$\iint_S \frac{\partial}{\partial x} \left( \frac{1}{\sqrt{x^2 + y^2}} \right) dS = \sum_{i=1}^3 n_{xi} \frac{\sin(\theta_{li} - \theta_i) - \sin(\theta_{2i} - \theta_i)}{h_i} n_{xi} \quad (4.22)$$

#### 4.2.2 Limiting Procedure:

The limiting procedure for evaluation of strongly singular integrals is introduced in [5], which in fact is valid for any type of singularity in electromagnetic problems. The geometry of the problem is plotted in Figure 4.4, where a small area around the singular point is extracted from the integration domain and the remaining integral is evaluated first. Secondly the contribution of the extracted surface is evaluated by assuming the observation point to be outside the source patch at  $(0,0,h)$  and the integral is evaluated at this point. Then the limit  $P_1 \rightarrow P_0$  is applied which gives a finite result for the integral. It can be shown that the singular terms of the two separately evaluated integrals cancel yielding a finite result [50].

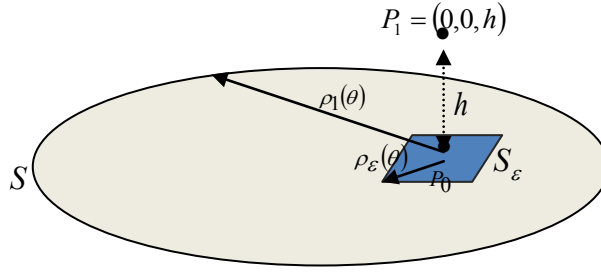


Figure 4.4 The surface  $S$  over which strongly singular integral is defined and the extracted surface  $S_\epsilon$

Specifically for a strongly singular integral defined on the surface  $S$  one writes,

$$I = \iint_S \frac{f(\theta)}{r^2} r dr d\theta = \lim_{\epsilon \rightarrow 0} \iint_{S-S_\epsilon} \frac{f(\theta)}{r^2} r dr d\theta + \lim_{h \rightarrow 0} \left\{ \lim_{\epsilon \rightarrow 0} \iint_{S_\epsilon} \frac{f(\theta)}{(r^2 + h^2)} r dr d\theta \right\} \quad (4.23)$$

To illustrate that the above mentioned procedure is valid, consider the same strongly singular integral considered in the previous subsection,

$$\iint_S \frac{\partial}{\partial x} \left( \frac{1}{\sqrt{x^2 + y^2}} \right) dS = \iint_S \frac{-\cos \theta}{r^2} r dr d\theta \quad (4.24)$$

which is written in polar coordinates in the format given in (4.23). The first integral on the RHS can be evaluated as,

$$I_1 = \lim_{\epsilon \rightarrow 0} \int_0^{2\pi} \int_{\rho_\epsilon(\theta)}^{\rho(\theta)} \frac{-\cos \theta}{r^2} r dr d\theta = - \int_0^{2\pi} \cos \theta [\ln(\rho(\theta)) - \ln(\rho_\epsilon(\theta))] d\theta \quad (4.25)$$

and the second integral is written as,

$$I_2 = \lim_{h \rightarrow 0} \left[ \lim_{\epsilon \rightarrow 0} \int_0^{2\pi} \int_0^{\rho_\epsilon(\theta)} \frac{-\cos \theta}{r^2 + h^2} r dr d\theta \right] = - \lim_{h \rightarrow 0} \left[ 0.5 \int_0^{2\pi} \cos \theta [\ln(\rho_\epsilon^2(\theta) + h^2) - \ln(h^2)] d\theta \right] \quad (4.26)$$

It should be noted that as  $h \rightarrow 0$  the first term in (4.26) is a divergent term and cancels the second term in (4.25). The second divergent term  $\ln(h^2)$  in (4.26) is

eliminated by the angular integral and the sum  $I_1 + I_2$  is a finite integral so that we can write,

$$\iint_s \frac{\partial}{\partial x} \left( \frac{1}{\sqrt{x^2 + y^2}} \right) dS = - \int_0^{2\pi} \cos \theta \ln \left( \frac{h_i}{\cos(\theta - \theta_i)} \right) d\theta \quad (4.27)$$

on a subtriangle shown in Fig. 4.2. Although no explicit formula can be obtained for (4.27) it can be evaluated by numerical methods to a high accuracy since the singularity of the original integral is removed.

#### *Numerical tests:*

To illustrate the accuracy of these formulas, two tests are conducted to evaluate the integral given in (4.19). One case is for nearly strongly singular integral and the other case is for strongly singular integrals. For both problem the integration domain is a square with corner points  $(1,1)$ ,  $(-1,1)$ ,  $(1,-1)$  and  $(-1,-1)$ .

For the nearly strongly singular problem, the observation point is taken outside the square patch but close to it so that near singular behavior of the integrand is still observed although integrand does not become infinite. So observation point for this problem is located at  $(0,2)$ . Since the integrand is bounded, quadrature rules are also applicable for the integral given in (4.19). Thus integration domain is divided into  $N^2$  square elements and the value of the integrand is sampled at the center of each element. Table 4.3 summarizes the results obtained with formulas (4.22) and (4.27) as well as those obtained with Newton-Cotes quadrature formula.

As expected, both (4.22) and (4.27) give the same values for the integral. It is also observed that accuracy of the quadrature formula increases as the number of quadrature points is increased and for a tenfold increase in accuracy a tenfold increase in number of quadrature points is required. This behavior is also observed for nearly weakly singular integrals in the previous section.

Table 4.3 Results obtained for nearly strongly singular integral on a square patch

Analytical Result (4.22) and (4.27)	Quadrature Rule	$N$	Accuracy (%)
1.1078468735646	1.1060106034721	$10^1$	$1.7 \times 10^1$
1.1078468735646	1.1078249180330	$10^2$	$1.9 \times 10^{-1}$
1.1078468735646	1.1078466500219	$10^3$	$2.0 \times 10^{-3}$
1.1078468735646	1.1078468713257	$10^4$	$2.0 \times 10^{-5}$
1.1078468735646	1.1078468735507	$10^5$	$1.8 \times 10^{-7}$

As a second numerical test, the integral in (4.19) is considered when observation point is within the domain of integration so the integrand becomes unbounded at that point. The integration domain is again a square patch with corner points located at  $(1,1)$ ,  $(-1,1)$ ,  $(1,-1)$ , and  $(-1,-1)$ , and the observation point is located at  $(0.5,0.5)$ . Similar to the previous case the patch is divided into  $N^2$  square elements with side length  $dl = 2/N$ . The results obtained via derived formulas (4.22) and (4.27) are compared with those obtained with a quadrature rule. Since conventional quadrature rules lead to incorrect results when observation point is within the domain of integration, we used modified quadrature rules introduced in [58] for evaluation of the integral.

Table 4.4 Results obtained for strongly singular integral on a square patch

Analytical Result (4.22) and (4.27)	Quadrature Rule	$N$	Accuracy (%)
1.4909963089948	1.3676690976234	$10^1$	$2.2 \times 10^0$
1.4909963089948	1.4883717449217	$10^2$	$1.76 \times 10^{-1}$
1.4909963089948	1.4906869417489	$10^3$	$2.07 \times 10^{-2}$
1.4909963089948	1.4909654577391	$10^4$	$2.12 \times 10^{-3}$
1.4909963089948	1.4909932247245	$10^5$	$2.06 \times 10^{-4}$

Simulation results show that for strongly singular integrals performance of quadrature rules is not as good as nearly strongly singular integrals as presented in Table 4.3. Also when compared to nearly singular case, increment in accuracy is

not as rapid as number of quadrature points is increased. For a tenfold increase in accuracy the number of quadrature points must be increased by a factor of 100 compared to 10 for nearly singular case. This behavior is due to the limiting procedure in evaluation of quadrature rules which puts a lower limit to the accuracy.

### 4.3 Hypersingular Integrals and Their Evaluation

Hypersingular integrals arise in many areas of engineering sciences such as crack problems and fluid flow problems in applied mechanics, acoustic and elastic wave scattering in physics and recently electromagnetic scattering problems in electrical engineering. In EM scattering problems one encounters hypersingular dyadic integrals in the form,

$$\bar{\nabla} \iint_S \bar{\nabla} \frac{e^{-jkR}}{R} dS' \quad (4.28)$$

These dyadic integrals are defined as the derivative of *CPV* integrals and therefore possess a stronger singularity with  $1/R^3$  terms. The literature dealing with hypersingular integrals is diverse and a detailed review can be found in [4,52]. The extensive literature on hypersingular integrals introduced many different methods for their evaluation. Despite the wide attention of other fields of engineering on the topic, publications in EM community basically deal with evaluation of weakly singular and strongly singular integrals and systematic evaluation of hypersingular integrals is introduced only in a few papers [4]. This is due to common convention of reducing hypersingular kernels to strongly singular or weakly singular kernels by transferring the differential operator acting on Green's function to the unknown source function. Since singularity is weakened, accurate evaluation of integrals can be done more efficiently. The cost of weakening the kernels however is the requirement to introduce basis functions on which derivative operation can be applied. Introduction of such basis functions, called divergence conforming basis functions, for the unknown density, again increases numerical complexity and therefore computation time.



In this thesis we aim to introduce new explicit formulas for the evaluation of hypersingular integrals to a high degree of accuracy so that divergence conforming basis functions are not necessary anymore and the complexity in formulation is reduced.

Two major methods to evaluate integrals with hypersingular kernels are contour integration method and evaluation of Hadamard finite part of the integral. In application of Stoke's procedure the domain of integration is changed to the contour of the surface which cancels divergent terms. This is the cheapest and most effective solution as far as numerical effort is considered [59]. To the best of author's knowledge, there are few papers which use this procedure to evaluate hypersingular integrals for the solution of EM scattering problems. [6] uses this method to evaluate hypersingular surface integrals in a scattering problem by two dielectric spheres but does not give explicit formulas which can be directly introduced to the formulation whereas [4] uses Stoke's theorem along with a limiting procedure to obtain explicit formulas, but these formulas are rather complex. In this study, we obtain explicit expressions for hypersingular surface integrals which can be directly used in numerical implementations and are less complex than those introduced in [4]. Hadamard finite part interpretation for hypersingular kernels on the other hand discards the divergent terms in the resulting expression for the integrals and uses nondivergent terms. To our knowledge, there are no explicit formulas for hypersingular integrals which use Hadamard finite part interpretation in the literature which are first introduced in this study. It will be shown by numerical tests that both methods have same accuracy although they lead to different expressions for the same integrands.

Apart from the contributions mentioned above, hypersingular integrals on nonplanar surfaces are also considered in this study. In EM literature, we could determine only a single paper [6] that discusses the evaluation of such integrals on nonplanar surfaces and it proposes a transformation from curvilinear surface elements to flat, square elements. Instead of introducing an extra coordinate

transformation, following [60], we used a modified kernel which also possesses information on the curvature of the surface.

#### 4.3.1 Contour Integration for Flat Surfaces:

In this section, hypersingular integrals on flat triangular elements are considered. As in previous chapters, we assume that the triangle lies on the  $xy$ -plane and its contour is defined by  $\Gamma$ . The triangle is divided into three subtriangles each having their vertex point at integration point as shown in Figure 4.2.

As discussed previously by Taylor series expansion of Green's function in relation with (4.5) and (4.6), divergent behavior of the integral in (4.28) is the same as the behavior of the dyadic integral

$$\bar{\nabla} \iint_S \bar{\nabla} \frac{1}{R} dS' \quad (4.29)$$

Therefore, we will be interested in evaluation of (4.29) rather than (4.28). The  $\bar{\nabla}$  operator outside the integral cannot be brought under the integral sign unless a limiting procedure is applied. Thus we have

$$\bar{\nabla} \iint_S \bar{\nabla} \frac{1}{R} dS' = \lim_{\varepsilon \rightarrow 0} \iint_S \bar{\nabla} \bar{\nabla} \frac{1}{\sqrt{R^2 + \varepsilon^2}} dS' \quad (4.30)$$

proof of which is given in [48].

Application of vector identity in (4.15) to the integral on the RHS of (4.30) result in,

$$\lim_{\varepsilon \rightarrow 0} \iint_S \bar{\nabla} \bar{\nabla} \frac{1}{\sqrt{R^2 + \varepsilon^2}} dS' = \lim_{\varepsilon \rightarrow 0} \oint_{\Gamma} \hat{n} \bar{\nabla} \frac{1}{\sqrt{R^2 + \varepsilon^2}} dl' \quad (4.31)$$

where  $\hat{n}$  is the unit normal to the surface and  $\Gamma$  defines the contour of the surface.

Note that since the integration domain is the contour of the triangle, the integrand is no more singular and one is free to take the limit under the integral sign. This is

in contrast to the approach in [4], where integral is evaluated first and limit is evaluated afterwards. Applying first the limit, one gets,

$$\lim_{\varepsilon \rightarrow 0} \oint_{\Gamma} \hat{n} \bar{\nabla} \frac{1}{\sqrt{R^2 + \varepsilon^2}} dl' = \oint_{\Gamma} \hat{n} \frac{-\hat{a}_R}{R^2} dl' \quad (4.32)$$

where  $\hat{a}_R$  is the radial unit vector.

Note that the integral on the RHS of (4.32) is a dyadic term that can be used to evaluate field in a specified direction due to a surface current in a specified direction. For example, the field in  $\hat{a}_x$  direction due to a current density in  $\hat{a}_x$  direction can be evaluated by writing,

$$I_{xx} = \oint_{\Gamma} \hat{n} \cdot \hat{a}_x \left( \frac{-\hat{a}_r}{R^2(\theta)} \right) \cdot \hat{a}_x d\ell. \quad (4.33)$$

Here  $I_{xx}$  is used to denote  $\hat{a}_x \hat{a}_x$  component of (4.32) and  $R(\theta)$  is defined in (4.8).

From Figure 4.2 one can set

$$\hat{a}_r \cdot \hat{a}_x = \cos \theta \quad (4.34a)$$

$$\hat{n}_i \cdot \hat{a}_x = \cos \theta_i \quad (4.34b)$$

$$\Gamma = \Gamma_1 + \Gamma_2 + \Gamma_3 \quad (4.34c)$$

$$d\ell = \frac{r(\theta)d\theta}{\cos(\theta - \theta_i)} \quad (4.34d)$$

Using (4.34) an explicit formula for result of (4.33) can be given as,

$$I_{xx} = \sum_{i=1}^3 \frac{\cos \theta_i}{h_i} (\sin \theta_{2i} - \sin \theta_{1i}) \quad (4.35a)$$

And, in a similar way, other components of (4.32) can be written as:

$$I_{xy} = \sum_{i=1}^3 \frac{\cos \theta_i}{h_i} (\cos \theta_{2i} - \cos \theta_{1i}) \quad (4.35b)$$

$$I_{yx} = \sum_{i=1}^3 \frac{\sin \theta_i}{h_i} (\sin \theta_{2i} - \sin \theta_{1i}) \quad (4.35c)$$

$$I_{yy} = \sum_{i=1}^3 \frac{\sin \theta_i}{h_i} (\cos \theta_{2i} - \cos \theta_{1i}) \quad (4.35d)$$

The resulting expressions for the hypersingular integral (4.29) appear less complicated than their counterparts introduced previously in [4] since the limit is applied before integration. As will be shown later they have the same accuracy as the formulas introduced in those studies.

Using polar coordinate system in evaluation of the above integrals introduces extra coordinate transformation since the observation point should be at the center of the coordinate system. In order to get rid of this inconveniency, we converted the results obtained in Eqn. (4.35) to a Cartesian local coordinate system. In this local coordinate system the triangular patch on which the integral is to be evaluated lies on the  $xy$ -plane. The vertices of the triangle are located at points  $(x_1, y_1)$ ,  $(x_2, y_2)$  and  $(x_3, y_3)$ . The observation point is assumed to be within the triangle and is located at  $(x_0, y_0)$ . By using trigonometric identities one obtains,

$$h_i = \frac{|(y_{i+1} - y_i)(x_i - x_0) - (x_{i+1} - x_i)(y_i - y_0)|}{\sqrt{(y_{i+1} - y_i)^2 + (x_{i+1} - x_i)^2}} \quad (4.36a)$$

$$\cos(\theta_{2i}) = \frac{x_{i+1} - x_0}{\sqrt{(y_{i+1} - y_0)^2 + (x_{i+1} - x_0)^2}} \quad (4.36b)$$

$$\cos(\theta_{1i}) = \frac{x_i - x_0}{\sqrt{(y_i - y_0)^2 + (x_i - x_0)^2}} \quad (4.36c)$$

$$\cos(\theta_i) = \frac{y_{i+1} - y_i}{\sqrt{(y_{i+1} - y_i)^2 + (x_{i+1} - x_i)^2}} \operatorname{sgn}((y_{i+1} - y_i)(x_i - x_0) - (x_{i+1} - x_i)(y_i - y_0)) \quad (4.36d)$$

$$\sin(\theta_{2i}) = \frac{y_{i+1} - y_0}{\sqrt{(y_{i+1} - y_0)^2 + (x_{i+1} - x_0)^2}} \quad (4.36e)$$

$$\sin(\theta_{1i}) = \frac{y_i - y_0}{\sqrt{(y_i - y_0)^2 + (x_i - x_0)^2}} \quad (4.36f)$$

$$\sin(\theta_i) = \frac{-x_{i+1} + x_i}{\sqrt{(y_{i+1} - y_i)^2 + (x_{i+1} - x_i)^2}} \operatorname{sgn}((y_{i+1} - y_i)(x_i - x_0) - (x_{i+1} - x_i)(y_i - y_0)) \quad (4.36g)$$

When applying formulas (4.36) one should use  $(x_4, y_4) = (x_0, y_0)$ . Using (4.36), (4.35) can be written as,

$$I_{xx} = \sum_{i=1}^3 \frac{y_{i+1} - y_i}{y_{i+1}x_i - y_ix_{i+1} + y_0(x_{i+1} - x_i) - x_0(y_{i+1} - y_i)} \left( \frac{y_{i+1} - y_0}{\sqrt{(x_{i+1} - x_0)^2 + (y_{i+1} - y_0)^2}} - \frac{y_i - y_0}{\sqrt{(x_{i+1} - x_0)^2 + (y_{i+1} - y_0)^2}} \right) \quad (4.37a)$$

$$I_{xy} = \sum_{i=1}^3 \frac{-y_{i+1} + y_i}{y_{i+1}x_i - y_ix_{i+1} + y_0(x_{i+1} - x_i) - x_0(y_{i+1} - y_i)} \left( \frac{x_{i+1} - x_0}{\sqrt{(x_{i+1} - x_0)^2 + (y_{i+1} - y_0)^2}} - \frac{x_i - x_0}{\sqrt{(x_{i+1} - x_0)^2 + (y_{i+1} - y_0)^2}} \right) \quad (4.37b)$$

$$I_{yx} = \sum_{i=1}^3 \frac{x_i - x_{i+1}}{y_{i+1}x_i - y_ix_{i+1} + y_0(x_{i+1} - x_i) - x_0(y_{i+1} - y_i)} \left( \frac{y_{i+1} - y_0}{\sqrt{(x_{i+1} - x_0)^2 + (y_{i+1} - y_0)^2}} - \frac{y_i - y_0}{\sqrt{(x_{i+1} - x_0)^2 + (y_{i+1} - y_0)^2}} \right) \quad (4.37c)$$

$$I_{yy} = \sum_{i=1}^3 \frac{x_{i+1} - x_i}{y_{i+1}x_i - y_ix_{i+1} + y_0(x_{i+1} - x_i) - x_0(y_{i+1} - y_i)} \left( \frac{x_{i+1} - x_0}{\sqrt{(x_{i+1} - x_0)^2 + (y_{i+1} - y_0)^2}} - \frac{x_i - x_0}{\sqrt{(x_{i+1} - x_0)^2 + (y_{i+1} - y_0)^2}} \right) \quad (4.37d)$$

The formulas in (4.37) can be tailored to be used to any flat surface element with a defined number of edges as long as they can be represented as a combination of triangular elements. Application of these formulas is easy since they only use coordinate information of the corner points. In a numerical implementation one requires only single coordinate transformation to represent any mesh in  $xy$ -plane and no extra coordinate transformation in polar coordinates is necessary.

### 4.3.2 Hadamard Finite Part Interpretation:

Hadamard finite part of a hypersingular integral is obtained by keeping the nondivergent part of the integral and discarding the part that diverges. A one dimensional hypersingular integral can be written as,

$$I = \int_a^b \frac{f(x)}{(x-c)^2} dx \quad (4.38)$$

where  $f(x)$  is called the density function and  $a \leq c \leq b$ .

Definitely, the integral in (4.38) does not exist in the Riemann sense and should be defined in a special sense. Approaching the singular point in a limiting sense (4.38) can be written as,

$$\begin{aligned} \int_a^b \frac{f(x)}{(x-c)^2} dx &= \lim_{\varepsilon \rightarrow 0^+} \left\{ \int_a^{c-\varepsilon} \frac{f(x)}{(x-c)^2} dx + \int_{c+\varepsilon}^b \frac{f(x)}{(x-c)^2} dx \right\} \\ &= \lim_{\varepsilon \rightarrow 0^+} \frac{2f(c)}{\varepsilon} + F(c) \end{aligned} \quad (4.39)$$

Using Taylor series expansion of  $f(x)$  around singular point  $c$ ,  $F(c)$  is given as,

$$\begin{aligned} F(c) &= f(c) \left( \frac{1}{a-c} - \frac{1}{b-c} \right) + f'(c) (\ln(b-c) - \ln(a-c)) \\ &\quad + \sum_{m=2}^{\infty} \frac{f^{(m)}(c)}{m!(m-1)} [(b-c)^{m-1} - (a-c)^{m-1}] \end{aligned} \quad (4.40)$$

The term  $F(c)$  represents the finite part of the integral in (4.38) and does not blow-up as singular point is approached. Thus Hadamard finite part of a hypersingular integral is defined and denoted by,

$$HFP \int_a^b \frac{f(x)}{(x-c)^2} dx = \lim_{\varepsilon \rightarrow 0^+} \left\{ \int_a^{c-\varepsilon} \frac{f(x)}{(x-c)^2} dx + \int_{c+\varepsilon}^b \frac{f(x)}{(x-c)^2} dx - \frac{2f(c)}{\varepsilon} \right\} \quad (4.41)$$

Although the last term in (4.41) eliminates the divergent part of the integral, for the integral in (4.38) to exist the density function should meet certain smoothness criteria. Specifically the derivative of the density function should be Hölder continuous around the point of singularity [61]. That is

$$|f(x_1) - f(x_2)| \leq A|x_1 - x_2|^\alpha \quad (4.42)$$

where  $A$  is a finite constant and  $0 \leq \alpha < 1$ . This requirement is proved in Appendix C.

The use of Hadamard finite part interpretation to evaluate hypersingular surface integrals in EM problems relies on the equality,

$$\bar{\nabla} \iint_S \bar{\nabla} \left( \frac{1}{R} \right) dS' = HFP \iint_S \bar{\nabla} \bar{\nabla} \left( \frac{1}{R} \right) dS' \quad (4.43)$$

An interpretation to (4.43) can be provided in the following way: The expression on the LHS of the equation gives a bounded value since it is the derivative of a strongly singular integral and can be evaluated by finding derivative of  $CPV$  integrals. Nevertheless, taking the  $\bar{\nabla}$  operator under the integral sign produces divergent terms and the integral on RHS is not bounded. Still discarding the divergent terms and keeping the finite part on RHS lead to same results as the LHS of the equation. The proof for (4.43) is given in Appendix B.

With the above interpretation  $I_{xx}$  term of the dyadic in (4.43) integrated over a triangular patch, can be evaluated as,

$$\begin{aligned} I_{xx} &= HFP \iint_S \frac{\partial^2 (1/R)}{\partial x \partial x} dS' = \sum_{i=1}^3 HFP \int_{\theta_i}^{\theta_{2i}} \left( 2 \cos^2 \theta - \sin^2 \theta \right) \int_0^{r(\theta)} \frac{1}{R^3} R dR d\theta \\ &= \sum_{i=1}^3 \int_{\theta_i}^{\theta_{2i}} \left( 2 \cos^2 \theta - \sin^2 \theta \right) HFP \int_0^{r(\theta)} \frac{1}{R^2} dR d\theta = \sum_{i=1}^3 \int_{\theta_i}^{\theta_{2i}} \frac{(\sin^2 \theta - 2 \cos^2 \theta)}{h_i} \cos(\theta - \theta_i) d\theta \quad (4.44) \end{aligned}$$

This result in,

$$I_{xx} = \sum_{i=1}^3 \frac{1}{h_i} \left[ \sin(\theta_{2i} + \theta_i) + \cos^2(\theta_{2i}) \sin(\theta_{2i} - \theta_i) - \sin(\theta_{1i} + \theta_i) - \cos^2(\theta_{1i}) \sin(\theta_{1i} - \theta_i) \right] \quad (4.45a)$$

Similarly other terms in the dyadic can be evaluated as,

$$I'_{yy} = \sum_{i=1}^3 \frac{-1}{h_i} \left[ \sin(\theta_{2i} + \theta_i) + \sin^2(\theta_{2i}) \sin(\theta_{2i} - \theta_i) + \sin(\theta_{1i} + \theta_i) - \sin^2(\theta_{1i}) \sin(\theta_{1i} - \theta_i) \right] \quad (4.45b)$$

$$I'_{xy} = \sum_{i=1}^3 \frac{1}{h_i} \left[ \sin^3(\theta_{2i}) \sin(\theta_i) - \cos^3(\theta_{2i}) \cos(\theta_i) - \sin^3(\theta_{1i}) \sin(\theta_i) + \cos^3(\theta_{1i}) \cos(\theta_i) \right] \quad (4.45c)$$

$$I'_{yx} = \sum_{i=1}^3 \frac{1}{h_i} \left[ \sin^3(\theta_{2i}) \sin(\theta_i) - \cos^3(\theta_{2i}) \cos(\theta_i) - \sin^3(\theta_{1i}) \sin(\theta_i) + \cos^3(\theta_{1i}) \cos(\theta_i) \right] \quad (4.45d)$$

To test the accuracy of the formulas derived for hypersingular surface integrals, we evaluated these integrals on a randomly chosen triangle. Observation point is randomly selected within the triangle and we compare the results obtained with expressions (4.37) and (4.45) with the results given in [4]. In order to allow comparison of the results, the same triangle in [4] is used. The triangle has its vertices at (0.7,0.1,0), (0.4,0.3,0) and (0.1,0.2,0), while the observation point is located at (0.4,0.2,0). The results are presented in Table 4.5.

Table 4.5: The components of hypersingular dyadic on a triangle with random shape

	Reference [3]	Reference [4]	Equation (4.37)	Equation (4.45)
$I_{xx}$	13.16227766016	13.16227766016	13.16227766016	13.16227766016
$I_{xy}$	3.162277660168	3.162277660168	3.162277660168	3.162277660168
$I_{yx}$	3.162277660168	3.162277660168	3.162277660168	3.162277660168
$I_{yy}$	58.46049894151	58.46049894151	58.46049894151	58.46049894151



As observed from Table (4.5) the results obtained with (4.37) and (4.45) are same with references up to the 14<sup>th</sup> digit. In fact following these numbers up to 100<sup>th</sup> digit still gives same result. This makes us to believe that the new formulas are analytically equivalent to the previously published formulas in [3,4]. However we were not able to obtain the new formulas by algebraic operations.

#### 4.4 Hypersingular Integrals on Nonplanar Surfaces:

Previous sections deal with evaluation of singular surface integrals over flat surfaces. For EM scattering problems from nonplanar surfaces on the other hand, special care should be exercised for evaluation of singular integrals. Generally fine meshing approximates the surface with enough accuracy but increases computation time since computation time increases with the square of the number of meshes for iterative methods. Thus one is required to take into account the nonplanar parameters of the surface if one desires to obtain high accuracy with relatively small number of meshes. Typically, hypersingular integrals dominate in self cell or near cell interaction terms over strongly singular and weakly singular integrals. Thus accurate evaluation of hypersingular integrals is of utmost importance for high order accuracy.

In this study we introduce a new kernel for hypersingular integrals on nonplanar surfaces based on Hadamard finite part interpretation. This approach was suggested in [61] for evaluation of hypersingular integrals of acoustic wave scattering problems where normal gradient of the static Green's function should be evaluated. However for EM scattering problems tangential derivative of the static Green's function should be evaluated and the kernel must be modified for its tangential derivatives.

The surface over which the hypersingular integral is to be evaluated is shown in Fig. 4.5. It is defined in a local coordinate system with  $w = S(u_1, u_2)$  and observation point is located at  $(0, 0, w_0)$  with  $w_0 = S(0, 0)$ . The surface is defined by the expression,

$$\Omega: w = S(u_1, u_2) \quad u_1, u_2 \in D \quad (4.46)$$

where  $D$  is the projection of  $\Omega$  on  $u_1 u_2$  plane and is a quadrilateral. The normal to the surface at a given point is defined by the vector  $\hat{n}$ . Moreover, two vectors are defined which are tangential to the surface. One is in  $u_1$ -direction and is given by the expression  $\hat{t}_1 = \hat{u}_2 \times \hat{n}$ ; and the other is in  $u_2$ -direction and is given by the expression  $\hat{t}_2 = -\hat{u}_1 \times \hat{n}$ . Thus we define,

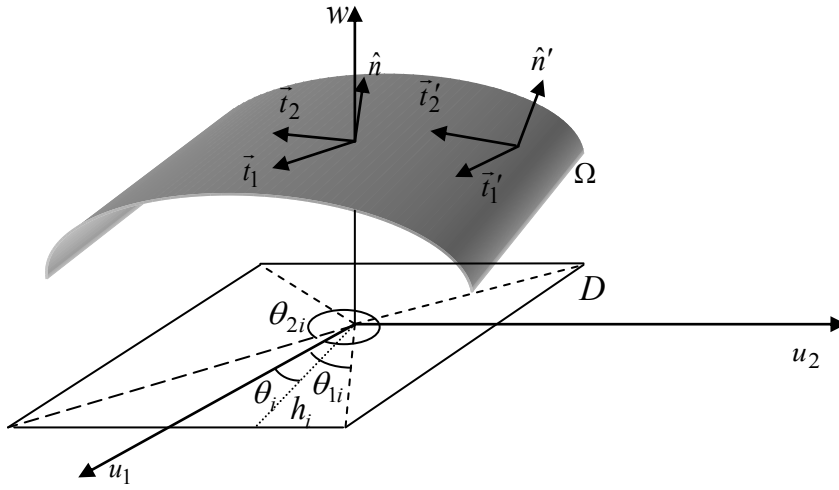


Figure 4.5 Nonplanar surface  $\Omega$  and its projection  $D$  on  $u_1 u_2$  plane

$$\vec{N} = \left( -\frac{\partial S}{\partial u_1}, -\frac{\partial S}{\partial u_2}, 1 \right) \text{ with } \hat{n} = \frac{\vec{N}}{|\vec{N}|} \quad (4.47)$$

$$\vec{T}_1 = \left( 1, 0, \frac{\partial S}{\partial u_1} \right) \quad \text{with } \hat{t}_1 = \frac{\vec{T}_1}{|\vec{T}_1|} \quad (4.48)$$

$$\vec{T}_2 = \left( 0, 1, \frac{\partial S}{\partial u_2} \right) \quad \text{with } \hat{t}_2 = \frac{\vec{T}_2}{|\vec{T}_2|} \quad (4.49)$$

The surface current density can be represented with two components one in  $\hat{t}_1$  direction and the other in  $\hat{t}_2$  direction. Similarly the tangential electric field on the

surface can be represented with two components again in  $\hat{t}_1$  and  $\hat{t}_2$  directions. In evaluating the field at observation point one is required to evaluate four integrals. Specifically to evaluate  $\hat{t}_i$  directed field due to  $\hat{t}'_j$  directed current one needs to handle the hypersingular integral,

$$I_{ij} = HFP \iint_{\Omega} \frac{\partial}{\partial \hat{t}_i} \frac{\partial}{\partial \hat{t}'_j} \left( \frac{1}{R} \right) d\Omega' \quad (4.50)$$

where  $R = \sqrt{u_1'^2 + u_2'^2 + \left( S(0,0) - S(u_1', u_2') \right)^2}$  and,

$$\frac{\partial}{\partial \hat{t}'_2} \left( \frac{1}{R} \right) = \hat{t}'_2 \cdot \vec{\nabla}' \left( \frac{1}{R} \right) \quad (4.51)$$

Projecting the integral in (4.50) over curved surface  $\Omega$  onto the surface  $D$ , one obtains,

$$I_{ij} = HFP \iint_{\Omega} \left\{ \frac{\delta_{ij} + F_i F'_j}{R^3} - \frac{3(u'_i + F_i(S(u'_1, u'_2) - w_0))(u'_j + F'_j(S(u'_1, u'_2) - w_0))}{R^5} \right\} du'_1 du'_2 \quad (4.52)$$

where  $F_i = \partial S(u_1, u_2) / \partial u_i$  and  $F'_j = \partial S(u'_1, u'_2) / \partial u'_j$ .

The analytical solution for (4.52) is not possible for every surface function  $w = S(u_1, u_2)$ . So we need to express the surface in a form that is suitable for analytical evaluation. In this study we purpose two approximations for the surface function for the solution of (4.52). First approximation uses Taylor series expansion of the surface function around the observation point and the second uses bicubic spline interpolation of the surface function. Two cases lead to different expressions with different accuracy and will be handled separately.

#### 4.4.1 Taylor series expansion for surface function

In the first case the surface function is expanded around the singular point so that,

$$S(u'_1, u'_2) = w_0 + \sum_m \sum_n \frac{1}{m!n!} \frac{\partial^{m+n} S(u_1, u_2)}{\partial u_1^m \partial u_2^n} \Big|_{(0,0)} u_1'^m u_2'^n \quad (4.53)$$

Using (4.53) in (4.52) results in four hypersingular integrals given as,

$$\begin{aligned} I_1 &= HFP \iint_S \left( \frac{1}{R^3} - \frac{3u_1'^2}{R^5} \right) du'_1 du'_2, \quad I_2 = HFP \iint_S \left( \frac{1}{R^3} - \frac{3u_2'^2}{R^5} \right) du'_1 du'_2, \\ I_3 &= HFP \iint_S \left( \frac{3u'_1 u'_2}{R^5} \right) du'_1 du'_2, \quad I_4 = HFP \iint_S \frac{1}{R^3} du'_1 du'_2 \end{aligned} \quad (4.54)$$

Except for the fourth integral  $I_4$ , integrals  $I_1$ ,  $I_2$ , and  $I_3$  are encountered previously, and explicit expressions for them are given in (4.45a)-(4.45c), respectively. These formulas can be used for the first three integrals keeping in mind that they should be defined over four subtriangles since the projection of the nonplanar surface is a quadrilateral in this case. For  $I_4$ , again finite part interpretation is utilized which leads to,

$$I_4 = \sum_{i=1}^3 \frac{1}{h_i} [\sin(\theta_{li} - \theta_i) - \sin(\theta_{2i} - \theta_i)]. \quad (4.55)$$

The other terms in (4.52) resulting from the Taylor series approximation have weaker singularities and can either be treated as finite part integrals or other techniques in literature can be employed.

#### *Numerical Tests:*

In order to test the accuracy of modified kernel on a curvilinear surface  $I_{22}$  is evaluated on a surface with constant curvature. Resulting values for the integral of modified kernel is compared with the analytical result. The surface is represented by  $w = \sqrt{a^2 - u_2'^2}$  for  $-0.5 \leq u_1 \leq 0.5$  and  $-0.5 \leq u_2 \leq 0.5$  with "a" being the radius of curvature. The current on the surface flows in  $u_2$  direction and resulting field in  $u_2$  direction is observed at the point  $(0,0,a)$ .

For the first case the radius of curvature surface is taken as a small value, namely  $a = 2$ . Table 4.6 gives the results obtained by using (4.52) and the exact solution.

Table 4.6 Comparison of (4.52) with analytical solution for  $a = 2$

Order of Expansion	Results obtained for $-I_{22}$		
	Exact	(4.52)	Error(%)
0	6.148666256	5.656854249	$7.9 \times 10^0$
2	6.148666256	6.141123332	$1.2 \times 10^{-1}$
4	6.148666256	6.148447612	$3.7 \times 10^{-3}$

From Table 4.6 it is observed that (4.52) provides higher accuracy as the order of Taylor series expansion is increased.

As a second example we consider a larger radius of curvature so that the effect of curvature decreases. For that purpose integral in (4.52) is evaluated for  $a = 5$ . The results for this case are given in Table 4.7

Table 4.7 Comparison of (4.52) with analytical solution for  $a = 5$

Order of Expansion	Results obtained for $-I_{22}$		
	Exact	(4.52)	Error(%)
0	5.734523235	5.656854249	$1.4 \times 10^0$
2	5.734523235	5.734334808	$3.3 \times 10^{-3}$
4	5.734523235	5.734428556	$1.6 \times 10^{-5}$

From Table 4.7 it is observed that when the curvature of the surface is decreased, the accuracy of approximation increases. So the accuracy for  $a = 2$  less than the accuracy obtained for  $a = 5$ . This behavior is expected since (4.52) is exact for planar surfaces but is an approximation for nonplanar surfaces. As the surface approaches a flat surface accuracy is expected to increase. It is also observed that the rate of convergence is faster for  $a = 5$  as the surface is more accurately represented for larger radius of curvature.

#### 4.4.2 Bicubic Spline Interpolation of surface function

Spline interpolation of a function is used to represent a function with piecewise polynomials between sample points. As the polynomials are defined piecewise, low degree polynomials are adequate for fine representation without stability problems. Moreover spline interpolation forces the derivatives of the function to be equal at sample points so that smoothness is still preserved when piecewise polynomials are connected at sample points. These properties make spline interpolation a favorable method to represent curved functions in numerical simulations. Bicubic interpolation is the two dimensional extension of spline interpolation. Cubic polynomials are utilized to represent surface functions. The surface function  $w = S(u_1, u_2)$  can be represented by using bicubic splines as,

$$S(u_1, u_2) = \sum_{m=0}^3 \sum_{n=0}^3 a_{mn} u_1^m u_2^n \quad (4.56)$$

where  $a_{mn}$  are constants and  $u_1, u_2$  are defined within the quadrilateral: This bicubic spline form is defined by four sample points  $P_1 - P_4$ . In order to evaluate sixteen coefficients  $a_{mn}$ , sixteen equations are required. Four equations are obtained by the values of surface function at sample points, four equations are obtained by  $u_1$  derivative at sample points, four equations are obtained by  $u_2$  derivative and four equations are obtained by  $u_1 u_2$  derivatives making a total of sixteen equations. Using (4.56) in (4.52) results in eight hypersingular integrals, whose singularities are stronger than  $1/R^2$ . These are written as,

$$\begin{aligned} I_1 &= \iint_S \frac{1}{R^5} dS', I_2 = \iint_S \frac{u_1'}{R^5} dS', I_3 = \iint_S \frac{u_2'}{R^5} dS', I_4 = \iint_S \frac{u_1' u_2'}{R^5} dS', \\ I_5 &= \iint_S \frac{1}{R^4} dS', I_6 = \iint_S \frac{u_1'}{R^4} dS', I_7 = \iint_S \frac{u_2'}{R^4} dS' \text{ and } I_8 = \iint_S \frac{1}{R^3} dS' \end{aligned} \quad (4.57)$$

Other emerging integrals are at most strongly singular integrals and can be evaluated either by using finite part interpretation or by using techniques previously introduced in the literature. Using Fig. 4.4, integrals in (4.57) are

evaluated on the projection of  $\Omega$  on  $D$ , which is a quadrilateral formed by four subtriangles. The subtriangles have their common vertex at the observation point which is the origin of the local coordinate system. Finite part interpretation results in following expressions for the integrals in (4.57).

$$I_1 = \sum_{i=1}^4 \frac{1}{h_i^3} \left[ \frac{3}{4} \sin(\theta - \theta_i) + \frac{1}{12} \sin(3\theta - 3\theta_i) \right]_{\theta_{1i}}^{\theta_{2i}} \quad (4.58a)$$

$$I_2 = \sum_{i=1}^4 \frac{1}{h_i^2} \left[ \frac{1}{2} \sin(\theta) + \frac{1}{4} \sin(\theta - 2\theta_i) + \frac{1}{12} \sin(3\theta - 2\theta_i) \right]_{\theta_{1i}}^{\theta_{2i}} \quad (4.58b)$$

$$I_3 = \sum_{i=1}^4 \frac{1}{h_i^2} \left[ -\frac{1}{2} \cos(\theta) + \frac{1}{4} \cos(\theta - 2\theta_i) - \frac{1}{12} \sin(3\theta - 2\theta_i) \right]_{\theta_{1i}}^{\theta_{2i}} \quad (4.58c)$$

$$I_4 = \sum_{i=1}^4 \frac{1}{h_i^2} \left[ -\frac{1}{4} \cos(\theta + \theta_i) - \frac{1}{12} \cos(\theta - 3\theta_i) \right]_{\theta_{1i}}^{\theta_{2i}} \quad (4.58d)$$

$$I_5 = \sum_{i=1}^4 \frac{1}{h_i^2} \left[ \frac{1}{2} \theta + \frac{1}{4} \sin(2\theta - 2\theta_i) \right]_{\theta_{1i}}^{\theta_{2i}} \quad (4.58e)$$

$$I_6 = \sum_{i=1}^4 \frac{1}{h_i^2} \left[ \frac{1}{2} \theta \cos(\theta_i) + \frac{1}{4} \sin(2\theta - \theta_i) \right]_{\theta_{1i}}^{\theta_{2i}} \quad (4.58f)$$

$$I_7 = \sum_{i=1}^4 \frac{1}{h_i^2} \left[ \frac{1}{2} \theta \sin(\theta_i) - \frac{1}{4} \cos(2\theta - \theta_i) \right]_{\theta_{1i}}^{\theta_{2i}} \quad (4.58g)$$

$$I_8 = \sum_{i=1}^4 \frac{1}{h_i} [\sin(\theta - \theta_i)]_{\theta_{1i}}^{\theta_{2i}} \quad (4.58h)$$

*Numerical Tests:*

Bicubic spline interpolation of the surface function is used to represent the patch  $w = \sqrt{a^2 - u_2^2}$  which is also used in Taylor series expansion approach. In order to allow comparison we evaluate the same integral  $I_{22}$  for different values of radius of curvature. The values for exact result as well as those obtained using (4.58) are presented in Table 4.8.

Table 4.8 Comparison of (4.58) with exact results

Radius of Curvature “ $a$ ”	Results obtained for $-I_{22}$		
	Exact	(4.58)	Error(%)
2	6.148666256	6.164626498	$2.6 \times 10^{-1}$
3	5.873544249	5.876425660	$4.9 \times 10^{-2}$
4	5.778378936	5.779308711	$1.6 \times 10^{-2}$

It can be seen from Table 4.8 that like the Taylor series expansion case, the accuracy of the expressions in (4.58) increases as the radius of curvature increases. It is also observed that for the radius of curvature  $a = 2$  using Taylor series expansion of surface function gives more accurate results even for an expansion order of two. This behavior is attributed to inaccurate estimation of observation point when bicubic splines are used since sample points are at the corners of the quadrilateral. In Fig. 4.6 we plot the relative error for different radius of curvatures and using different expressions which utilize Taylor series expansion, bicubic spline interpolation, and flat patch approximation.

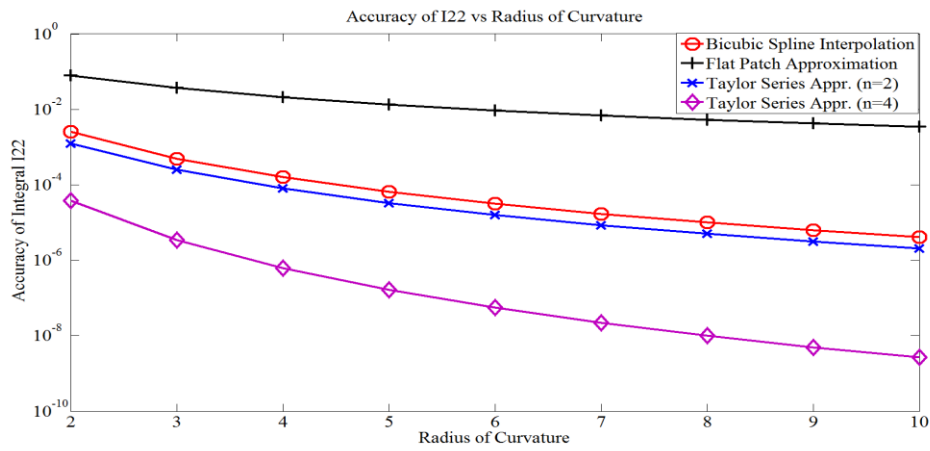


Fig. 4.6 Accuracy of  $I_{22}$  with different approximations of surface function



## 4.5 Numerical Results

In this section we consider some generic frequency domain scattering problems for the solution of which Nyström procedure is followed. The first problem is EM scattering from a dielectric cube and volume electric field integral equation is constructed to calculate radar cross section (RCS) of the cube. Second problem is scattering problem from a long PEC cylinder for which we evaluated induced current on the cylinder for  $TM^z$  and  $TE^z$  polarizations.

### 4.5.1 Scattering from Dielectric Cube

As the first problem we employed Nyström method for the solution of volume electric field equation in (2.15) to find the RSC of a dielectric cube. As volume current densities are the unknown sources to be determined, the integration domain is a volume so we encounter at most strongly singular integrals which are due to  $1/R^3$  terms defined within the volume. Apart from integrals with  $1/R^3$  terms in the kernel, we also encounter weakly singular integrals with  $1/R^2$  terms in the kernel and regular integrals. The geometry of the problem is plotted in Fig. 4.7.

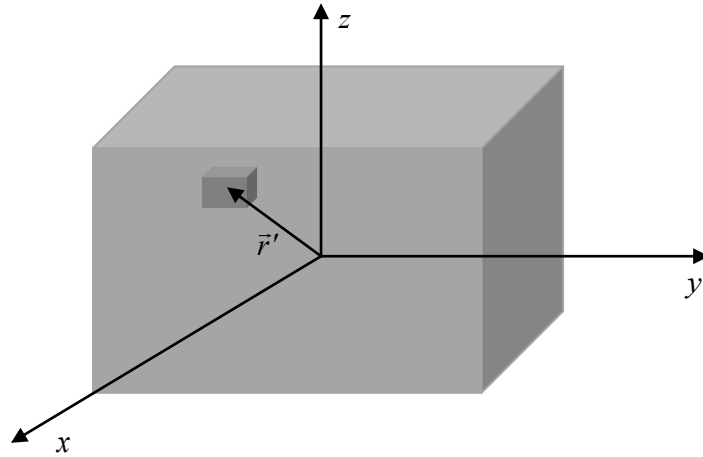


Fig 4.7. Geometry for dielectric cube scattering problem

The cube has a side length of 0.15m and is represented with cubic cells with side length of 0.015m so that there are a total of 1000 cells within the cube. The relative permeability  $\epsilon_r$  of the cube is selected as 3. The incident wave is a plane

wave propagating in  $-x$  direction and is represented by  $E^i = E_0 \exp(jkx)$ . In the first case the frequency of the incident wave is chosen as 300 MHz so that the cube is a  $0.15\lambda$  cube. The RCS of the cube is plotted in Fig 4.8.

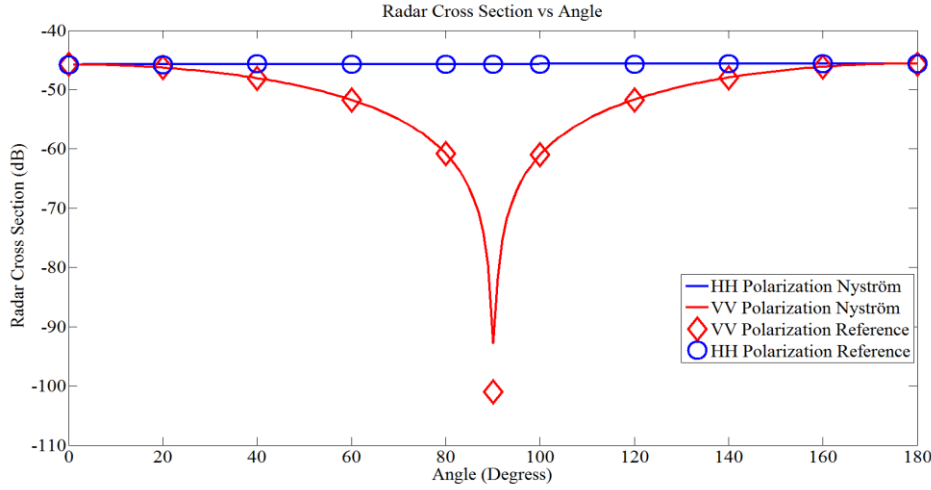


Fig. 4.8. Bistatic radar cross section of dielectric cube with  $a=0.15\lambda$  for both vertical and horizontal polarizations.

It is observed from Fig. 4.8 that RCS results obtained using Nyström method with singularity extraction is coherent with the results obtained using commercial simulation software CST Studio Suit 2013.

As the second case the frequency of the incident plane wave is increased to 900 MHz so that the cube is a  $0.05\lambda$  cube. As the previous case the cube is represented by 1000 cubic cells. The results of Nytröm method again agree well with the results of CST Studio Suit which are both plotted in Fig. 4.9.

#### 4.5.2 Scattering from PEC Cylinder ( $TM^z$ polarization)

As the second problem we consider scattering from a long PEC Cylinder for  $TM^z$  scattering. The length of the cylinder is selected long enough such that edge effects have minor contribution to the field in the middle region of the cylinder and results can be compared with analytical solution obtained by using Mie series [62]. The length of the cylinder is chosen as  $10\lambda$  and the radius of the cylinder is selected as  $0.5\lambda$ . The surface of the cylinder is represented by flat square patches

with 64 angular nodes. The incident wave is a plane wave with  $E^i = E_0 \exp(jkx)$  which has an amplitude of  $120\pi$ . The hypersingular integrals for the solution of EFIE are evaluated using (4.45) which were obtained by using Hadamard finite part interpretation on flat surfaces. Same formulas are used to evaluate nearly hypersingular integrals due to neighboring cells. The geometry of the problem and the current induced on the cylinder are plotted in Fig. 4.10 and in Fig 4.11 respectively.

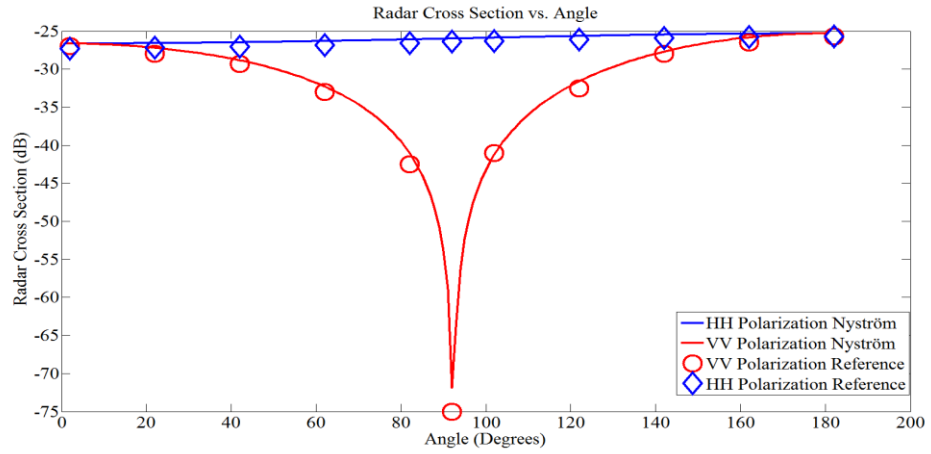


Fig. 4.9. Bistatic radar cross section of dielectric cube with  $a=0.05\lambda$  for both vertical and horizontal polarizations.

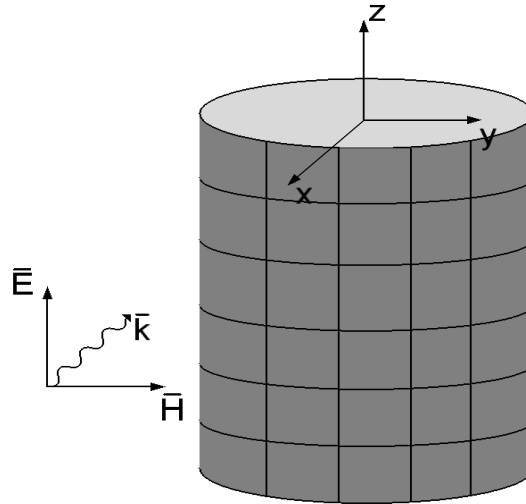


Fig. 4.10 Geometry of the PEC cylinder problem ( $TM^z$  polarization)

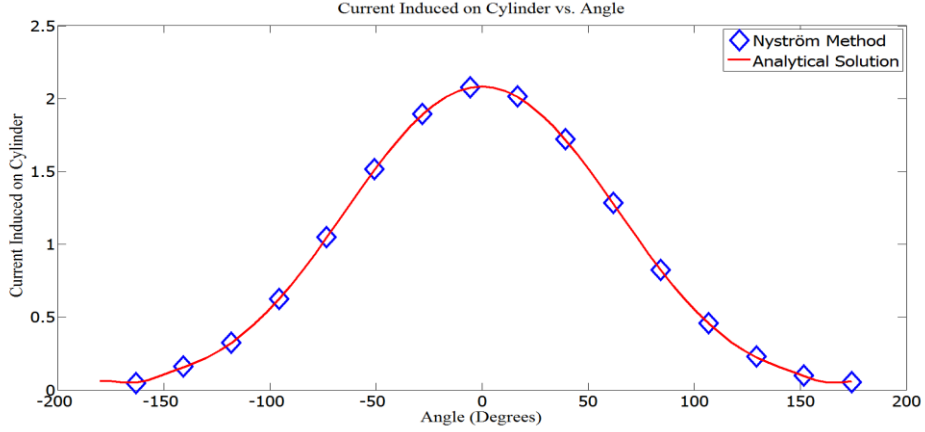


Fig. 4.11 Current induced on PEC cylinder versus angle for  $TM^z$  polarization

#### 4.5.3 Scattering from PEC Cylinder ( $TE^z$ polarization)

As a final problem we consider scattering from a PEC cylinder with  $TE^z$  polarized incident field. The geometry of the problem is the same as  $TM^z$  scattering problem which is plotted in Fig. 4.9. For evaluation of hypersingular integrals that arise in the solution of EFIE we used (4.58) which were obtained for hypersingular integrals on nonplanar surfaces. Same expressions are utilized for neighboring cells and sixteen point Newton-Cotes quadrature rules are used to account for far cell contribution. Fig. 4.12 plots the amplitude of current induced on PEC cylinder with  $r = 2\lambda$  with 200 angular nodes.

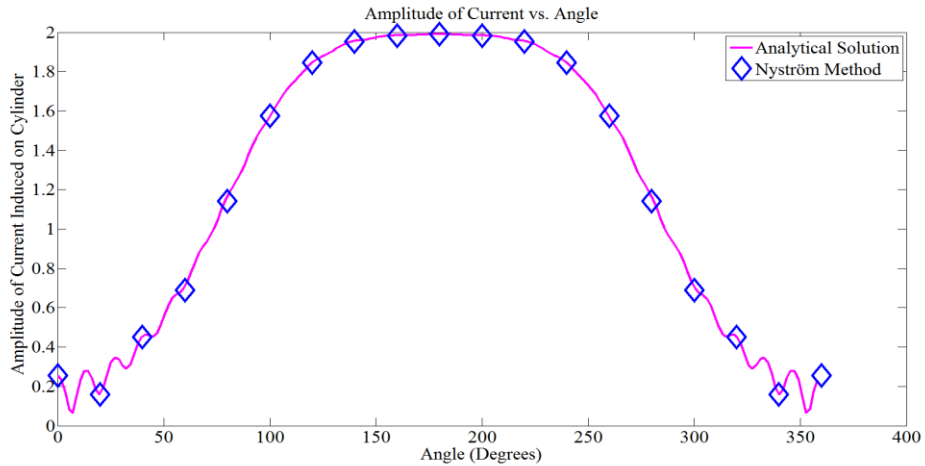


Fig 4.12 Current induced on PEC cylinder versus Angle for  $TE^z$  polarization

In order to assess the performance of (4.58) which is used to evaluate hypersingular integrals on nonplanar surfaces, we solved the same problem by using (4.45) which were introduced for flat surfaces. We changed the number of angular nodes and observed the accuracy for the amplitude of current so that,

$$Error = \frac{\|I_{Numerical} - I_{Analytical}\|_2}{\|I_{Analytical}\|_2} \quad (4.59)$$

on angular nodes. Fig. 4.13 plots error as a function of nodes obtained both by using (4.58) and (4.45).

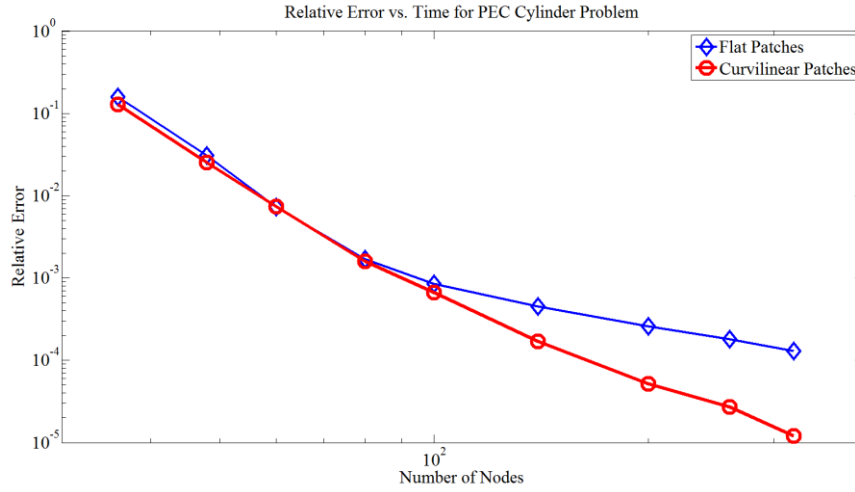


Figure 4.13 Accuracy obtained for  $TE^z$  scattering problem when number of nodes is increased

It can be observed from Fig. 4.13 that as the number of nodes is increased the accuracy is increased for both curvilinear patch representation and flat patch representation. When the number of nodes is small, similar accuracy is obtained for both cases although curvilinear patch representation gives slightly better accuracy. However when the number of nodes is further increased the hypersingular integrals start to dominate the total accuracy. This behavior can be explained by larger contribution of hypersingular terms when the patch sizes get smaller. This is obvious from expressions in (4.45) and (4.58), whose magnitudes

are inversely proportional to the height of subtriangles  $h_i$ . As a result, the rate of convergence for flat patch representation is limited by inaccurately evaluated hypersingular integrals on these surfaces. It can be seen from Fig. 4.12 that when hypersingular terms are evaluated on curvilinear patches using (4.58) the rate of convergence preserves its slope. This figure shows the importance of using curvilinear elements in high order methods for which the rate of convergence is a major concern and that without using curvilinear elements such methods are of little benefit.

Having evaluated hypersingular integrals to a high accuracy we are now in a position to develop a time domain locally corrected Nyström method which will be introduced in chapter 5.

## CHAPTER 5

### A TIME DOMAIN NYSTRÖM METHOD FOR THE SOLUTION OF EFIE

Although Maxwell's equations are first introduced in time domain, until recent time majority of research in computational electromagnetics was conducted in frequency domain. This situation is explained by some advantages of frequency domain study such as being easily tractable analytically and availability of hardware for practical experiments [63]. However, with the advent of fast computers, the inferior position of time domain methods over frequency domain methods start to change. For certain problems, such as wide band radiation and scattering or problems involving time varying media, direct time domain methods are employed since these problems are more efficiently treated in time domain. Despite the advantages of integral equation methods over differential equation methods as mentioned in chapter 2, time domain integral equation (TDIE) methods lagged behind time domain differential equation (TDDE) methods due to their computational complexity and late time instability, which is caused by accumulated error in marching on in time (MoT) procedure.

In this study we propose a new formulation for time domain electric field integral equation (TDEFIE) for scattering problems from PEC objects. Unlike the conventional TDEFIE which uses RWG basis functions, the new formulation applies Nyström scheme. Employing Nyström method aims to reduce the computational complexity of the method since it applies quadrature rules instead of evaluating double surface integrals of basis and testing functions. This is because the location of quadrature nodes and their weights can be found by using the tables developed for quadrature rules. Moreover, the difficulties that arise from singular integrals for self-cell interaction in Nyström method are alleviated by using explicit expressions for hypersingular integrals. These explicit expressions

are obtained for both flat and curvilinear surfaces in chapter 4 and high accuracy is obtained. Moreover, we applied interpolation in time to account for near cell contribution and this increase stability of the procedure as will be shown by numerical simulations.

### 5.1 Formulation

When illuminated by a transient electromagnetic pulse, surface current is induced on the surface of a PEC object which then reradiates the scattered field. Boundary conditions force the tangential component of the electric field to be zero on the surface so that we require the scattered field cancel the incident field on the surface at all times. The system equation for TDEFIE can be obtained by using the inverse Fourier transform of the frequency domain counterpart introduced in chapter 2 and written here again for convenience,

$$\hat{n} \times \vec{E}^i(\vec{r}) = \hat{n} \times \left[ j\omega\mu \iint_S \frac{e^{-jk|\vec{r}-\vec{r}'|}}{4\pi|\vec{r}-\vec{r}'|} \vec{J}(\vec{r}') dS' + \frac{j\omega\mu}{k^2} \vec{\nabla} \left( \vec{\nabla} \cdot \iint_S \frac{e^{-jk|\vec{r}-\vec{r}'|}}{4\pi|\vec{r}-\vec{r}'|} \vec{J}(\vec{r}') dS' \right) \right] \quad (5.1)$$

Evaluating the inverse Fourier transform of (5.1) one obtains an equation for TDEFIE as,

$$\vec{E}_{\tan}^i(\vec{r}, t) = \left[ \frac{\mu}{4\pi} \iint_S \frac{\frac{\partial}{\partial t} \left\{ \vec{J}\left(\vec{r}', t - \frac{R}{c}\right) \right\}}{R} dS' - \frac{1}{4\pi\epsilon} \vec{\nabla} \left( \vec{\nabla} \cdot \iint_S \frac{\int_{-\infty}^{t-\frac{R}{c}} \vec{J}(\vec{r}', \tau) d\tau}{R} dS' \right) \right]_{\tan} \quad (5.2)$$

In writing (5.2) we have used,

$$j\omega \vec{J}(\vec{r}') = \frac{\partial \vec{J}(\vec{r}')}{\partial t} \quad (5.3a)$$

$$\frac{1}{j\omega} \vec{J}(\vec{r}') = \int \vec{J}(\vec{r}', \tau) d\tau \quad (5.3b)$$



$$e^{-j\omega\frac{R}{c}}\vec{J}(\vec{r}') = \vec{J}\left(\vec{r}', t - \frac{R}{c}\right) \quad (5.3c)$$

$$k^2 = \omega^2 \mu \epsilon \quad (5.3d)$$

### 5.1.1 Conventional Formulation for TDEFIE

The conventional approach for numerical solution of (5.2) is to expand the unknown current in terms of  $N_s$  spatial and  $N_t$  temporal basis functions as

$$\vec{J}(\vec{r}, t) = \sum_{j=1}^{N_t} \sum_{n=1}^{N_s} I_{jn} T(t - j\Delta t) \vec{S}_n(\vec{r}) \quad (5.4)$$

where  $I_{jn}$  are the unknown coefficients to be determined,  $\vec{S}_n(\vec{r})$  are the spatial basis functions,  $T(t)$  is the temporal basis function and  $\Delta t$  is the time step.

Selection of temporal and spatial basis functions is critical as far as accuracy and late time stability are concerned. Late time stability is often attributed to inaccurate evaluation of surface integrals [64] which accumulate in MoT scheme, or to insufficient representation of low and high frequency components which again result in propagating error in MoT scheme [65-67]. Studies to obtain stable solution to MoT scheme often deals with designing new temporal basis functions [68-69]. The desired properties of the temporal basis functions are causality to satisfy MoT criterion, short temporal support to reduce the complexity of the formulation and being band limited to eliminate unwanted oscillations due to high and low frequency components. The selection of spatial basis functions is usually underestimated and conventional RWG basis functions are used in the majority of studies concerning late time stability.

Discretization of (5.2) is achieved by using (5.4) for the density function, multiplying the derivative of (5.2) with  $\delta(t - i\Delta t) \vec{S}_m(\vec{r})$  and by integrating over the surface of the scattering object and over all time [70]. This amounts to Galerkin in

space , point matching in time. The derivative is taken to eliminate the time integral of the current function. This yields the matrix equation

$$\bar{V}_i = \sum_{j=1}^{N_t} \bar{Z}_{i-j} \bar{I}_j \quad \text{for } i = 1, 2, \dots, N_t \quad (5.5)$$

In (5.5)  $\bar{V}_i$  is an  $N_s \times 1$  vector and denotes the excitation matrix at time  $t = i\Delta t$ . The elements of the excitation vector are given as,

$$[\bar{V}_i]_m = \iint_{S_m} \dot{\vec{E}}_{\tan}^{inc}(\vec{r}, i\Delta t) \cdot \vec{S}_m(\vec{r}) dS \quad (5.6)$$

Also  $\bar{I}_j$  is an  $N_s \times 1$  vector, whose elements are the unknown coefficients of the expansion function in (5.4) at time  $t = j\Delta t$ . This is written as,

$$[\bar{I}_j]_n = I_{jn} \quad (5.7)$$

Finally  $\bar{Z}_{i-j}$  is an  $N_s \times N_s$  matrix, whose elements  $Z_{i-j,mn}$  relate the field at observation patch  $m$ , at time  $t = i\Delta t$  to the current at source cell  $n$  at time  $t = j\Delta t$ .

$$Z_{k,mn} = \frac{\mu}{4\pi} \iint_{S_m} \iint_{S_n} \frac{\vec{S}_m(\vec{r}) \cdot \vec{S}_n(\vec{r}')}{R} \ddot{T}\left(k\Delta t - \frac{R}{c}\right) dS' dS - \frac{1}{4\pi\epsilon} \iint_{S_m} \iint_{S_n} \frac{[\vec{\nabla} \cdot \vec{S}_m(\vec{r})][\vec{\nabla} \cdot \vec{S}_n(\vec{r}')] }{R} T\left(k\Delta t - \frac{R}{c}\right) dS' dS \quad (5.8)$$

with  $k = i - j$  and  $R$  is the distance between patch  $m$  and  $n$ .

It can be deduced from (5.8) that for temporal basis functions with finite duration, some of the impedance matrices  $\bar{Z}_{i-j}$  are zero. For a causal temporal basis function of duration  $l\Delta t$  and with the maximum distance between two elements on the surface being  $R_{\max}$ , the contribution of current at time  $j\Delta t$  to the field at time  $i\Delta t$  is between,

$$j\Delta t + \frac{R_{\max}}{c} < t_{\text{interaction}} < j\Delta t + \frac{R_{\max}}{c} + l\Delta t \quad (5.9)$$

It can be seen from (5.9) that for  $i - j < \frac{R_{\max}}{c\Delta t} + l$  the impedance matrices are all zero. This condition suggests to use of basis functions with short temporal support to reduce the memory requirement and computational complexity.

Another subject to be mentioned about the temporal basis functions is the marching condition. For temporal basis functions with,  $T(t) = 0$  for  $t < -\Delta t$ , (5.5) can be written as [71],

$$\bar{\bar{Z}}_0 \bar{I}_i = \bar{V}_i - \sum_{j=1}^{i-1} \bar{\bar{Z}}_{i-j} \bar{I}_j \quad (5.10)$$

which writes the current at time  $i\Delta t$  in terms of the excitation at the same time and in terms of currents earlier than  $i\Delta t$  in an iterative manner. Note that the upper limit in the summation on the RHS of (5.10) is up to  $i-1$  due to marching condition. If this condition is not met, information of future currents would be required for which extrapolation methods should be employed [72]. Since using future currents is not compatible with causality, in most cases extrapolation schemes lead to unwanted oscillations.

Moreover for  $\Delta t < R_{\min}/c$  with  $R_{\min}$  being the minimum distance between two patches, the interaction matrix on the LHS of (5.10) is a diagonal matrix and the marching is called as explicit. Similarly with  $\Delta t > R_{\min}/c$  the interaction matrix is not diagonal and the marching scheme is called as an implicit scheme.

Finally for each  $\bar{\bar{Z}}_{i-j}$ ,  $N_s$  equations are obtained which relate the field at time  $t = i\Delta t$  to the currents earlier than  $t = i\Delta t$ . Also  $N_t$  such groups are obtained yielding a total of  $N_s N_t$  equations for  $N_s N_t$  unknown coefficients  $I_{jn}$ .

### 5.1.2 Nyström Method for the solution of TDEFIE

It was mentioned in chapter 3 that the main difference between Nyström method and MoM procedure in frequency domain is the replacement of the surface

integrals in MoM procedure with quadrature rules. This can be seen as a change of basis functions where impulse functions are employed for spatial basis functions in Nyström method. Thus unlike the MoM procedure which seeks the coefficients of expansion functions, Nyström method searches for the samples of the current at selected quadrature nodes. In this study, using explicit MoT scheme, we aim to obtain a discretization of (5.2) which is in the form,

$$\vec{E}_{\text{tan}}^i(\vec{r}_{kl}, n\Delta t) = \left[ \sum_{z=1}^n \sum_{i=1}^N \sum_{j=1}^q w_{zij} \vec{G}(\vec{r}_{kl}, \vec{r}_{ij}) \cdot \vec{J}(\vec{r}_{ij}, z\Delta t) \right]_{\text{tan}} \quad (5.11)$$

In (5.11) the field at point  $\vec{r}_{kl}$  and at time step  $n\Delta t$  is written in terms of sample of current at points  $\vec{r}_{ij}$ , i.e. at  $j^{\text{th}}$  quadrature node of mesh  $i$ , and at time instants  $t = z\Delta t$  earlier than  $n\Delta t$ . This eliminates the use of temporal as well as spatial basis functions in conventional MoM. That is, (5.11) is discretization of TDEFIE which applies Nyström scheme.

Nyström discretization is achieved by first applying the differential operators in (5.2) to the kernel in order to obtain the dyadic Green's function for electric field. This yields,

$$\begin{aligned} \vec{E}(\vec{r}, t) = & \frac{\mu_0}{4\pi} \iint_S \left( \vec{I} - \hat{a}_R \hat{a}_R \right) \cdot \frac{\partial \vec{J} \left( \vec{r}, t - \frac{R}{c} \right)}{\partial t} \frac{dS'}{R} - \frac{\mu_0 c}{4\pi} \iint_S \left( \vec{I} - 3\hat{a}_R \hat{a}_R \right) \cdot \vec{J} \left( \vec{r}, t - \frac{R}{c} \right) \frac{dS'}{R^2} \\ & + \frac{\mu_0 c^2}{4\pi} \iint_S \left( \vec{I} - 3\hat{a}_R \hat{a}_R \right) \cdot \int_{-\infty}^{t - \frac{R}{c}} \vec{J}(\vec{r}, \tau) d\tau \frac{dS'}{R^3} \end{aligned} \quad (5.12)$$

multiplying (5.12) with  $\delta(t - n\Delta t) \delta(\vec{r} - \vec{r}_{kl})$ , which is point matching both in time and space, integrating over the surface and over all time and replacing the integrals with quadrature rules we obtain,

$$\begin{aligned} \vec{E}_{\tan}^i(\vec{r}_{kl}, n\Delta t) = \sum_{i=1}^N \sum_{j=1}^q w'_{zij} \frac{\mu_0}{4\pi} \left\{ \left( \vec{I} - \hat{a}_R \hat{a}_R \right) \cdot \frac{\partial \vec{J} \left( \vec{r}_{ij}, n\Delta t - \frac{R}{c} \right)}{\partial t} \frac{1}{R} - c \left( \vec{I} - 3\hat{a}_R \hat{a}_R \right) \cdot \vec{J} \left( \vec{r}_{ij}, n\Delta t - \frac{R}{c} \right) \frac{1}{R^2} \right. \\ \left. + c^2 \left( \vec{I} - 3\hat{a}_R \hat{a}_R \right) \cdot \int_{-\infty}^{n\Delta t - \frac{R}{c}} \vec{J}(\vec{r}, \tau) d\tau \frac{1}{R^3} \right\}_{\tan} \quad (5.13) \end{aligned}$$

Equation (5.13) uses the samples of current, its integral and its first derivative at time instants, which are not multiples of time step  $\Delta t$  due to the delay exhibited by the electromagnetic field. In order to obtain an accurate representation of TDEFIE, the derivative and the integral of the current function should be adequately represented by the samples of current at integer multiples of time step.

It has been shown in [73-74] that using numerical differentiation and integration of the current function can yield quite accurate results. Thus the derivative of the current sample is approximated by backward difference scheme so that,

$$\frac{\partial \vec{J} \left( \vec{r}_{kl}, n\Delta t - \frac{R}{c} \right)}{\partial t} = \frac{\vec{J} \left( \vec{r}_{kl}, n\Delta t - \frac{R}{c} \right) - \vec{J} \left( \vec{r}_{kl}, (n-1)\Delta t - \frac{R}{c} \right)}{\Delta t} \quad (5.14)$$

and for the integral of the sample of current we write the iterative equation,

$$\int_{-\infty}^{n\Delta t - R/c} \vec{J}(\vec{r}_{kl}, \tau) d\tau = \int_{-\infty}^{n\Delta t - R/c - \Delta t} \vec{J}(\vec{r}_{kl}, \tau) d\tau + \vec{J}(\vec{r}_{kl}, n\Delta t) \Delta t \quad (5.15)$$

In (5.13-15), we also need to express the current at time  $n\Delta t - R/c$  in terms of the samples of current at time instants that are multiples of the time step. This is achieved by using Taylor series expansion of the retarded current function. That is,

$$\vec{J}\left(\vec{r}_{kl}, n\Delta t - \frac{R}{c}\right) = \vec{J}\left(\vec{r}_{kl}, n\Delta t - \frac{R_{\text{int } eger}}{c}\right) + \frac{\partial \vec{J}\left(\vec{r}_{kl}, n\Delta t - \frac{R_{\text{int } eger}}{c}\right)}{\partial t} \frac{(R_{\text{int } eger} - R)}{c} + \dots \quad (5.16)$$

where  $R_{\text{int } eger}$  is the closest value to  $R$  which is larger than  $R$  and for which we have,

$$R_{\text{int } eger} = mc\Delta t \quad (5.17)$$

$m$  being an integer.

Using (5.14) for the derivative operator in (5.16), (5.16) can be rewritten as,

$$\vec{J}\left(\vec{r}_{kl}, n\Delta t - \frac{R}{c}\right) \cong \left(1 - \frac{R_{\text{int } eger} - R}{c}\right) \vec{J}\left(\vec{r}_{kl}, n\Delta t - \frac{R_{\text{int } eger}}{c}\right) + \frac{R_{\text{int } eger} - R}{c} \vec{J}\left(\vec{r}_{kl}, n\Delta t - \frac{R_{\text{int } eger}}{c} + \Delta t\right) \quad (5.18)$$

Using (5.14)-(5.18) in (5.13) we can now obtain (5.11) where all integrals in EFIE are replaced by quadrature rules. In this formulation only samples of current at specific quadrature nodes and discrete time instants are unknowns. Higher order accuracy can be obtained if high order terms in (5.16) are used for the estimation of early current. However this will introduce samples of current at very early time instants so that summation over time index in (5.11) will involve more terms and the computational complexity will be increased.

Similar to the case of frequency domain counterpart however, (5.11) is only valid for far cell interactions and again local corrections should be applied to account for near-cell and self-cell contribution. This is achieved by extracting the singular core from the integrand of TDEFIE before differential operators are applied to Green's function. We first write the frequency domain EFIE as,

$$\hat{n} \times \vec{E}^i(\vec{r}) = \hat{n} \times \left[ j\omega\mu \iint_S \frac{e^{-jkR}}{4\pi R} \vec{J}(\vec{r}') dS' + \frac{j\omega\mu}{k^2} \vec{\nabla} \left( \vec{\nabla} \cdot \iint_S \frac{(e^{-jkR} - 1)}{4\pi R} \vec{J}(\vec{r}') dS' \right) + \frac{1}{j\omega\epsilon_0} \iint_S \vec{\nabla} \vec{\nabla} \left( \frac{1}{R} \right) \cdot \vec{J}(\vec{r}') dS' \right] \quad (5.19)$$

The first integral on the RHS of (5.19) is a weakly singular integral. Using Taylor series expansion of  $e^{-jkR} - 1$ ,

$$e^{-jkR} - 1 = -jkR + (-jkR)^2 / 2! + (-jkR)^3 / 3! \dots \quad (5.20)$$

in (5.19), we see that the second integral on the RHS is also at most weakly singular. The first two integrals in (5.19) can be evaluated by using one of the methods for evaluation of weakly singular integrals presented in chapter 4.

The last integral in (5.19) is a hypersingular integral and should be evaluated by using Hadamard finite part interpretation which is described in chapter 4. With all of these discussions we write (5.19) in time domain as,

$$\hat{n} \times \vec{E}^i(\vec{r}_m, t) = \frac{\mu_0}{4\pi} \hat{n} \times \frac{\partial \vec{J}\left(\vec{r}_m, t - \frac{R}{c}\right)}{\partial t} \iint_S \frac{dS'}{R} - \frac{1}{4\pi\epsilon_0} \hat{n} \times \sum_{n=0}^{\infty} \iint_S \nabla \nabla (R^n) dS' \cdot \frac{(-1)^{n+1}}{(n+1)! c^{n+1}} \frac{\partial^n \vec{J}\left(\vec{r}_m, t - \frac{R}{c}\right)}{\partial t^n} + \frac{1}{4\pi\epsilon_0} \hat{n} \times HFP \iint_S \vec{\nabla} \vec{\nabla} \frac{dS'}{R} \cdot \int_{-\infty}^{t-\frac{R}{c}} \vec{J}(\vec{r}_m, \tau) d\tau \quad (5.21)$$

The time integral and time derivative of the current density is evaluated by using (5.14)-(5.18) so that (5.21) allows us to evaluate the near-cell and self-cell interactions accurately using again the samples of current at quadrature nodes at discrete time instants. That is we can write (5.21) in the form of (5.11) which uses quadrature rules. Discretization of (5.13) and (5.21) completes the formulation of the novel Nyström method proposed in this study for the solution of TDEFIE.

## 5.2 Numerical Results

In order to verify the validity of the derived formulas, three surface scattering problems are solved. In the first problem transient scattering from an electrically large PEC plate is analyzed. In the second problem transient scattering from a PEC cylinder is analyzed and in the last problem scattering from a long PEC strip is analyzed. In the series in the second integral on RHS in (5.21) only the first two terms are taken into account. One point quadrature rule is applied for far cells and 25 point quadrature rule is applied for close cells. The excitation pulse for the problem is a Gaussian pulse multiplied with a carrier to avoid DC breakdown. The transient pulse can be represented by,

$$E^i(t) = 120\pi \exp\left(-\frac{(t-t_0)^2}{\beta^2}\right) \cos(2\pi f_c t) \quad (5.22)$$

### 5.2.1 Electrically Large Plate

Plate is square in shape with side length of 10m. Geometry for the problem is plotted in Fig. 5.1. Incident pulse is a  $TM^x$  pulse with  $f_c=300$  MHz,  $t_0$  is selected as 7.5 ns and  $\beta$  as 3.4ns. Surface of plate is represented by square patches each having side length of 0.1m. Fig. 5.2 plots x-directed induced current on plate calculated by Nyström method as well as analytical solution.



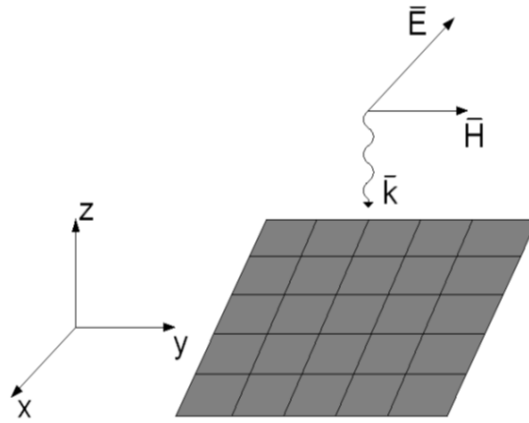


Fig. 5.1 Geometry for PEC plane problem

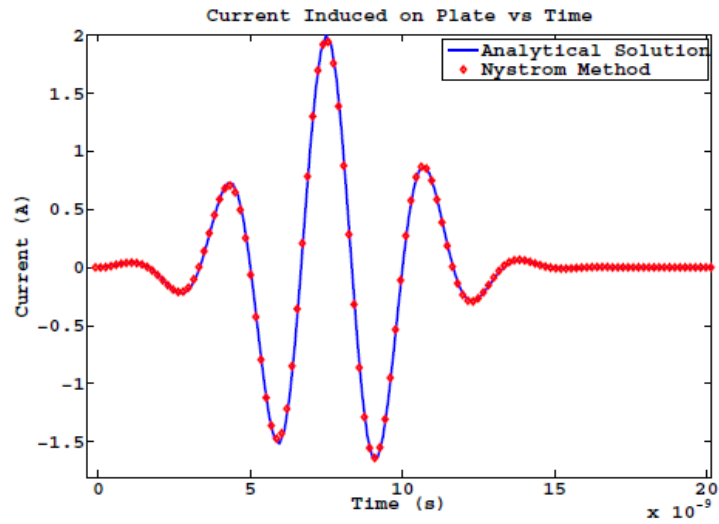


Fig. 5.2 Amplitude of induced current on PEC plate

It is observed from Fig 5.2 that the numerical result is coherent with the analytical result. Although this is a simple problem since the plate is both electrically and physically large and no reflections occur at the edges. It is useful to demonstrate that the time domain formulation obtained by using hypersingular terms is valid.

### 5.2.2 PEC Cylinder

In the second numerical problem we analyzed a long cylinder with radius of 1m and length 5m. The excitation pulse is a  $TM^z$  pulse with carrier frequency of 750 MHz,  $t_0=2.4\text{ns}$  and  $\beta$  1ns. The cylinder is represented with square patches having side length of 0.1m. Fig. 5.3 and Fig. 5.4 plot the geometry for the problem and amplitude of  $z$ -directed current on the cylinder, respectively.

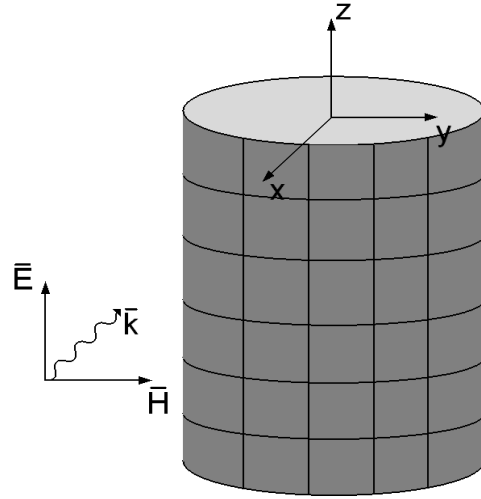


Fig. 5.3 Geometry for PEC cylinder problem

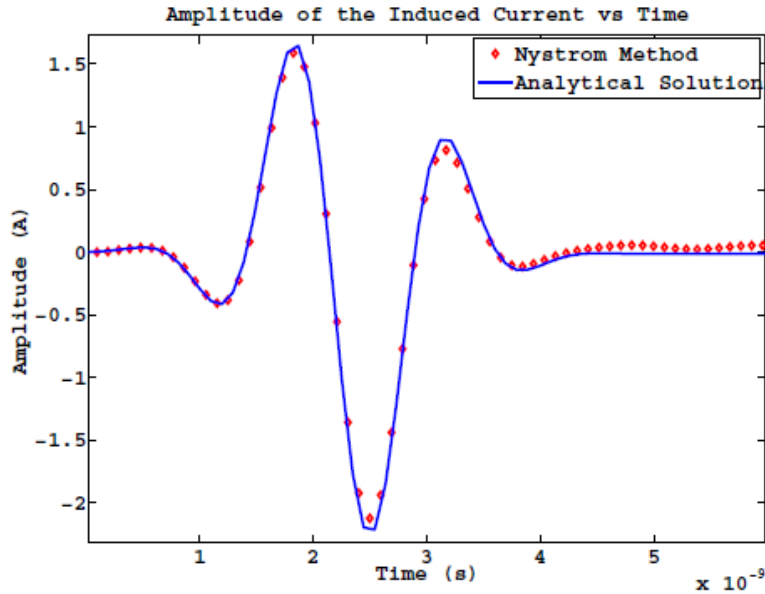


Fig. 5.4 Amplitude of the induced current on cylinder

It can be observed from Fig. 5.4 that the numerical results are close to the numerical results obtained by using new formulation. The analytical solution is obtained by inverse Fourier transform of the Mie series solution which is then convolved with the excitation pulse. This problem demonstrates that the formulation yields correct results for objects with smooth surfaces.

### 5.2.3 PEC Strip

In the last problem we consider  $TM^z$  scattering from a long PEC strip lying along  $z$ -direction. The length of strip is 10 m and the width is 0.5m. The strip is represented with square patches of sidelength 0.1 m. Incident pulse is a  $TM^z$  pulse with  $f_c=300$  MHz,  $t_0$  is 7.5 ns and  $\beta$  is 3.4ns. Fig. 5.5 plots the current induced at the center of the strip. The results are compared with the method proposed in [63]. In both methods no stabilization scheme is used. When no stabilization is applied, it is shown that the method proposed in this study remains stable although oscillation is observed in the reference solution at late times. This improvement is attributed to high order quadrature rules and interpolation in time, which are utilized to account for near cell contribution. On the other hand the disadvantage of using high order quadrature rules is increased simulation time and increased computational complexity to apply interpolation in time.

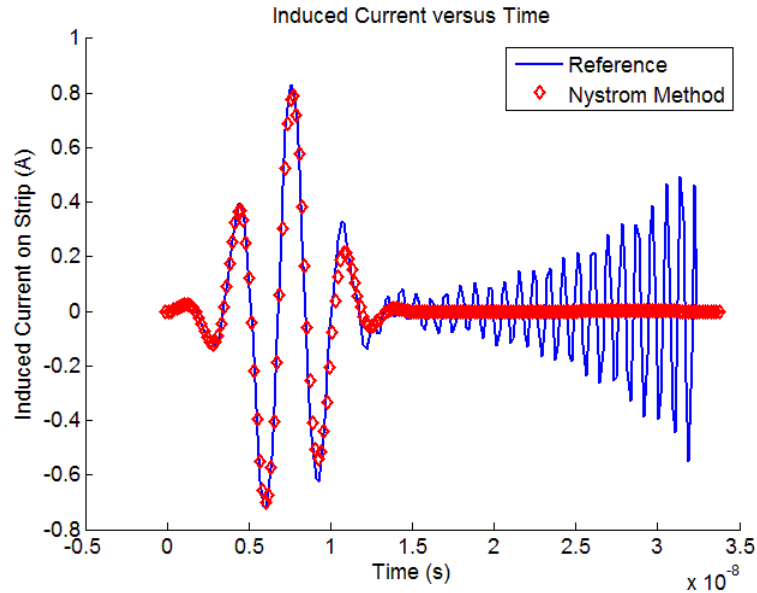


Fig. 5.5 Amplitude of current induced on PEC strip



## CHAPTER 6

### CONCLUSION

#### 6.1 Conclusion

Nyström method is successfully applied for the solution of TDEFIE. Although the method introduces some advantages when compared to MoM procedure in frequency domain, no attempt was made to apply it in time domain. In contrast to the conventional MoM procedure for the solution of TDIE, Nyström method does not use temporal and spatial basis functions and uses samples of current at selected quadrature points. Since repeated evaluation of double surface integrals of divergence conforming basis and testing functions are avoided, simpler formulation is obtained for the solution of integral equations.

One drawback of the frequency domain Nyström method is the failure of the classical quadrature rules when the kernel of the integrand is singular. Although local corrections are applied to overcome this difficulty, evaluation of hypersingular integrals increase the computational complexity. We have used Hadamard finite part interpretation for evaluation of hypersingular integrals and obtained explicit expressions for these integrals. These explicit expressions reduce the computational complexity of local corrections. When compared to other formulas previously introduced in literature, the new expressions are simpler and have the same accuracy. We have also purposed new formulas for hypersingular integrals on curvilinear surfaces. Improved accuracy is obtained when compared to flat facet approximations. Numerical studies conducted in frequency domain have shown that accurate representation of nonplanar characteristics of surface is important to preserve the rate of convergence of the solution.

Transient scattering problems are solved to test the accuracy of the purposed time domain method. It has been observed that results are coherent with analytical

results and with the results obtained by using conventional MoM procedure. Also the results are stable even at late times even if no stabilization techniques are employed. This behavior is attributed to the applied interpolation in time, which better approximated retarded interactions.

Finally it is foreseen that time domain formulation using Nyström method is also valid for solution of TDMFIE and TDCFIE as the singular integrals in these equations are not worse than hypersingular integrals. Also time domain analysis of integral equations using volume equivalent sources can be conducted by this method. Moreover we have used Newton-Cotes quadrature rules throughout the thesis but application of other rules such as Gauss-Legendre or Gauss-Lobatto is expected to give more accurate results.

## REFERENCES

- [1] L.F.Canino, J.J.Ottusch, M.A.Stalzer, J.L.Visher, S.M.Wandzura, “Numerical Solution of the Helmholtz Equation in 2D and 3D Using a High-Order Nystrom Discretization”, *J. Comp. Physics*, vol. 146, pp. 627–663, 1998. DOI: 10.1006/jcph.1998.6077
- [2] S.D. Gedney, J.Ottusch, P. Petre, J.Visher, and S.Wandzura, “Efficient high-order discretization schemes for integral equation methods,” *Digest of the 1997 IEEE Antennas and Propagation International Symposium*, Montreal, CA, pp. 1814–1817, July 1997
- [3] S. Kapur and D. E. Long, “High order Nyström schemes for efficient 3-D capacitance extraction,” *Digest of Technical Papers of the IEEE/ACM International Conference on Computer-Aided Design (ICCAD 98)*, pp. 178–185, November 1998. DOI: 10.1145/288548.288604
- [4] Mei Song Tong, Weng Cho Chew, “A Novel Approach for Evaluating Hypersingular and Strongly Singular Surface Integrals in Electromagnetics,” *IEEE Trans. on Antennas Propag.*, vol. 58, no. 11, Nov 2010
- [5] Mei Song Tong, Weng Cho Chew, “Super-Hyper Singularity Treatment for Solving 3D Electric Field Integral Equations”, *Microwave and Optical Technology Letters*, vol. 49, No.6, June 2007
- [6] J. C. Chao, Y. J. Liu, F. J. Rizzo, P.A. Martin, L. Udpa, “Regularized Integral Equations and Curvilinear Boundary Elements for Electromagnetic Wave Scattering in Three Dimensions,” *IEEE Trans. on Antennas Propag.*, vol. 43, No. 12, December 1995
- [7] K. Umashankar, A. Taflove, Computational Electromagnetics, Artech House, MA, 1993.
- [8] K.S. Yee, “Numerical solution of initial boundary value problems involving Maxwell’s equations in isotropic media,” *IEEE Trans. on Antennas Propag.*, vol.14, 1966, pp.302-307.
- [9] C. Christopoulos, Transmission-Line Modeling Method: TLM, IEEE Press, New York, USA, 1995.
- [10] J. L. Volakis, A. Chatterjee, and L. C. Kempel, Finite Element Method for Electromagnetics, IEEE Press, New York, USA, 1998

- [11] Walton C. Gibson, The Method of moments in electromagnetics, McGraw Hill, 2005.
- [12] J. Jin, Finite Element Method in Electromagnetics, John Wiley and Sons, 1993.
- [13] M. Çiydem A Ray Based Finite Difference Method for Time Domain Electromagnetics, PhD Thesis, METU 2005.
- [14] R. Coifman, V. Rokhlin, and S. Wandzura, The fast multipole method for the wave equation: A pedestrian prescription, *IEEE Ant. Propagat. Magazine*, vol. 35, no. 3, pp. 7–12, June 1993.
- [15] J. B. Keller, Geometrical theory of diffraction, *J. Opt. Soc. Amer.*, vol 52, 116-130, 1962.
- [16] R. G. Kouyoumjian, P.H. Pathak, A uniform geometrical theory of diffraction for an edge in a perfectly conducting surface, *Proc. IEEE*, vol 62, 1448-1461, 1974.
- [17] T.W Veruttipong “Time Domain Version of Uniform GTD,” *IEEE Trans. on Antennas Propag.*, vol 42,1994, pp 9-15.
- [18] P. Ufimtsev, Approximate computation of the diffraction of plane electromagnetic waves at certain metal bodies, *Sov. Phys. Tech.* vol. 27, 1708-1718, 1957.
- [19] A. Michaeli, “Equivalent edge currents for arbitrary aspects of observation,” *IEEE Trans. on Antennas Propag.*, vol 23, 252-258, 1984.
- [20] CST Microwave User Guide, 2014.
- [21] C. Balanis, Advanced Engineering Electromagnetics, John Wiley and Sons, 1989.
- [22] C. Balanis, Antenna Theory, John Wiley and Sons, 1982
- [23] N. Günalp, EE523 Lecture Notes, METU 2005
- [24] S. A. Schelkunaff, “Some equivalence theorems of electromagnetic and their application to radiation problems” *Bell System Tech. J.*, vol. 15, pp. 92-112, 1936
- [25] J. D. Kraus, K.R. Carver, Electromagnetics, Second Edition, McGraw-Hill, New York 1973, pp 464-467
- [26] R. F. Harrington, Time Harmonic Electromagnetic Fields, McGraw-Hill, New York, 1961



- [27] A. E. H. Love “The integration of the equations of propagation of electric waves”, *Phil. Trans. Roy. Soc. London, Ser. A*, vol. 197, pp. 1-45, 1901
- [28] R. F. Harrington, *Field Computation by Moment Methods*, Macmillan, New York 1968
- [29] T. K. Sarkar, “A note on the choice of weighting functions in the method of moments,” *IEEE Trans. on Antennas Propag.*, vol. AP-33, no. 4, pp. 436–441, April 1985
- [30] G. H. Golub and C. F. V. Loan, *Matrix Computations*. Baltimore: Johns Hopkins University press, 1996
- [31] L. Gürel, K. Sertel, I. K. Sendur “On the choice of basis functions to model surface electric current densities in computational electromagnetic,” *Radio Science*, vol. 34, pp.1373-1387, November 1999.
- [32] T. K. Sarkar, A. R. Djorjevic “On the choice of expansion and testing functions in the numerical solution of operator equations,” *IEEE Trans. on Antennas Propag.*, vol. 33, pp. 988-996, 1985
- [33] J. H. Richmond “On the variational aspects of the moment method *IEEE Trans. on Antennas Propag.*, vol. 39, pp. 473-479, 1991
- [34] H. Kim, H. Ling, C. Lee “A fast moment method algorithm using spectral domain wavelet concepts,” *Rad. Sci.*, vol. 31, pp. 1253-1261, 1996
- [35] M. I. Aksun and R. Mittra, Choices of expansion and testing functions for the method of moments applied to a class of electromagnetic problems, *IEEE Trans. on Microwave Theory and Techniques*, vol. 41, no. 3, pp. 503–509, 1993
- [36] R. D. Graglia, D. R. Wilton, A. F. Peterson “Higher order interpolatory vector bases for computational electromagnetic,” *IEEE Trans. on Antennas Propag.*, vol. 45, 329-342, 1997
- [37] E. J. Nyström, “Über die praktische Auflösung von Integral-gleichungen mit Anwendungen auf Randwertaufgaben,” *Acta Math.*, vol. 54, pp. 185–204, 1930. DOI: 10.1007/BF02547521
- [38] M.S.Tong and W. C. Chew, “A higher-order Nyström scheme for electromagnetic scattering by arbitrarily shaped surfaces,” *IEEE Antennas and Wireless Propagation Letters*, vol. 4, pp. 277-280, 2005
- [39] S. D. Gedney, “On deriving a locally-corrected Nyström scheme from a quadrature sampled moment method,” *IEEE Trans. on Antennas Propag.*, vol. 51, pp. 2402–2412, September 2003

- [40] A. F. Peterson, M. M. Biby “ An introduction to locally corrected Nyström method” , Morgan&Claypool 2010, ISBN: 9781608452996
- [41] R. Kress, “Numerical solution of boundary integral equations in time-harmonic electromagnetic scattering,” *Electromagnetics*, vol. 10, pp. 1–20, 1990.
- [42] R. Kress, “A Nyström method for boundary integral equations in domains with corners” *Numerische Mathematik*, vol. 58, pp. 145–161, 1990
- [43] J. S. Kot, “Computer modeling of MM-wave integrated circuit antennas using the Nyström method” *International Conference on Computation in Electromagnetics*, London, UK, pp. 288-291 ,1991
- [44] J. S. Kot, “Application of Nyström methods to electric- and magnetic-field integral equations” *Proceedings of the 1992 URSI International Symposium on Electromagnetic Theory*, Sydney pp. 125-127, 1992
- [45] L. M. Delves and J. L. Mohamed, Computational Methods for Integral Equations (Cambridge Univ. Press, New York, 1985).
- [46] J. Strain, “Locally corrected multidimensional quadrature rules for singular functions,” *SIAM J. Scientific Computing*, vol. 16, pp. 992–1017, 1995
- [47] J. M. Song and W. C. Chew, Multilevel fast-multipole algorithm for solving combined field equations of electromagnetic scattering, *Microwave Opt. Technol. Lett.* **10**, 14 (1995).
- [48] S. G. Samko. “Hypersingular Integrals and Their Applications” Taylor&Francis, 2002, ISBN 0415272688
- [49] L. J. Gray, J. Glaeser, T. Kaplan “ Direct evaluation of hypersingular Galerkin surface integrals” *SIAM J. Sci. Comput.*, 25 (2005) pp. 1534-1556
- [50] Krishnasamy G. , Schmerr L. W., Rudolphi T. J., Rizzo F. J., “Hypersingular Boundary Integral Equations: Some Applications in Acoustic and Elastic Wave Scattering”, *Transactions on ASME*, Vol 57, pp 404-414, June 1990
- [51] P. A. Martin, F. J. Rizzo, I. R. Gonsalves “ On hypersingular boundary integral equations for certain problems in mechanics” *Mechanics Research Comm.* vol. 16 (2), pp. 65-71, 1989
- [52] A. G. Polimeridis, M. Tamayo, J. M. Rius, J. R. Mosing “ Fast and accurate computation of hypersingular integrals in Galerkin surface integral equation formulations via the direct evaluation methods” *IEEE Trans. on Antennas Propag.*, vol. 59, pp. 2329-2340, June 2011

- [53] N. I. Ioakimidis "A natural approach to the introduction of finite part integrals into crack problems of three dimensional elasticity" *Engng. Fract. Mech.*, 16 (1982) pp. 669-673
- [54] M. G. Duffy, "Quadrature over a pyramid or cube of integrands with a singularity at the vertex," *SIAM Journal of Numerical Analysis*, vol. 19, pp. 1260-1262, December 1982
- [55] A. D. Yaghjian, "Electric Dyadic Green's Functions in the Source Region" *Proceedings of the IEEE*, 68, February 1980, p.248-263.
- [56] J. Van Bladel, "Some remarks on Green's dyadic for infinite space," *IRE Trans. Antennas Propag.*, Vol. AP-9, pp. 563-566, Nov. 1961
- [57] R. D. Graglia, "On the numerical integration of the linear shape functions times the 3-D Green's function or its gradient on a plane triangle," *IEEE Trans. on Antennas Propag.*, vol. 41, pp. 1448-1455, 1993.
- [58] Venturino E. "On The Numerical Calculation of Hadamard Finite Part Integrals" *Le Matematiche*, Vol 15 (1998)- Fasc. 2, pp.277-292
- [59] P. A. Martin, F. J. Rizzo "On boundary integral equations for crack problems" *Proc. R. Soc. Lond.* 421 (1989), pp. 341-355
- [60] P. A. Martin "Diffraction from nonplanar cracks" 4<sup>th</sup> International Conference on Mathematical and Numerical Aspects of Wave Propagation 1998
- [61] P. A. Martin. F. J. Rizzo. "Hypersingular integrals: How smooth must the density be?" *International Journal for Numerical Methods in Engineering*. Vol. 39, pp. 687-704, 1996
- [62] Bowman, Senior, Uslengi, "Electromagnetic and Acoustic Scattering By Simple Shapes", North-Holland Publishing Company-Amsterdam, 1969
- [63] S. D. Rao, "Time domain electromagnetics" Academic Press, San Diego, 1999 ISBN:012580190
- [64] T. Abboud, J.-C. Nédélec, and J. Volakis, "Stable solution of the retarded potential integral equations," in *Applied Computational Electromagnetics Symp.*, Monterey, CA, 2001
- [65] T. K. Sarkar, W. Lee, and S. M. Rao, "Analysis of transient scattering from composite arbitrarily shaped complex structures," *IEEE Trans. Antennas Propagat.*, vol. 48, pp. 1625-1634, 2000

- [66] G. Manara, A. Monorchio, and R. Reggiannini, "A space-time discretization criterion for a stable time-marching solution of the electric field integral equation," *IEEE Trans. Antennas Propagat.*, vol. 45, pp 527–532, 1997.
- [67] S. Dodson, S. P. Walker, and M. J. Bluck, "Implicitness and stability of time domain integral equation scattering analysis," *Appl. Computat. Electromagn. Soc. J.*, vol. 13, pp. 291–301, 1998.
- [68] J.-L. Hu and C. H. Chan, "Improved temporal basis functions using for time domain electric field integral equation method," *Electron. Lett.*, vol. 35, pp. 883–885, 1999.
- [69] J.-L. Hu, C. H. Chan, and Y. Xu, "A new temporal basis function for the time-domain integral equation method," *IEEE Microwave Wireless Comp. Lett.*, vol. 11, pp. 465–466, 2001
- [70] D. S. Weile, B. Shanker, and E. Michielssen, "An accurate scheme for the numerical solution of the time domain electric field integral equation," in *IEEE Antennas and Propagation Int. Symp.*, Boston, MA, 2001.
- [71] D. S. Weile, B. Shanker, and E. Michielssen "A novel scheme for the solution of the time-domain integral equations of electromagnetics," *IEEE Trans. on Antennas Propag.*, vol.52 no.1 2004.
- [72] R.A. Wildman, D. Weile "Two-Dimensional transverse-magnetic time-domain scattering using the Nyström method and bandlimited extrapolation," *IEEE Trans. on Antennas Propag.*, vol.53 no.7, 2005.
- [73] S. M. Rao, T. K. Sarkar "An alternative version of the time-domain electric field integral equation for arbitrarily shaped conductors," *IEEE Trans. on Antennas Propag.*, vol.41 no.6 1993.
- [74] J. B. Ho, T. K. Sarkar. " Time-domain electric field integral equation with central finite difference," Electrical Engineering Computer Science Paper 99, 2001
- [75] H. B. Dwight, "Table of integrals and other mathematical data," 4<sup>th</sup> ed. New York: Macmillan 1961

## APPENDIX A

### NUMERICAL INTEGRATION AND QUADRATURE RULES

The numerical evaluation of integrals is historically known by the name of quadrature, from the Latin word quadratura, which denotes the division of a region into squares to estimate its area. An  $n$ -point quadrature rule writes the integral as a summation with the form,

$$I(f) = \int_{-1}^1 f(x) dx = \sum_{i=1}^n w_i f(x_i) + E(n) \quad (\text{A.1})$$

The points  $x_i$  at which the function is evaluated are called as abscissas or the nodes. The multipliers  $w_i$  are called as the weights of the quadrature rule.  $E(n)$  denotes the error of the quadrature rule which in general decreases as the number of nodes is increased.

Here we introduce quadrature rules which approximate the integrals within unit domain  $-1 \leq x \leq 1$ . The integrals with domain  $(a, b)$  can be converted to unit domain by a change of variable,

$$z = x(b-a)/2 + (b+a)/2 \quad (\text{A.2})$$

and

$$\int_a^b g(z) dz = \int_{-1}^1 g(x(b-a)/2 + (b+a)/2) (b-a)/2 dx \quad (\text{A.3})$$

Quadrature rules are based on polynomial interpolation. The integrand function is evaluated at some nodes, the polynomial that interpolates the function at these nodes is determined and the integral of the interpolating polynomial is used as the approximation of the original function. Thus designing a quadrature

rules requires determination of the nodes and the weights of the summation. In this appendix we constrain ourselves the most common quadrature rules and their performance. These are the Newton-Cotes, Gauss-Legendre and the Gauss-Lobatto Quadrature rules.

### A.1. Newton-Cotes Quadrature Rules

Earlier quadrature rules use equally spaced nodes and are known as Newton-Cotes quadrature rules. In principle for an  $n$ -point quadrature rule with fixed nodes, the integrand can be approximated with polynomials at most of degree  $n - 1$ . If the nodes include the end points of the integration domain the quadrature rule is called as closed, otherwise it is called as an open quadrature rule. The weights are determined by solving the matrix equation,

$$\begin{bmatrix} \int 1 dx \\ \int x dx \\ \vdots \\ \int x^{n-1} dx \end{bmatrix} = \begin{bmatrix} 1 & 1 & 1 & 1 \\ x_1 & x_2 & \cdots & x_n \\ \vdots & \vdots & \ddots & \vdots \\ x_1^{n-1} & x_2^{n-1} & \cdots & x_n^{n-1} \end{bmatrix} \begin{bmatrix} w_1 \\ w_2 \\ \vdots \\ w_n \end{bmatrix} \quad (\text{A.3})$$

The advantage of Newton-Cotes quadrature rule is that the weights associated to the quadrature rule can be determined easily by using (A.3). On the other hand using fixed nodes reduces the degree of freedom and limits the degree of interpolating polynomials.

### A.2. Gauss-Legendre Quadrature Rules

Gauss has observed that if the position of nodes is not kept fixed, their position can be optimized to give better accuracy for smooth function when compared with Newton-Cotes quadrature rules. That is for a cubic polynomial with four degrees of freedom, two point quadrature rules may be used since both weights and positions of quadrature nodes can be optimized. Specifically, for interpolating polynomials at most of degree 3 two node quadrature rule can be constructed by solving,

$$\int 1dx = w_1 + w_2 \quad (\text{A.4})$$

$$\int xdx = w_1x_1 + w_2x_2 \quad (\text{A.5})$$

$$\int x^2dx = w_1x_1^2 + w_2x_2^2 \quad (\text{A.6})$$

$$\int x^3dx = w_1x_1^3 + w_2x_2^3 \quad (\text{A.7})$$

The advantage of using Gauss-Legendre rules is that an  $n$ -point quadrature rule can integrate polynomials of degree  $2n - 1$ . However solution of (A.4)-(A.7) is more difficult when compared with (A.3) as they are nonlinear equations. Nevertheless the system of equations (A.4)-(A.7) need not be solved since it has been shown that for an  $n$ -point quadrature rule the nodes are the roots of the Legendre polynomials and the weights are given by,

$$w_i = \frac{2}{(1 - x_i^2)[P'_n(x_i)]^2} \quad (\text{A.8})$$

with  $P_n(x)$  being the Legendre polynomial of degree  $n$ .

### A.3. Gauss-Lobatto Quadrature Rules

Gauss-Lobatto quadrature rules are similar to Gauss-Legendre rules but they include the end points of the integration domain. As two nodes are fixed they do integrate polynomials of degree  $2n - 3$  exactly. The nodes for an  $n$ -point rule are  $(i - 1)^{th}$  zero of  $P'_{n-1}(x)$  and the weights are given by

$$w_i = \frac{2}{n(n-1)[P'_{n-1}(x_i)]^2} \quad (\text{A.9})$$

#### A.4 Relative Performance of Quadrature Rules

In order to compare the performance of quadrature rules, the above mentioned rules are employed to evaluate a one dimensional integral and the error is compared for different number of nodes. Specifically we evaluate the integral,

$$I(x) = \int_{-1}^1 \frac{1}{x-1.1} dx \quad (\text{A.10})$$

The integral in (A.10) is a nearly strongly singular integral according to the convention introduced in chapter 4.

Table A.1 gives the error of different quadrature rules. The error is calculated by using,

$$Error = \frac{|I_{analytical} - I_{numercal}|}{I_{analytical}} \quad (\text{A.11})$$

Table (A.1) Relative performance of quadrature rules

<i>Number of Nodes</i>	<i>Newton-Cotes</i>	<i>Gauss-Lobatto</i>	<i>Gauss-Legendre</i>
5	$1.5 \times 10^{-1}$	$5.9 \times 10^{-2}$	$1.4 \times 10^{-2}$
7	$5.7 \times 10^{-2}$	$8.7 \times 10^{-3}$	$2.4 \times 10^{-3}$
9	$2.5 \times 10^{-2}$	$1.4 \times 10^{-3}$	$4.2 \times 10^{-4}$

It can be observed from table (A.1) that Gauss-Legendre has the best accuracy and Newton-Cotes rule has the worst accuracy. As the number of nodes is increase the accuracy of all rules of increased. The rate of convergence is similar in Gauss-Legendre and Gauss-Lobatto rules but it is relatively slow for Newton-Cotes quadrature rule. This is expected since as the order of nodes is increased by one,



the degree of interpolating polynomials increase by two for Gauss-Legendre and Gauss-Lobatto rules. It is also observed from the table that regardless of the employed quadrature rule, accuracy improves as the degree of interpolating polynomials is increased.

## APPENDIX B

### EQUIVALENCE OF FINITE PART INTEGRALS TO PHYSICAL FIELDS

In this Appendix we prove the validity of (4.43) on a flat surface defined on a coordinate system  $(x_1, x_2, y)$  which is plotted in Fig. B.1.

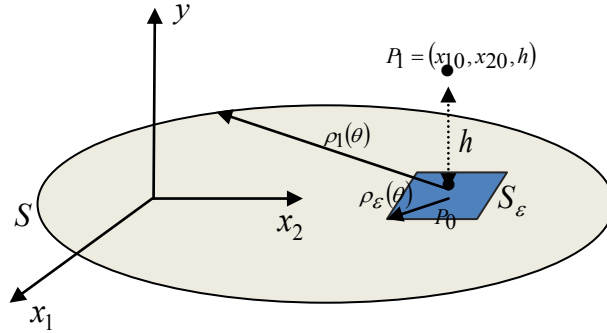


Fig. B1. Geometry on which (4.43) is defined

We rewrite (4.43) here in a different format as,

$$\frac{\partial}{\partial x_i} \iint_S \frac{\partial}{\partial x_j} \left( \frac{1}{R} \right) f(x_1, x_2) dx_1 dx_2 = HFP \iint_S \frac{\partial}{\partial x_i} \frac{\partial}{\partial x_j} \left( \frac{1}{R} \right) f(x_1, x_2) dx_1 dx_2 \quad (B.1)$$

where  $R$  is the distance between source point  $(x_1, x_2)$  and observation point  $(x_{10}, x_{20}, y)$ .

Unlike the equation in Chapter 4 we also included the density function  $f(x_1, x_2)$  in the integrand in (B.1). This results in a more general proof that is valid unless the density function is not Hölder continuous that is  $f(x_1, x_2) \in C^{1,\alpha}$ .

We start the proof by assuming the observation point is off the source plane at  $P_1$  such that the integral in the LHS of (B.1) is not singular. Also we extract a

small patch  $S_\varepsilon$  from the source plane and evaluate the contribution of  $S - S_\varepsilon$  and  $S_\varepsilon$  separately. It will be shown that the contribution of  $S - S_\varepsilon$  and  $S_\varepsilon$  will diverge separately as  $P_1 \rightarrow P_0$  and  $S_\varepsilon \rightarrow 0$ . Nevertheless it will be shown that divergent terms from both surfaces are same with opposite signs so that the resulting integral is finite. Having discarded the divergent terms on LHS in (B.1) we arrive to the Hadamard finite part of the integral which is on RHS of (B.1) and is already defined in Chapter 4. It should also be noted that although the proof is given on a flat surface it is also valid for smooth nonplanar surfaces since the extracted surface element  $S_\varepsilon$  can be considered as locally flat as its area diminishes.

We start the proof dividing the domain of integration it two parts and rewrite the integral on the LHS of (B.1)

$$\begin{aligned} \lim_{S\varepsilon \rightarrow 0} \left\{ \lim_{P_1 \rightarrow P_0} \iint_{S-S_\varepsilon} \frac{\partial}{\partial x_i} \frac{\partial}{\partial x_j} \left( \frac{1}{R} \right) f(x_1, x_2) dx_1 dx_2 \right\} &= \lim_{S\varepsilon \rightarrow 0} \left\{ \lim_{P_1 \rightarrow P_0} \iint_{S-S_\varepsilon} \frac{\partial}{\partial x_i} \frac{\partial}{\partial x_j} \left( \frac{1}{R} \right) f(x_1, x_2) dx_1 dx_2 \right\} \\ &+ \lim_{S\varepsilon \rightarrow 0} \left\{ \lim_{P_1 \rightarrow P_0} \iint_{S_\varepsilon} \frac{\partial}{\partial x_i} \frac{\partial}{\partial x_j} \left( \frac{1}{R} \right) f(x_1, x_2) dx_1 dx_2 \right\} \quad (B.2) \end{aligned}$$

where we have  $R = \sqrt{r^2 + h^2}$  and  $r = \sqrt{(x_1 - x_{10})^2 + (x_2 - x_{20})^2}$ .

In the first integral on the RHS of (B.2) the limit  $P_1 \rightarrow P_0$  can directly be applied since the singular point is not included in  $S - S_\varepsilon$ . Applying this limit result in the following integral,

$$I_1 = \lim_{S\varepsilon \rightarrow 0} \left\{ \lim_{P_1 \rightarrow P_0} \iint_{S-S_\varepsilon} \frac{\partial}{\partial x_i} \frac{\partial}{\partial x_j} \left( \frac{1}{R} \right) f(x_1, x_2) dx_1 dx_2 \right\} = \lim_{S\varepsilon \rightarrow 0} \left\{ \iint_{S-S_\varepsilon} \frac{\partial}{\partial x_i} \frac{\partial}{\partial x_j} \left( \frac{1}{r} \right) f(x_1, x_2) dx_1 dx_2 \right\} \quad (B.3)$$

The density function is expanded around the singular point so that we write,

$$f(x_1, x_2) = f(x_{10}, x_{20}) + f_1(x_{10}, x_{20}) \times (x_1 - x_{10}) + f_2(x_{10}, x_{20}) \times (x_2 - x_{20}) + H.O.T. \quad (B.4)$$

where  $f_1(x_{10}, x_{20}) = \partial f(x_1, x_2) / \partial x_1$  and  $f_2(x_{10}, x_{20}) = \partial f(x_1, x_2) / \partial x_2$  evaluated at  $(x_{10}, x_{20})$ .

Substituting (B.4) for the density function in (B.3),  $I_1$  is rewritten as,

$$I_1 = \lim_{S_\varepsilon \rightarrow 0} \left\{ \iint_{S-S_\varepsilon} \frac{\partial}{\partial x_i} \frac{\partial}{\partial x_j} \left( \frac{1}{r} \right) f(x_{10}, x_{20}) dx_1 dx_2 + \iint_{S-S_\varepsilon} \frac{\partial}{\partial x_i} \frac{\partial}{\partial x_j} \left( \frac{1}{r} \right) f_1(x_{10}, x_{20}) (x_1 - x_{10}) dx_1 dx_2 \right. \\ \left. + \lim_{S_\varepsilon \rightarrow 0} \iint_{S-S_\varepsilon} \frac{\partial}{\partial x_i} \frac{\partial}{\partial x_j} \left( \frac{1}{r} \right) f_2(x_{10}, x_{20}) (x_2 - x_{20}) dx_1 dx_2 \right\} \quad (B.5)$$

The first integral on the RHS of (B.5) is written in a local coordinate system whose origin is at the observation point at  $(x_{10}, x_{20})$ . This result in,

$$I_{1a} = \lim_{S_\varepsilon \rightarrow 0} \left\{ \iint_{S-S_\varepsilon} \frac{\partial}{\partial x_i} \frac{\partial}{\partial x_j} \left( \frac{1}{r} \right) f(x_{10}, x_{20}) dx_1 dx_2 \right\} = \lim_{S_\varepsilon \rightarrow 0} \left\{ f(x_{10}, x_{20}) \int_0^{2\pi} \int_{\rho_\varepsilon(\theta)}^{\rho_1(\theta)} \left( \frac{g_{ij}(\theta) - \delta_{ij}}{r^3} \right) r dr d\theta \right\} \quad (B.6)$$

where

$$g_{11}(\theta) = 3 \cos^2(\theta) \quad (B.7a)$$

$$g_{12}(\theta) = g_{21}(\theta) = 3 \cos(\theta) \sin(\theta) \quad (B.7b)$$

$$g_{22}(\theta) = 3 \sin^2(\theta) \quad (B.7c)$$

with  $\cos \theta = x_1 / r$ ,  $\sin \theta = x_2 / r$  and  $\delta_{ij} = 1$  for  $i = j$  and  $\delta_{ij} = 0$  for  $i \neq j$ .

Evaluating the integral of the radial component yields,

$$I_{1a} = \lim_{\varepsilon \rightarrow 0} \left\{ f(x_{10}, x_{20}) \int_0^{2\pi} \left[ -\frac{g_{ij}(\theta) - \delta_{ij}}{r} \right]_{\rho_\varepsilon(\theta)}^{\rho_1(\theta)} d\theta \right\} \quad (B.8)$$

for which the divergent part as  $S_\varepsilon \rightarrow 0$  is,

$$I_{1a}^d = \lim_{\varepsilon \rightarrow 0} \left\{ f(x_{10}, x_{20}) \int_0^{2\pi} \frac{g_{ij}(\theta) - \delta_{ij}}{\rho_\varepsilon(\theta)} d\theta \right\} \quad (\text{B.9})$$

Next consider the second integral on the RHS of (B.5), which is written in polar coordinates as,

$$I_{1b} = \lim_{S_\varepsilon \rightarrow 0} \iint_{S-S_\varepsilon} \frac{\partial}{\partial x_i} \frac{\partial}{\partial x_j} \left( \frac{1}{r} \right) f_1(x_{10}, x_{20}) (x_1 - x_{10}) dx_1 dx_2 = \lim_{S_\varepsilon \rightarrow 0} \left\{ f_1(x_{10}, x_{20}) \int_0^{2\pi} \int_{\rho_\varepsilon(\theta)}^{\rho_1(\theta)} \left( \frac{(g_{ij}(\theta) - \delta_{ij}) \cos \theta}{r^2} \right) r dr d\theta \right\} \quad (\text{B.10})$$

where  $(x_1 - x_{10}) = r \cos \theta$  is used in (B.10). Evaluating the integral of the radial component yields,

$$I_{1b} = \lim_{\varepsilon \rightarrow 0} \left\{ -f_1(x_{10}, x_{20}) \int_0^{2\pi} (g_{ij}(\theta) - \delta_{ij}) \cos \theta [\ln(r)]_{\rho_\varepsilon(\theta)}^{\rho_1(\theta)} d\theta \right\} \quad (\text{B.11})$$

and the divergent part as  $S_\varepsilon \rightarrow 0$  is,

$$I_{1b}^d = \lim_{\varepsilon \rightarrow 0} \left\{ -f_1(x_{10}, x_{20}) \int_0^{2\pi} (g_{ij}(\theta) - \delta_{ij}) \cos \theta [\ln(\rho_\varepsilon(\theta))] d\theta \right\} \quad (\text{B.12})$$

Same procedure can be used the divergent term for the third integral on the RHS of (B.5) and the result is,

$$I_{1c}^d = \lim_{\varepsilon \rightarrow 0} \left\{ f_1(x_{10}, x_{20}) \int_0^{2\pi} (g_{ij}(\theta) - \delta_{ij}) \sin \theta [\ln(\rho_\varepsilon(\theta))] d\theta \right\} \quad (\text{B.13})$$

$I_{1a}^d, I_{1b}^d$  and  $I_{1c}^d$  are the divergent terms that result for evaluation of the integral in (B.5) whose domain of integration is  $S - S_\varepsilon$ . Next we consider the second integral on the RHS of (B.2) which is defined on  $S_\varepsilon$  and write explicitly the divergent terms resulting from this integral. Thus,

$$I_2 = \lim_{S_\varepsilon \rightarrow 0} \left\{ \lim_{P_1 \rightarrow P_0} \iint_{S_\varepsilon} \frac{\partial}{\partial x_i} \frac{\partial}{\partial x_j} \left( \frac{1}{R} \right) f(x_1, x_2) dx_1 dx_2 \right\} = \lim_{S_\varepsilon \rightarrow 0} \left\{ \lim_{h \rightarrow 0} \iint_{S_\varepsilon} \frac{\partial}{\partial x_i} \frac{\partial}{\partial x_j} \left( \frac{1}{\sqrt{r^2 + h^2}} \right) f(x_1, x_2) dx_1 dx_2 \right\} \quad (\text{B.12})$$

and the expansion of the density function  $f(x_1, x_2)$  in (B.4) is used to in (B.12) which yields,

$$I_2 = I_{2a} + I_{2b} + I_{2c} \quad (\text{B.13})$$

with

$$I_{2a} = \lim_{S_\varepsilon \rightarrow 0} \left\{ \lim_{h \rightarrow 0} \iint_{S_\varepsilon} \frac{\partial}{\partial x_i} \frac{\partial}{\partial x_j} \left( \frac{1}{\sqrt{r^2 + h^2}} \right) f(x_{10}, x_{20}) dx_1 dx_2 \right\} \quad (\text{B.14})$$

$$I_{2b} = \lim_{S_\varepsilon \rightarrow 0} \left\{ \lim_{h \rightarrow 0} \iint_{S_\varepsilon} \frac{\partial}{\partial x_i} \frac{\partial}{\partial x_j} \left( \frac{1}{\sqrt{r^2 + h^2}} \right) f_1(x_{10}, x_{20}) (x_1 - x_{10}) dx_1 dx_2 \right\} \quad (\text{B.15})$$

$$I_{2c} = \lim_{S_\varepsilon \rightarrow 0} \left\{ \lim_{h \rightarrow 0} \iint_{S_\varepsilon} \frac{\partial}{\partial x_i} \frac{\partial}{\partial x_j} \left( \frac{1}{\sqrt{r^2 + h^2}} \right) f_2(x_{10}, x_{20}) (x_2 - x_{20}) dx_1 dx_2 \right\} \quad (\text{B.16})$$

In order to find divergent term due to  $I_{2a}$ , this integral is written in local coordinates as,

$$I_{2a} = \lim_{S_\varepsilon \rightarrow 0} \left\{ \lim_{h \rightarrow 0} \int_0^{2\pi\rho_\varepsilon(\theta)} \int_0^\theta f(x_{10}, x_{20}) \left\{ \frac{(g_{ij}(\theta))r^2}{(\sqrt{r^2 + h^2})^5} - \frac{\delta_{ij}}{(\sqrt{r^2 + h^2})^3} \right\} r dr d\theta \right\} \quad (\text{B.17})$$

Using

$$I_{2a}^1 = \int_0^{\rho_\varepsilon(\theta)} \frac{(g_{ij}(\theta))r^3}{(\sqrt{r^2 + h^2})^5} dr = \left\{ -\frac{r^2}{(\sqrt{r^2 + h^2})^3} - \frac{2h^2}{3(\sqrt{r^2 + h^2})^3} \right\} \bigg|_0^{\rho_\varepsilon(\theta)} (g_{ij}(\theta))$$

(B.18)

for the first integral in the brackets of the radial component and evaluating this expression in the boundaries yield,

$$I_{2a}^1 = \left\{ -\frac{\rho_\varepsilon^2(\theta)}{(\sqrt{\rho_\varepsilon^2(\theta) + h^2})^3} - \frac{2h^2}{3(\sqrt{\rho_\varepsilon^2(\theta) + h^2})^3} + \frac{2h^2}{3h^3} \right\} (g_{ij}(\theta)) \quad (\text{B.19})$$

Similarly using

$$I_{2a}^2 = \int_0^{\rho_\varepsilon(\theta)} \frac{-\delta_{ij} r}{\left(\sqrt{r^2 + h^2}\right)^3} dr = \left\{ \frac{r^2}{\left(\sqrt{r^2 + h^2}\right)^3} + \frac{h^2}{\left(\sqrt{r^2 + h^2}\right)^3} \right\} \bigg|_0^{\rho_\varepsilon(\theta)} (\delta_{ij}) \quad (\text{B.20})$$

for the second integral in the brackets of the radial component and evaluating this expression in the boundaries yield,

$$I_{2a}^2 = \left\{ -\frac{\rho_\varepsilon^2(\theta)}{\left(\sqrt{\rho_\varepsilon^2(\theta) + h^2}\right)^3} + \frac{h^2}{\left(\sqrt{\rho_\varepsilon^2(\theta) + h^2}\right)^3} - \frac{h^2}{h^3} \right\} (\delta_{ij}) \quad (\text{B.21})$$

Adding the two integrals  $I_{2a}^1$  and  $I_{2a}^2$  yields,

$$I_{2a} = \left\{ -\frac{\rho_\varepsilon^2(\theta)[g_{ij}(\theta) - \delta_{ij}]}{\left(\sqrt{\rho_\varepsilon^2(\theta) + h^2}\right)^3} - \frac{h^2 \left[ \frac{2}{3}(g_{ij}(\theta) - \delta_{ij}) \right]}{\left(\sqrt{\rho_\varepsilon^2(\theta) + h^2}\right)^3} + \frac{h^2 \left[ \frac{2}{3}(g_{ij}(\theta) - \delta_{ij}) \right]}{h^3} \right\} \quad (\text{B.22})$$

When the limit  $h \rightarrow 0$  applied it can be shown that the first term produces a divergent term which has the same magnitude as (B.6) but has opposite sign, that is,

$$I_{2a}^d = \lim_{\varepsilon \rightarrow 0} \left\{ \int_0^{2\pi} -\frac{[g_{ij}(\theta) - \delta_{ij}]}{\rho_\varepsilon(\theta)} f(x_{10}, x_{20}) d\theta \right\} \quad (\text{B.23})$$

Also the second term in (B.22) vanishes as the limit is applied. The third term however is also a divergent term as  $h \rightarrow 0$  but fortunately the angular integral removes this singularity so that this term also vanishes yielding  $I_{1a}^d = -I_{2a}^d$ .

Also writing  $I_{2b}$  in polar coordinates result in,

$$I_{2b} = \lim_{S_\varepsilon \rightarrow 0} \left\{ \lim_{h \rightarrow 0} \int_0^{2\pi} \int_0^{\rho_\varepsilon(\theta)} \frac{[g_{ij}(\theta) - \delta_{ij}] \cos \theta}{\left(\sqrt{r^2 + h^2}\right)^5} r^4 f_1(x_{10}, x_{20}) dr d\theta \right\} \quad (\text{B.24})$$

The integral of the radial component is evaluated using

$$\int \frac{r^3}{(\sqrt{r^2 + h^2})^4} = \frac{1}{2} \ln(r^2 + h^2) + \frac{h^2}{2(r^2 + h^2)} \quad (\text{B.25})$$

Substituting (B.21) in (B.20) result in,

$$I_{2b} = \lim_{h \rightarrow 0} \int_0^{2\pi} (g_{ij}(\theta) - \delta_{ij}) \cos \theta \left[ \frac{1}{2} \ln(\rho_\varepsilon^2(\theta) + h^2) + \frac{h^2}{2(h^2 + \rho_\varepsilon^2(\theta))} - \frac{1}{2} \ln(h^2) - \frac{1}{2} \right] d\theta \quad (\text{B.22})$$

Application of the limit  $h \rightarrow 0$  eliminates second and fourth term within the brackets whereas the fourth term is still unbounded. However since the integration of angular component along the fourth term result in a vanishing integral and this term does not contribute a divergent value. The remaining divergent term due to  $I_{2b}$  can be written as,

$$I_{2b}^d = \lim_{\varepsilon \rightarrow 0} \int_0^{2\pi} (g_{ij}(\theta) - \delta_{ij}) \cos \theta \ln(\rho_\varepsilon(\theta)) d\theta \quad (\text{B.26})$$

Similar inspection on  $I_{2c}$  leads to the divergent integral,

$$I_{2c}^d = \lim_{\varepsilon \rightarrow 0} \int_0^{2\pi} (g_{ij}(\theta) - \delta_{ij}) \sin \theta \ln(\rho_\varepsilon(\theta)) d\theta \quad (\text{B.27})$$

Having explicitly written divergent terms for  $I_1$  and  $I_2$ , we see that these divergent terms cancel so that,

$$I_{1a}^d + I_{1b}^d + I_{1c}^d + I_{2a}^d + I_{2b}^d + I_{2c}^d = 0 \quad (\text{B.28})$$

which leads to the definition of Hadamard finite part of the integral on the LHS of (B.1) and this completes the proof.



## APPENDIX C

### REQUIREMENT ON THE DENSITY FUNCTION FOR THE EXISTENCE OF FINITE PART OF A HYPERSINGULAR INTEGRAL

In Appendix B tangential components of a hypersingular integral is evaluated by extracting a small surface  $S_\varepsilon$  from the domain of integration and finding the divergent terms resulting from the integral on  $S_\varepsilon$  and  $S - S_\varepsilon$  separately. It was shown that the divergent terms of the resulting integrals are same but have opposite signs such that the result is bounded. Specifically we proved that the sum,

$$\lim_{S_\varepsilon \rightarrow 0} \left\{ \lim_{P_1 \rightarrow P_0} \iint_{S - S_\varepsilon} \frac{\partial}{\partial x_i} \frac{\partial}{\partial x_j} \left( \frac{1}{R} \right) f(x_1, x_2) dx_1 dx_2 \right\} + \lim_{S_\varepsilon \rightarrow 0} \left\{ \lim_{P_1 \rightarrow P_0} \iint_{S_\varepsilon} \frac{\partial}{\partial x_i} \frac{\partial}{\partial x_j} \left( \frac{1}{R} \right) f(x_1, x_2) dx_1 dx_2 \right\} = 0 \quad (C.1)$$

is finite by using the expansion of the surface function  $f(x_1, x_2)$  around the observation point  $(x_{10}, x_{20})$ . In order the proof given in Appendix A to be complete we need to prove either the remaining terms of the Taylor series expansion of density function do not introduce new divergent terms or these new divergent (if any) terms cancel each other. That is we need also to show that,

$$\begin{aligned} & \lim_{S_\varepsilon \rightarrow 0} \left\{ \iint_{S - S_\varepsilon} \frac{\partial}{\partial x_i} \frac{\partial}{\partial x_j} \left( \frac{1}{R} \right) [f(x_1, x_2) - f(x_{10}, x_{20}) - f_1(x_{10}, x_{20})(x_1 - x_{10}) - f_2(x_{10}, x_{20})(x_2 - x_{20})] dx_1 dx_2 \right\} \\ & + \lim_{S_\varepsilon \rightarrow 0} \left\{ \iint_{S_\varepsilon} \frac{\partial}{\partial x_i} \frac{\partial}{\partial x_j} \left( \frac{1}{R} \right) [f(x_1, x_2) - f(x_{10}, x_{20}) - f_1(x_{10}, x_{20})(x_1 - x_{10}) - f_2(x_{10}, x_{20})(x_2 - x_{20})] dx_1 dx_2 \right\} = 0 \quad (C.2) \end{aligned}$$

either by showing that the two integrals are both finite or by showing that their divergent terms cancel each other. Here we use the first method which imposes a loose condition on the density function. Writing the first integral in polar coordinates,

$$I_3 = \lim_{\varepsilon \rightarrow 0} \int_0^{2\pi\rho_1(\theta)} \int_{0 \ \rho_\varepsilon(\theta)} \frac{g_{ij}(\theta)}{r^2} [f(x_1, x_2) - f(x_{10}, x_{20}) - f_1(x_{10}, x_{20})(x_1 - x_{10}) - f_2(x_{10}, x_{20})(x_2 - x_{20})] dr d\theta \quad (C.3)$$

it can be seen that this integral is finite if it is at most weakly singular. That is

$$[f(x_1, x_2) - f(x_{10}, x_{20}) - f_1(x_{10}, x_{20})(x_1 - x_{10}) - f_2(x_{10}, x_{20})(x_2 - x_{20})] \leq A|r|^{\alpha+1} \quad (C.4)$$

where  $A$  is finite number and  $0 \leq \alpha < 1$ . The condition in (C.4) is known as the Hölder continuity criteria of the density function and denoted by,

$$f(x_1, x_2) \in C^{1,\alpha} \quad (C.5)$$

Same discussion applies to the second integral in (C.2) which completes the proof.

## CURRICULUM VITAE

### PERSONAL INFORMATION

Surname, Name : Selçuk, Gökhun  
Nationality: Turkish (TC)  
Date and Place of Birth: 09 January 1981, İstanbul  
Marital Status: Married  
Phone: +90 312 592 3713  
Fax: +90 312 592 1403  
email: gselcuk@aselsan.com.tr

### EDUCATION

Degree	Institution	Year of Graduation
MS	METU,EE	2008
BS	METU,PHY	2005
BS	METU,EE	2004
High School	İstanbul Fen Lisesi	1999

### WORK EXPERIENCE

Year	Place	Enrollment
2005-Present	Aselsan Inc, Civil Comm. Dept.	Senior RF Eng.

### FOREIGN LANGUAGES

Fluent English, German

### PUBLICATIONS

1. Şahin B., Selçuk G., “İletişim Ağ Güvenliğinde Son Aşama: Kuantum Kriptografi ve Fiber Optik Ortamda Kuantum Temelli Rastsal Sayı Üretimi,” Ulusal Elektronik İmza Sempozyumu, Gazi Üniv., 7-8 Aralık 2006
2. Selcuk G., Koç S. S., “ Novel Nyström Method for TDEFIE” Proc. 8th Eur. Conf. Antennas Prop., Hague, Netherlands, April 2014
3. Selcuk G., Koç S. S., “ Evaluation of Hypersingular Integrals on Nonplanar Surfaces” Proc. Num. Electromag. Modelling and Opt., Pavia, Italy, May 2014

### HOBBIES

Football